2007

CONTROLS ON THERMAL DISCHARGE IN YELLOWSTONE NATIONAL PARK, WYOMING

Jacob Steven Mohrmann
The University of Montana

CONTROLS ON THERMAL DISCHARGE IN YELLOWSTONE NATIONAL PARK, WYOMING

By

Jacob Steven Mohrmann

B.A. Environmental Science, Northwest University, Kirkland, WA, 2003

Thesis

presented in partial fulfillment of the requirements
for the degree of Masters of Science in Geology

The University of Montana
Missoula, MT

Fall 2007

Approved by:

Dr. David A. Strobel, Dean
Graduate School

Dr. Nancy Hinman
Committee Chair

Dr. William Woessner
Committee Member

Dr. Solomon Harrar
Committee Member

Mohrmann, Jacob, M.S., Fall 2007 Geology

Controls on Thermal Discharge in Yellowstone National Park, Wyoming

Director: Nancy W. Hinman

Significant fluctuations in discharge occur in hot springs in Yellowstone National Park on a seasonal to decadal scale (Ingebritsen et al., 2001) and an hourly scale (Vitale, 2002).

The purpose of this study was to determine the interval of the fluctuations in discharge and to explain what causes those discharge patterns in three thermally influenced streams in Yellowstone National Park. By monitoring flow in these streams, whose primary source of input is thermal discharge, we were able to find several significant patterns of discharge fluctuations. Patterns were found by using two techniques of spectral analysis. The spectral analyses completed involved using the program "R" as well as Microsoft Excel, both of which use Fourier transforms. The Fourier transform is a linear operator that identifies frequencies in the original function.

Stream flow data were collected using a FloDar open channel flow monitor. The flow meter collected data at15-minute intervals at White Creek and Rabbit Creek for a period of approximately two weeks each during the Fall. Flow data were also used from 15-minute data interval from a USGS gaging station at Tantalus Creek.

Patterns of discharge fluctuation were found in each stream. By comparing spectral analysis results of flow data with spectral analysis of published tide data and barometric pressure data, connections were drawn between fluctuations in tidal and barometric-pressure patterns and flow patterns. Also, visual comparisons used to identify potential correspondence with earthquakes and precipitation events.

At Tantalus Creek, patterns were affected only by barometric pressure changes. At White Creek, one pattern was attributed to barometric pressure fluctuations, and another pattern was found that could be associated with earth-tide forces. At Rabbit Creek, these patterns were absent. A pattern at 8.55 hours, which could not be attributed to barometric pressure or earth tide forces, was found at Rabbit and White Creeks.

The 8.55 hour pattern in discharge found at both Rabbit and White Creeks may suggest a physical link between the sites, which are close (2.5 km). The time pattern could be a result of a shared hydrothermal aquifer, convectively heating and discharging at both streams. However, the common time pattern could also be the result of independent factors, which coincidentally caused a similar time pattern.

Acknowledgments

Thank you to my committee members: Nancy Hinman, Bill Woessner, and Solomon Harrar

Field assistants: Veronica Krings, Steve Mohrmann, Jan Mohrmann, Doc Richardson

Research was conducted under Yellowstone National Park Permit Yell-2006-SCI-5632.

Special thank you to Hank Heasler and other YNP personal that provided assistance throughout the project.

To Mike Kaczmarek and Morrison-Maierle of Helena, Montana for providing assistance throughout the project.

And to the USGS, NOAA, and Utah State University for providing station data at several sites throughout the park.

"I am convinced that, at its best, science is simple—that the simplest arrangement of facts that sets forth the truth best deserves the term science. So the geology I plead for is that which states facts in plain words—in language understood by the many rather than by the few."

--George Otis Smith, 1921
Director, U.S. Geological Survey 1907-1930

Page Number

Table of Contents

List of Tables

List of Figures

1.0 Introduction

Yellowstone National Park (YNP) holds half of the Earth's geothermal features including geysers, mud pots, fumaroles, and hot springs. These 10,000+ features are fed by water and steam heated at a variety of depths by a shallow magma plume sitting between 3 km to 5 km below the surface (Eaton et al., 1975; Iyer et al., 1981; Lehman et al., 1982; Smith and Braile, 1984; Benz and Smith, 1984; Miller and Smith, 1999; Finn and Morgan, 2002; Husen et al., 2004; Waite et al., 2005; Waite et al., 2005; Farnetani and Samuel, 2005; Yuan and Dueker, 2005). An abundant supply of recharge in the form of snow melt infiltrates the hydrothermal system in the Yellowstone caldera and is heated to ~ 350°C where it then rises through an extensive fracture network (Fournier, 1989; Fournier et al., 1994).

Hydrothermal water discharged from surface features can infiltrate back into the nearby subsurface and return to deep reservoirs recharging the system. However, much of the water discharged flows out of YNP in streams and rivers. Approximately 100 million metric tonnes of water are discharged by YNP hot springs annually (Fournier et al., 1976; Norton, 1989). Allen and Day first studied thermal discharge in YNP (1935). A better understanding of deep thermal water-rock interactions came through studies of hot-spring chemistry (Allen et al., 1935, White et al., 1975; Ingebritsen et al., 1993), which also serves to assess potential volcanic activity (Farrar et al., 1985; Sorey et al., 1991; Waite, 2002; Lowenstern et al., 2006) and to generate environmental baseline data in anticipation of possible future off-site geothermal development and other anthropogenic

influences (Sorey et al., 1991; Ingebritsen et al., 1988; Norton et al., 1989; Friedman, 2000). In these studies, many interesting phenomena have been reported, such as strong seasonal discharge pulses and decadal cyclical trends in discharge. In addition to pulses in water flux, changes in heat discharge and chemical discharges (chloride and arsenic) were also observed (Ingebritsen et al., 1993). Recent studies have suggested that shorter term daily cyclical patterns in discharge occur at Rabbit Creek in YNP (Vitale, 2002). Rabbit Creek's primary source of water comes directly from discharging hot springs that share a hydrothermal aquifer (Vitale, 2002). The hydrothermal reservoir is likely sensitive to pressure changes, as has been shown in several studies of subterranean aquifers (Bredehoeft, 1967; Freeze and Cherry 1979; Gieske et al., 1987; Hsieh et al., 1987; Furbish, 1997; Inkenbrandt et al., 2005).

1.1 Purpose of Research

This study's primary goals were to document temporal patterns in discharge cycles from two confined hydrothermal aquifers and to understand what causes these fluctuations. Our hypothesized controls include effects from earth tides, barometric pressure, seismic activity, and precipitation. To quantify fluctuations in discharge, we continuously monitored flow rates in two streams with inputs that were assumed to come primarily from hydrothermal discharge. Streams influenced heavily by geysers might show unpredictable pulses of water discharge related to geyser activity, and streams influenced heavily by shallow cold water aquifers would likely mask fluctuations caused by changes in hydrothermal discharge.

1.2 Geologic Setting of Yellowstone National Park

The stratigraphy of YNP provides the framework for an extensive and complex hydrothermal system. The Yellowstone Plateau covers an area of about 6,500 km^2 or roughly twice the size of the state of Rhode Island (Fenneman, 1931; Smith, 2000; Christiansen, 2001). Development of the plateau began ~ 100 to 50 million years ago (mya) with the collision of the North American and Pacific Ocean plates forcing uplift of the Rocky Mountains (Fenneman, 1931; Cohee, 1962; Thornbury, 1965). At 50 ma, volcanism started in central Idaho and southwestern Montana (Obradovich, 1992). Eruptions from these events deposited significant layers of andesite lava flows, basalt flows, and airfall ash (Boyd, 1961; Perkins and Nash, 2002). These eruptions were fueled by an upper crustal magma body (Blackwell, 1969; Eaton et al., 1975; Iyer et al., 1981; Lehman et al., 1982; Smith and Braile, 1984; Benz and Smith, 1984; Miller and Smith, 1999; Finn and Morgan, 2002; Husen et al., 2004; Waite et al., 2005; Waite et al., 2005; Farnetani and Samuel, 2005; Yuan and Dueker, 2005) that has produced approximately 142 caldera-forming eruptions as the continental plate moved over a hot spot (Perkins and Nash, 2002). The third most recent caldera-forming eruptions took place ~ 2.5 ma and were the first to occur in the greater YNP area (Obradovich, 1992; Christiansen 2001). Each caldera eruption followed three similar stages. However the magnitude of each caldera eruptive cycle differed significantly. During the first stage in the eruptive cycle an upwelling magma plume blistered and finally fractured the earth's surface (Figure 1A). This was followed by the second phase of the eruptive cycle, which

consisted of an explosive release of welded-ash flows that partially drained the upwelling magma chamber (Figure 1B). Nearly 3300 cubic kilometers of welded-ash were released during the 2.5 ma eruption (Christiansen, 2001). The drained portion of the upwelling magma chamber collapsed and formed a large caldera (Figure 1C). Finally, more lava, mostly rhyolite, flowed out, partially filling the caldera depression (Figure 1.D) (Christiansen, 2001). By comparison, the 2.5 ma caldera eruptive cycle deposited nearly ten thousand times more debris then erupted during the 1980 Mount St. Helens eruption (Fritz, 1985). Volcanic rocks of the 2.5 ma event are the Snake River Butte Rhyolite, the Huckleberry Ridge Tuff, and the Big Bend Ridge Rhyolite (Powers et al., 1958; Christiansen, 2001).

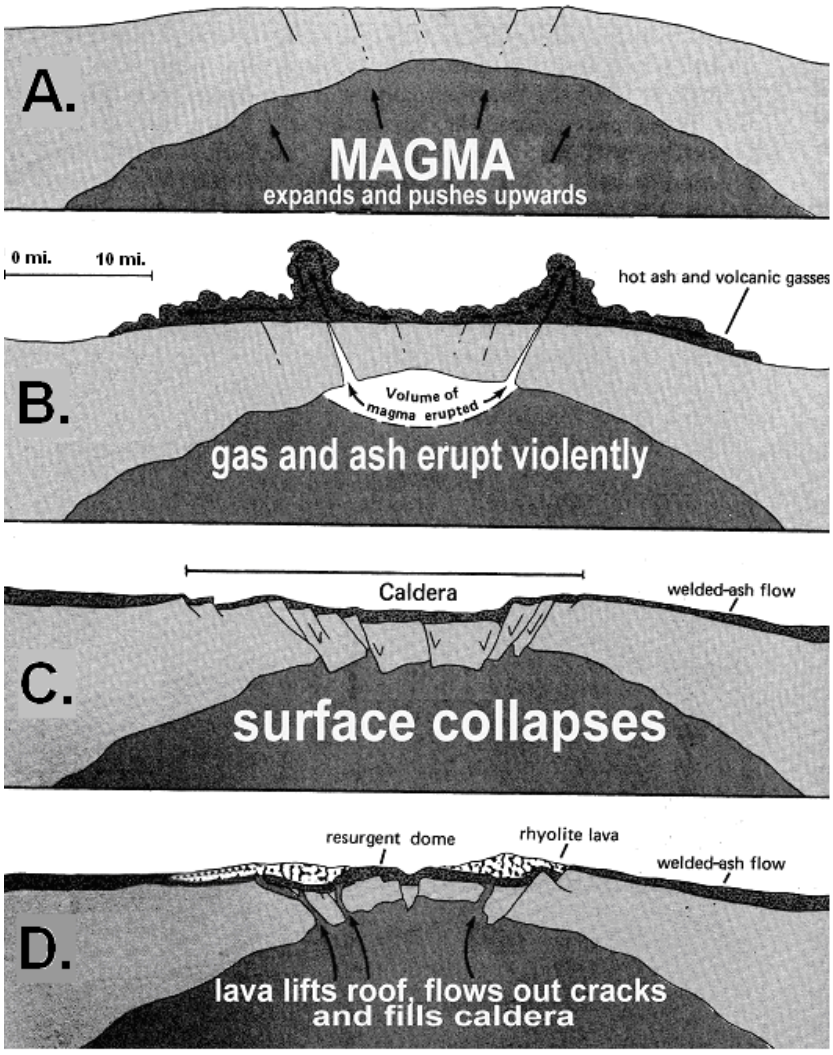

Figure 1. Illustration of sequence of caldera eruptions in Yellowstone National Park. Magma expands and pushes upwards (A.), gas and ash erupt (B.), surface collapses (C.), and finally lava lifts roof and flows out cracks filling the caldera (D.) modified from Fritz, 1985.

Two additional caldera eruptions followed this first eruptive sequence, one at 1.3 ma, and another at ~640 thousand years ago (ka) (Obradovich, 1992, Christiansen, 2001, Lanphere et al., 2002). The second eruptive cycle followed a similar series of eruptions and deposited a total of approximately 280 cubic kilometers of volcanic debris including a welded-ash, rhyolite and small amounts of basalt (Christiansen, 2001). This event was significantly smaller then the first and occurred inside the southwest corner of the 2.5 ma caldera (Figure 2). Layers deposited during this eruption from oldest to youngest include the Mesa Falls Tuff, and Island Park Rhyolite (Powers et al., 1958, Christiansen, 2001, 2002 et al., 1972, Lanphere et al., 2002). Strata from the second caldera event have been dated at ~1.2-1.3 ma using reverse paleomagnetic polarity and K-Ar techniques (Lanphere et al., 2002).

The third and most recent eruptive cycle occurred ~ 640 ka and was located near the center of what is now Yellowstone National Park (Christiansen et al., 1972; Obradovich, 1992, Christiansen, 2001) (Figure 2). This series of eruptions is following a similar pattern to the previous two eruptive cycles and has so far produced a total of about 1000 cubic kilometers of volcanic material (Christiansen, 2001); the current caldera may be in the hydrothermal phase, which is near the end of the caldera-eruption cycle and precedes final basaltic eruptions, or it may still be capable of erupting in another series of the explosive caldera-forming events (Christiansen, 2001). Smith and Brailey (1968)

designated this final phase as stage VII. Layers formed during this third event are, from oldest to youngest, Lewis Canyon and Mount Jackson Rhyolite, Lava Creek Tuff, and Plateau Rhyolite (Powers et al., 1958; Christiansen et al., 1972). The dominant stratigraphic layer, Lava Creek Tuff, has been dated at 640 ka using 40Ar/39Ar isotope age dating (Lanphere, 2002).

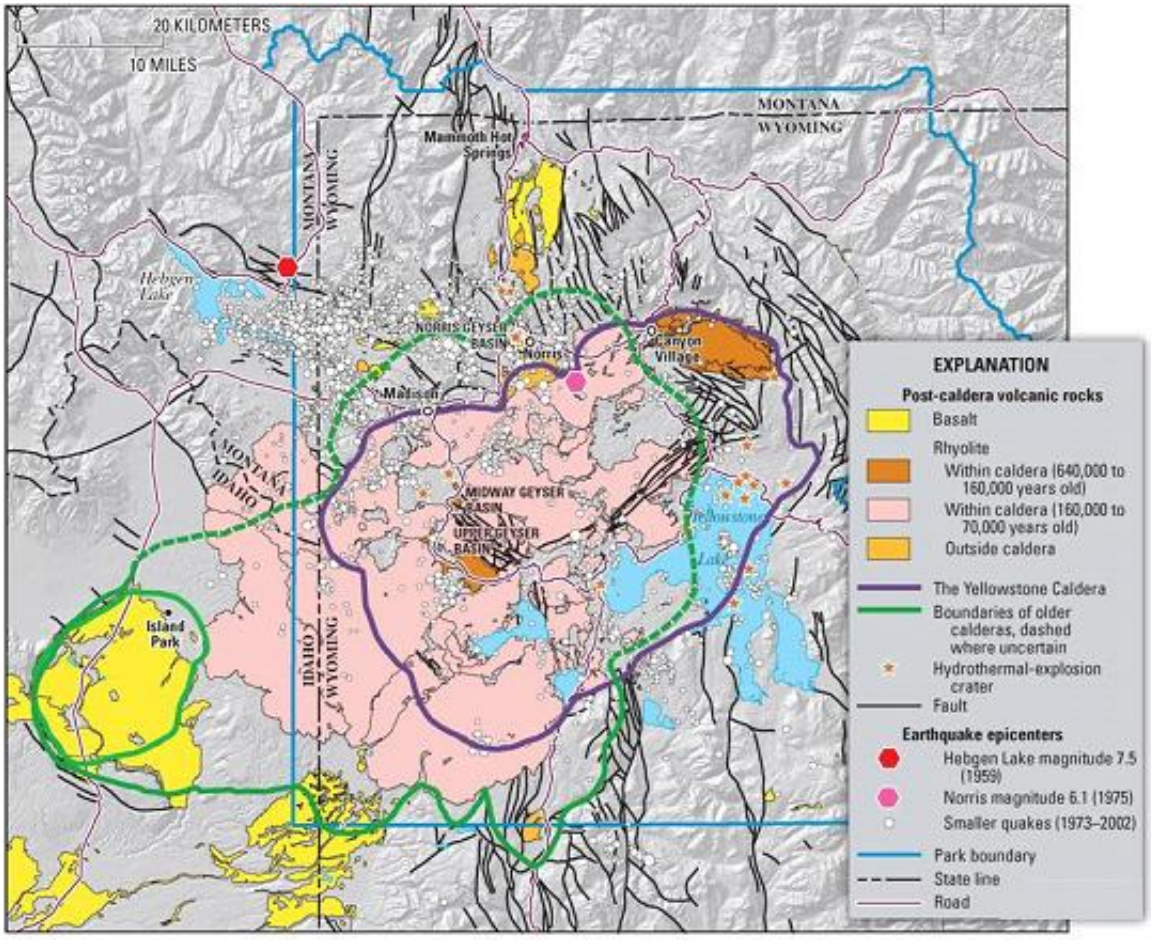

Figure 2. Geology of Yellowstone National Park courtesy of the U.S. Geological Survey (from http://www.usgs.gov, 2007).

Since the last major caldera eruption, there have been two significant periods of glaciation in YNP (Licciardi et al., 2001). The first, the Bull Lake stage, occurred between 160 and 130 ka, and the more recent, Pinedale stage, took place between 70 and 13 ka (Richmond, 1986, Licciardi et al., 2001). At the peak of the last ice age, massive sheets of ice covered most of the park to a depth of thousands of meters thick (Pierce et al., 1991). Glaciers in the YNP area have all been alpine as opposed to continental (Richmond, 1986). Ice cap glaciers developed throughout the park and fed outlet glaciers extending in many directions. Figure 3 shows the extent of glaciation during the Pinedale stage. Arrows indicate direction of ice flow (Baker, 1984).

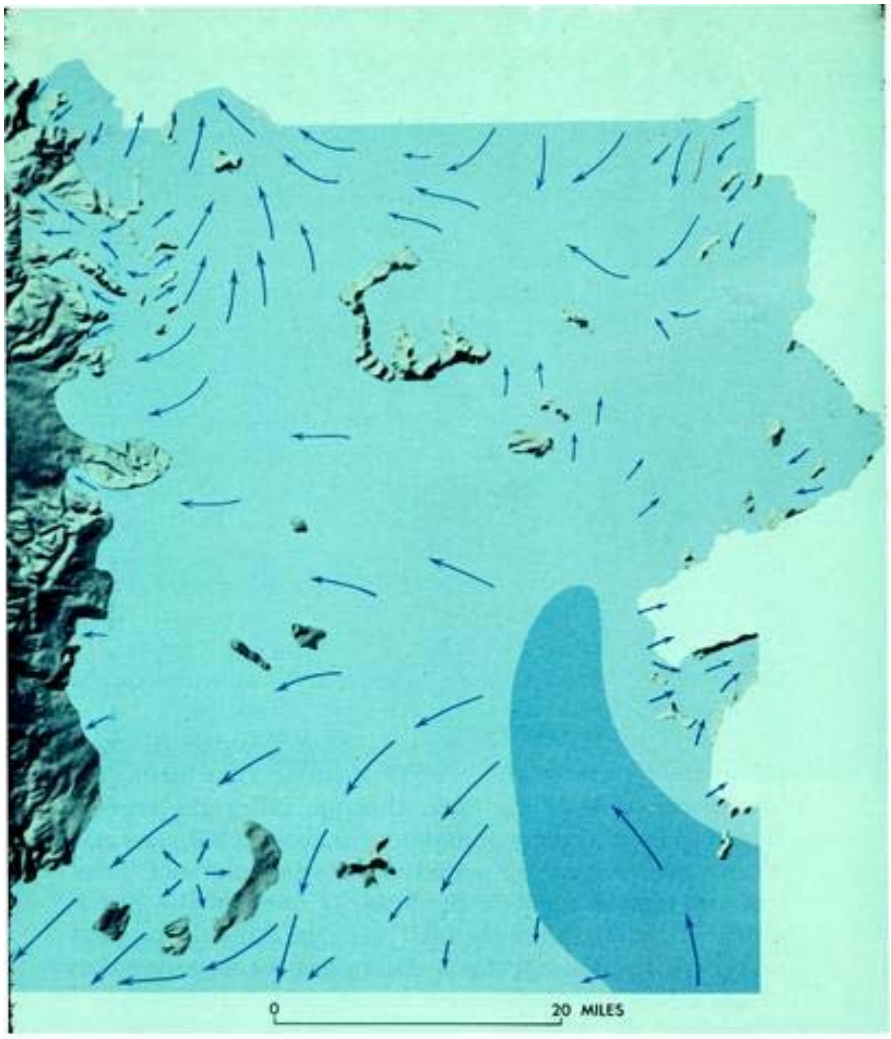

Figure 3.

Extent of Pinedale Glaciation in YNP (from Baker, 1984)

1.3 Hydrothermal Aquifer Structure

Caldera eruptive cycles and recent glaciation define the framework for YNP's unique hydrothermal system. The overall hydrothermal system varies greatly in character throughout the Park in its geochemical composition. A schematic of the structure of the system illustrates the pertinent and common features of hydrothermal systems (Figure 4). Cool meteoric surface water recharges the hydrothermal system through fracture networks (Kharaka, 2002). $^{18}O/^{16}O$ and $^{2}H/^{1}H$ isotopic analysis of thermal and non-thermal waters and snow revealed that recharge for the system originates as meteoric water (Kharaka et al., 1990, 1991). In the deepest layers of the system, hypersaline brine and gas with high concentrations of CO_2 and sulfur compounds permeates fractures just above the semi-molten magma plume at a depth of about 3 to 5 km (Kennedy et al., 1985; Kharaka et al., 1992; Fournier, 1989) (Figure 4.). This brine is a product of fluids being liberated from crystallizing magma (Fournier and Pitt, 1985). The brine does not appear to mix with other portions of the hydrothermal aquifer (Fournier and Pitt, 1985). Overlying the brine is a series of deep, local reservoirs sandwiched between layers of more and less permeable rhyolite (Fournier, 1989) (Figure 4). Water in these local reservoirs reaches temperatures of 350˚C - 430˚C (Fournier, 1989). These aquifers receive some meteoric recharge, and water from these aquifers can mix with higher aquifers as it rises through fracture networks (Fournier, 1989) (Figure 4). Water rises until it reaches highly-fractured rubble layers at the bottom and top of thick, silica-rich rhyolite flows (Fournier, 1989) (Figure 4). Meteoric water also recharges this main aquifer and can reside at this layer for relatively long periods of time at nearly constant

temperature, reaching chemical equilibrium with the surrounding rock (Kharaka et al., 1989; Fournier, 1989). Water in this aquifer ranges in temperature throughout the Park from 180˚C to 350˚C (Fournier, 1989). Some water continues to rise convectively in the system as it is forced into a network of fractures (Fournier, 1989) (Figure 4). The water decompresses as it rises towards the surface. Thermal waters commonly reach the surface where fractures cut across topographic lows, and hydrothermal features tend to also be more common at fault intersections (White et al., 1988). As thermal water moves upward, adiabatic boiling generates a steam phase, which can separate from the liquid phase along different paths through cracks and fissures to the surface (Henley, 1984) (Figure 4.). The steam phase may contain gases including H_2S, which oxidizes to H_2SO_4 when it comes into contact with oxygenated shallow ground water (Henley, 1984). These heated acidic, sulfate-rich waters reach the surface as acidic hot springs and mud pots.

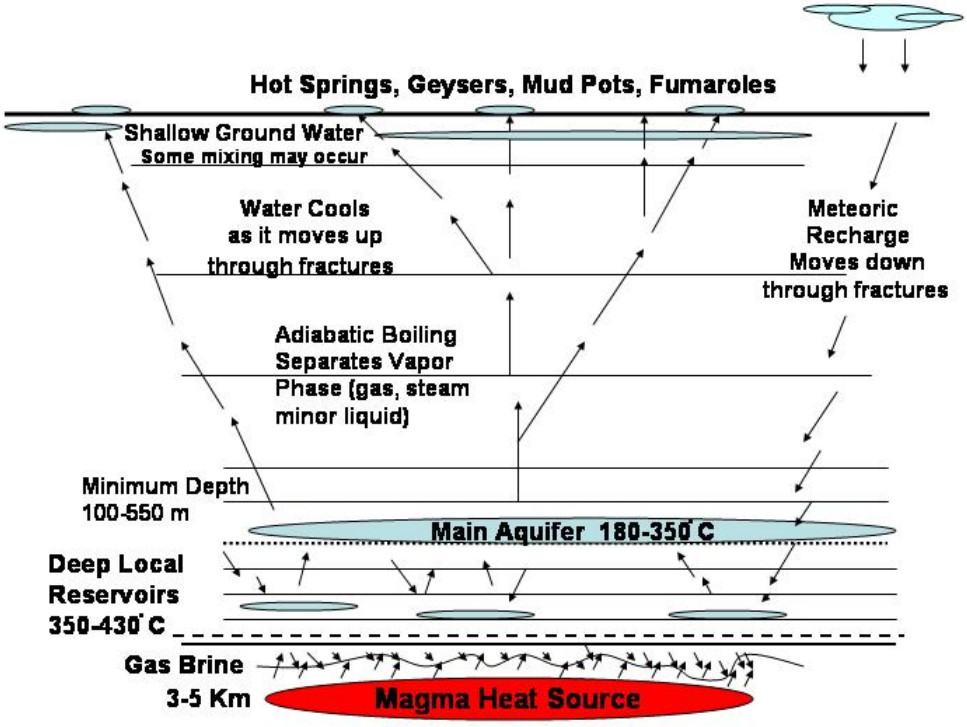

Figure 4: Hypothetical cross-section of the geothermal systems, YNP (created using Henley, 1984, Fournier and Pitt, 1985, White et al., 1988, Fournier, 1989, Kharaka et al., 1989)

1.4 Confined Aquifer Controls

An aquifer is defined as a geologic unit that can store and transmit water at a rate fast enough to be economically viable (Fetter, 2000). A confined aquifer is any aquifer or fully water-saturated earth material found to have a water table above its upper boundary (Fetter, 2000). A confined aquifer is usually pressurized due to the presence of a confining bed at its upper boundary. Because of this pressure, water levels in wells or water escaping through fractures in the confining layers rise to a level higher than the top of the aquifer. This level defines the potentiometric surface (Fetter, 2000). If the potentiometric surface for a given point in an aquifer is above land surface then water in a well or other natural conduit is able to discharge at the surface. In YNP, hot springs and geysers are good examples of water escaping confined aquifers through natural conduits. Interpreting well drillers logs for the local geologic stratigraphy is usually the easiest way to determine if an aquifer is confined. If drillers' logs are absent, interpreting known information about the local geology is the next best option. By knowing the stratigraphy and the permeability of the earth materials, aquifer properties and boundaries can be estimated (Fitts, 2002). In YNP, aquifers exist at more then one depth (Figure 4), and with the exception of the shallow cold-water aquifer, other aquifers are typically located beneath thick layers of low-permeability rhyolite (Fournier, 1989). Water trapped below rhyolite layers can build up immense pressure as it is heated, forcing liquid up through fracture networks (White et al., 1975).

Several factors have been shown to control pressure changes in confined aquifers. In a flowing well or spring, pressure changes in the aquifer translate to fluctuations in discharge at the surface (Fetter, 2000). We can extrapolate from concepts of pressure control in confined aquifers to hypothesize what factors may be controlling pressure changes in thermal aquifers. Factors affecting pressure changes in non-thermal aquifers include earth tides (Robinson, 1939, 1971; Bredehoeft, 1967; Gieske et al., 1985; Hsieh et al., 1987; Fitts, 2002), barometric pressure (Jacob, 1940; Clark, 1967; Pascal, 1973; Rojstaczer, 1988; Spane, 1999; Toll et al., 2007), earthquakes (Vorhis, 1955, 1964; Todd, 1980; Husen et al., 2004), and precipitation (Zarriello, 2001**,** Fleming, 2006).

Earth tides are induced stress and pressure changes that occur as a consequence of the daily revolution of the Earth in the gravitational fields of the Moon and Sun (Kvale, 2006). Generally, tidal effects are most easily observed on large, unbounded water bodies, such as the ocean or the Great Lakes (Kvale, 2003). Tidal forces can cause elastic deformation of solid and liquid earth bodies within the Earth's crust such as volcanic magma chambers and semi-elastic consolidated rock such as fractured limestone or other rock types (Robinson, 1939, 1971; Bredehoeft, 1967; Gieske et al., 1985; Hsieh et al., 1987; Fitts, 2002; Jaggar, 1924; Brown, 1925; Hamilton, 1973; Dzurisin, 1980; Davis, 1981; Berrino et al., 1988, 1991; Fadeli et al., 1991; Jentzsch, 1995). Two theories have been developed to understand tides and tidal processes, the equilibrium theory and the dynamic theory. The equilibrium theory of tides uses universal laws of physics as applied to a water-covered Earth (Kvale, 2006). It explains tides and tidal processes in an idealized Earth completely covered by deep water of uniform depth that is capable of

instantaneously responding to changes in gravitational forces (MacMillan, 1966). The dynamic theory of tides expands on the basic concepts of the equilibrium theory to include harmonic analysis of individual tidal constituents. The movements and angular speeds of the Moon and Sun relative to the Earth can be modeled as a combination of effects of a series of forces (Pugh, 1987). In short, the dynamic theory helps explain complexities of real world ocean tides.

On an idealized Earth, gravitational forces from the Moon and Sun combine with centripetal forces of the rotation of Earth about an Earth-Moon-Sun center of mass and produce oceanic bulges on opposite sides of the Earth (Figure 5A). The rotation of the Earth through each of these bulges produces semidiurnal tides. In the idealized Earth, intensity of tides can vary a number of ways. Spring tides, or maximum high tides and low tides, occur every 14.76 days when the Earth, Moon, and Sun are nearly aligned at a new or full Moon (Figure 5B.). The period of time from one full moon to the next is termed a synodic month and has a period of 29.53 days. Neap tides occur when the Moon and Sun are at right angles relative to the Earth. At this time, gravitational forces from the Moon and Sun oppose each other, in part resulting in smaller then average differences between high and low tides. Because the lunar orbit with the Earth and the Earth's orbit with the Sun are both slightly elliptical, perigee (closest approach to Earth) and apogee (farthest distance from Earth) periods can also have an affect on tidal amplitudes. For the Moon, the period of time perigees is 27.55 days (Figure 5C). During this time there are two spring tides and two neap tides often of unequal magnitudes.

Tidal amplitude is greater when spring tides occur near a time of lunar perigee and apogee.

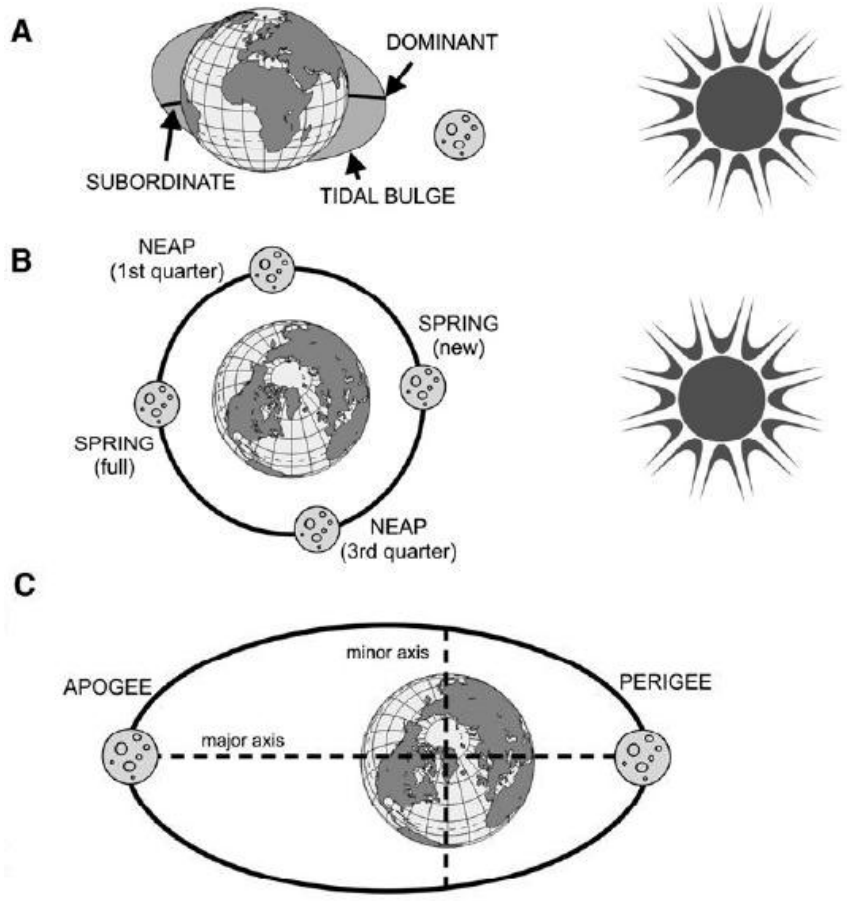

Figure 5. Model of idealized equilibrium theory of tides (modified from Kvale, 2006)

The dynamic tidal theory helps explain complexities of the real world ocean tidal system. By decomposing the harmonic tidal signal of an extended series of hourly tidal height measurements at a given tidal station, individual tidal constituents can be estimated (Ray and Cartwright, 2007). A tidal constituent is the result of gravitational effects from either or both the Sun and Moon at a particular position relative to the solar system. Each tidal constituent is modeled to generate its own tide with associated amplitude, period, and

tidal response time or phase angle (Ray and Cartwright, 2007). Tidal constituents are commonly reported in terms of alphanumeric terms. For example, S_2 symbolizes the principal solar tidal constituent at the 12-hour period. Although there can be over one hundred tidal constituents extracted from harmonic analysis of actual tides, seven represent over 80% of the variability recorded in tidal analyses (Defant, 1961) (Table 1). Each tidal constituent corresponds to its own tidal wave that moves around an amphidromic point. Amphidromic points are areas where the tidal range is almost zero (Kvale, 2006). They are a function of basin geometries and the Coriolis Effect deflecting oceanic currents to the right in the Northern Hemisphere and to the left in the Southern Hemisphere (Kvale, 2006). Tidal potential for any point in an ocean is a result of a series of tidal constituents specific to that location (Ray and Cartwright, 2007). Major tidal cycles are a function of harmonic convergence and divergence of certain tidal constituents (Ray and Cartwright, 2007). Timing for these cycles can be determined by: $[360^{o}/(\sigma_1-\sigma_2)]\ 24^{-1}$ = days where 360^{o} represents one complete rotation of the wave around the amphidromic point, and σ_1 and σ_2 represent the rotational speeds (^{o}/h) of the two tidal constituents of interest (Kvale, 2006) (Table 1).

Tidal constituent	Speed σ (°/h)	Origin	Period in solar hours
M_2	28.9841	Principal lunar	12.42
S_2	30	Principal solar	12
N_2	28.4397	Larger elliptical lunar	12.66
K_2	30.0821	Combined declinational lunar and declinational solar	11.97
K_1	15.0411	Combined declinational lunar and declinational solar	23.93
O_1	13.943	Principal lunar	25.82
P_1	14.9589	Principal solar	24.07

Table 1. Principal tidal constituents from the dynamic tidal theory (from Kvale, 2006).

Synodic neap and springs tides can be generated when the M_2 and S_2 tidal constituents come into phase (every 14.77 days) (Ray and Cartwright, 2007). Diurnal inequalities exist because O_1 and M_2 are in phase only once a day. If either O_1 is greatly diminished or M_2 is very small, diurnal inequalities will be very small (Ray and Cartwright, 2007). Table 2 and Figure 6 show interesting ranges of tidal stations and associated constituents (Kvale, 2006). Shown are stations from Do Son, Vietnam; Manila, Philippines; San Francisco, USA; and Immingham, England. Do Son and Manila are dominated by K_1 and O_1 and as a result, their tides are dominantly diurnal. In San Francisco, M_2, K_1 and O_1 dominate tides while S_2 has relatively little impact resulting in a predominately semidiurnal tide. At Immingham tides are dominated by the S_2 constituent resulting in a purely semidiurnal tide.

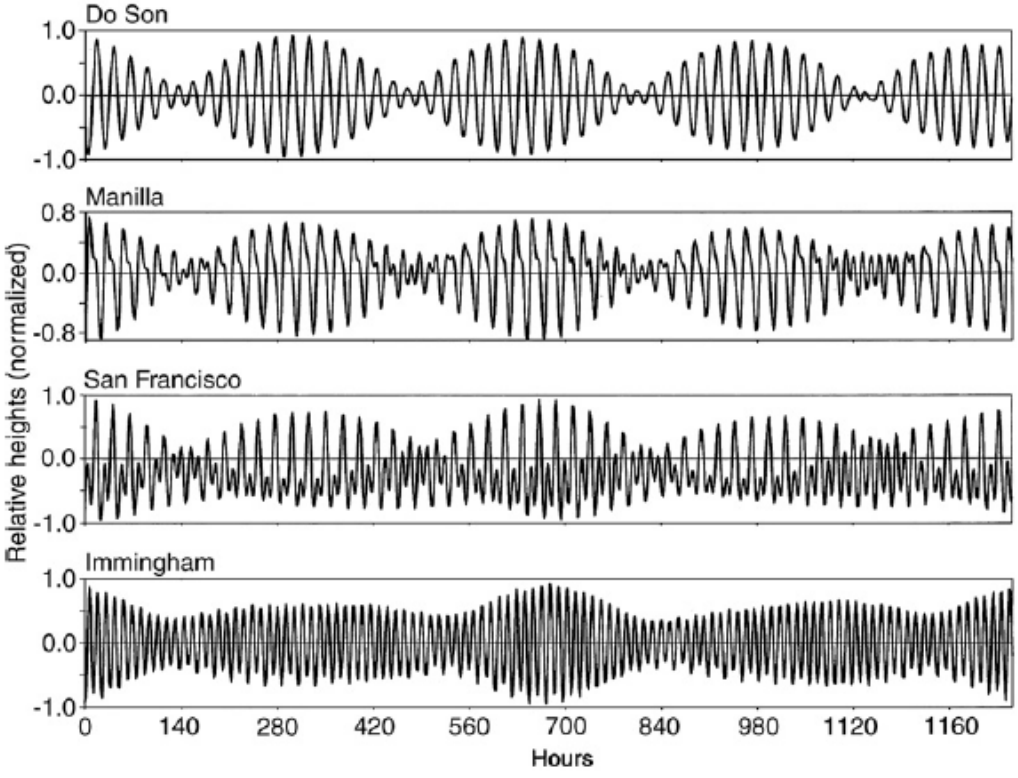

Figure 6. Tidal curves from Do Son, Vietnam, Manila, Philippines, San Francisco, USA Immingham, England (from Kvale, 2006).

Tidal constituent	Do Son	Manila	San Francisco	Immingham
	Amp.	Amp.	Amp.	Amp.
M_2	4.4	20.3	54.2	223.2
S_2	3.0	6.8	12.3	72.8
N_2	0.8	3.8	11.5	44.9
K_2	1.0	2.1	3.7	18.3
K_1	72.0	29.7	37.0	14.6
O_1	70.0	28.3	23.0	16.4
P_1	24.0	9.3	11.5	6.4

Table 2. Dominant tidal constituents and their amplitudes for 4 tidal stations (from Kvale, 2006).

The dynamic tidal theory explains real world variability in ocean tides. However the effects of earth tides on solid and liquid earth bodies within the Earth's crust are better explained by the traditional equilibrium theory (Arabelos et al., 2003). If tides had an affect on these earth bodies, expected timing and magnitude would follow those of the equilibrium theory (Arabelos et al., 2003). Figure 7 shows well water level responding to influence from earth tides (Kaczmarek, 2007). The well penetrates a confined aquifer in central Montana (Kaczmarek, 2007). The tidal data shown in the figure were collected at six-minute intervals at a tidal gauging station of similar latitude in Seattle, Washington and then was corrected to Mountain Time Zone (Kaczmarek, 2007). Earth tides cause pressure changes in semi-elastic solid bodies of some, but not all, confined aquifers (Bredehoeft, 1967; Gieske et al., 1985; Hsieh et al., 1987; Fitts, 2002). These pressure changes can cause fluctuations in well water levels. Rinehart (1972) hypothesized that earth tides may cause pressure changes in hydrothermal aquifers as well. These pressure changes would result in fluctuations in discharge at the surface.

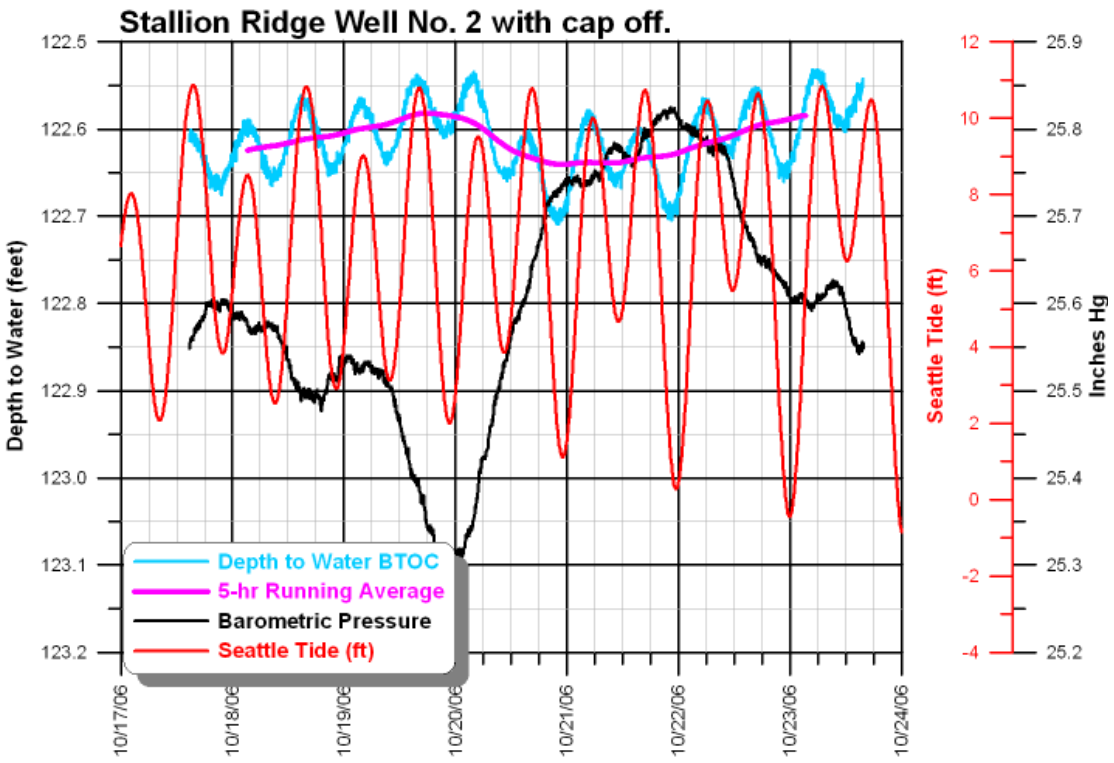

Figure 7. Well with earth tide effect in central Montana. (Kaczmarek, direct correspondence 2007).

Additionally, water-level fluctuations inversely correspond to barometric pressure changes in wells penetrating confined aquifers (Jacob, 1940; Clark, 1967; Pascal, 1973; Rojstaczer, 1988; Spane, 1999; Rush et al., 2002; Toll et al., 2007); as barometric pressure increases, water levels in observation wells decrease. This inverse relationship is observed when water levels are measured while the well cap is off showing the effect of barometric pressure directly on the water surface (Kaczmarek, 2007). With the well cap on, water levels can be measured with a downhole pressure transducer. Because the water surface in the well is isolated from the direct effect of atmospheric pressure, the pressure transducer may record water levels that directly relate to barometric pressure because it will show the effects of atmospheric pressure loading on the aquifer itself rather than the effects on well water-surface (Kaczmarek, 2007). The effect of

barometric pressure on confined wells is apparent in Figure 8. As atmospheric pressure drops, a corresponding drop in water level is observed. The change in water level is due to elastic deformation of the aquifer in response to barometric pressure changes. Figure 8 shows that as barometric pressure changes, hydrostatic pressure and compressive stress on the aquifer also change.

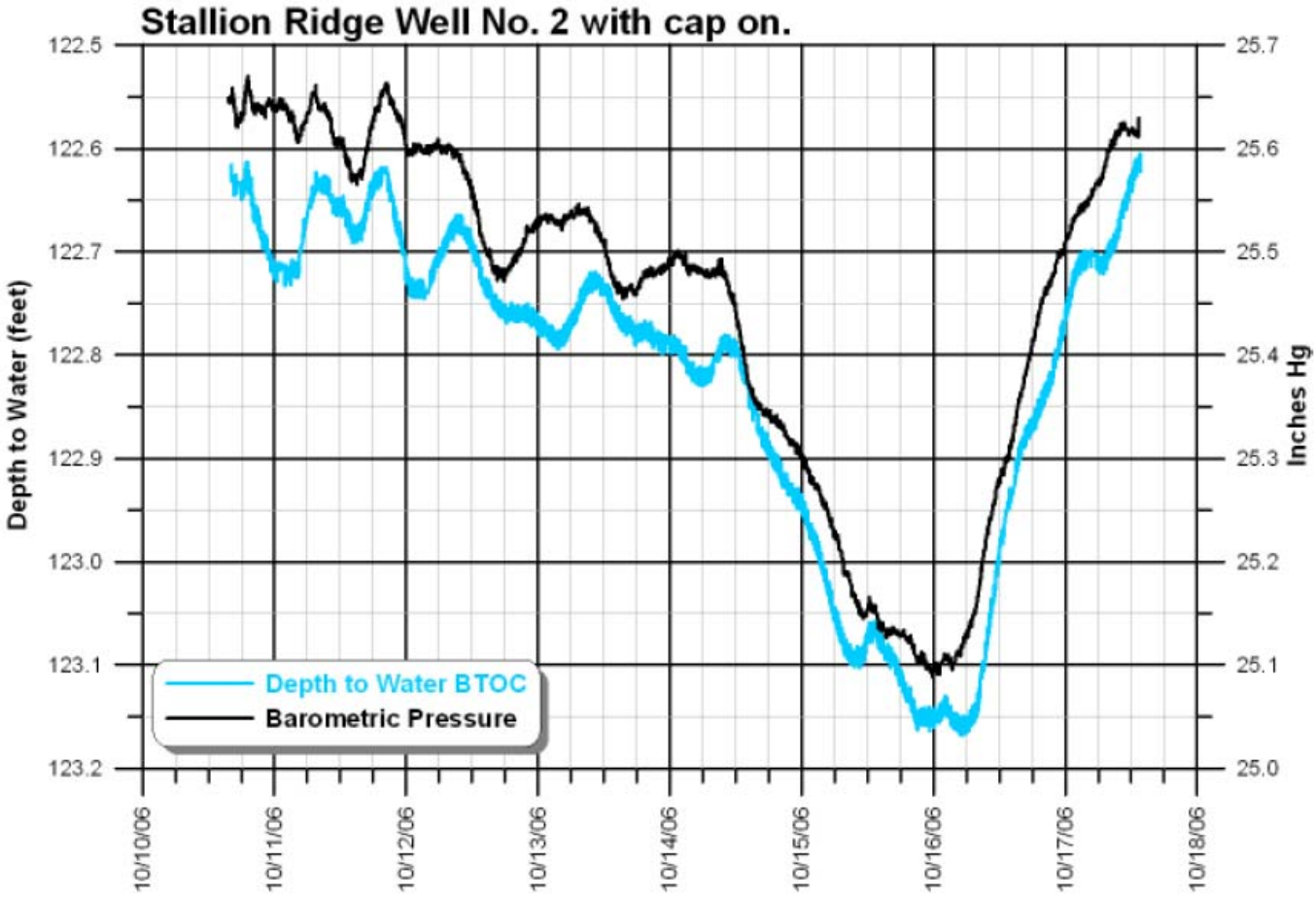

Figure 8. Example of a highly barometric efficient aquifer. (Kaczmarek direct correspondence, 2007).

Barometric efficiency of an aquifer is the ratio of change of hydraulic head in an aquifer to the change in barometric pressure. It can be calculated as $B = \gamma \, \delta h / \delta p_a$ where B is barometric efficiency, γ is the specific weight of water (density multiplied gravitational

acceleration, at 5°C the specific weight of water on Earth is 9807 Nm^{-3}), δh is the change in piezometric level, and δp_a is the change in atmospheric pressure. Most aquifers showing a response to barometric pressure will have barometric efficiency values ranging from 20% to 70%, higher efficiencies are observed in aquifers with a greater degree of barometric pressure influence. Atmospheric pressure forces (dp_a) load the upper aquifer confining layer, increasing pore water pressure (dp_w) and compressive stress of the aquifer (ds_c) (Figure 9).

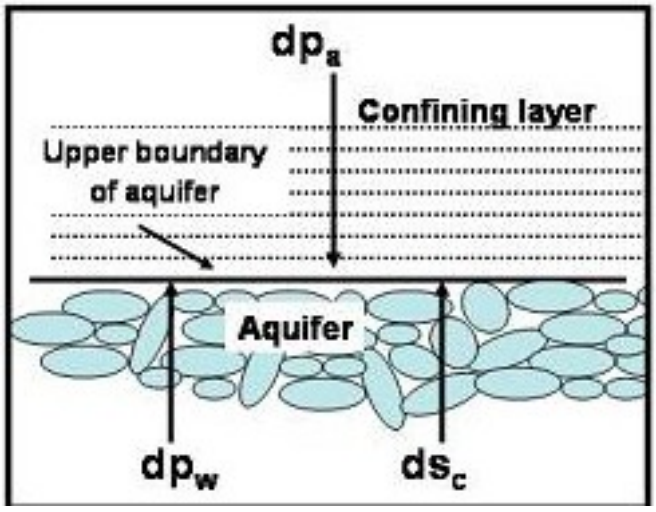

Figure 9. Distribution of forces at the upper boundary of confined aquifer (from Fitts, 2002).

Earthquakes have also been shown to effect water-level fluctuations in wells penetrating confined aquifers (Vorhis, 1955, 1964). Compression and expansion of semi-elastic confined aquifers caused by the passage of primary seismic waves produce water-level fluctuations in wells (Todd, 1980). Longevity of effects due to earthquakes are generally short lived depending on magnitude, but usually last less then 20 minutes (Igarashi, 1991). At best, discrete data recorders may only record one or two noticeable water-level changes. Continuous data recorders log the complete effect of earthquakes. Little is

known about the correspondence of earthquake magnitude and location and the corresponding effect on water levels in aquifers. Earthquakes can cause dramatic water-level changes in wells, but to the influences are not related to location and magnitude of the epicenter in a predictable manner (Todd, 1980). For example, on 27 March 27 1964, a large earthquake (8.4 to 8.8 on the Richter scale) near Anchorage, Alaska caused well water fluctuations around the world. However, the most dramatic effect was observed in South Dakota where water-level changes exceeding 7.0 m in an observation well tapping a confined aquifer (Vorhis, 1967).

Precipitation can affect aquifers several ways. Most aquifers depend on precipitation for recharge, which could lead to increases in discharge. However, a commonly overlooked effect of precipitation is direct system loading (Sophocleous et al., 2004). Significant weight can be added to the system from a large precipitation event. Similar to effects observed from earth tides and barometric pressure, precipitation loading to the aquifer may increase pore-water pressure and compressive stress of the aquifer, resulting in increased discharge in flowing springs.

1.5 Hydrothermal Aquifers

Hydrothermal aquifers exist at more than one level in the overall hydrothermal system in YNP (Truesdell and Fournier, 1976, White et al., 1988, Fournier, 1989) Truesdell and Fournier (1976) suggest a large hydrothermal aquifer may feed local shallow hydrothermal aquifers. The depth of this larger aquifer may lie is approximately 3 ±1 km

and is constrained by the volcanic stratigraphy of the Yellowstone Caldera (Truesdell and Fournier, 1976). Thermal aquifers in the hydrothermal system commonly occur in highly fractured contact zones between different volcanic strata (Fournier, 1989). Low permeability strata providing confining layers (Fournier, 1989). Heat from a relatively shallow magma source heats the aquifer water further pressurizing the system with expanding heat energy (White et al., 1988). Water rises through fracture networks and discharges at the surface.

Many investigations on the chemistry and hydrology of geothermal waters and gasses of YNP have taken place (e.g. Gooch and Whitfield, 1888, Allen and Day (1935), Rowe et al. (1973), Thompson et al. (1975), Thompson and Yadaw (1979), Fournier (1989), Norton et al., (1989), Fournier et al. (1994), Thompson and Demonge (1996), Friedman and Norton (2000)). Recently, Ingebretson et al. (2001) reported temporal variations in hydrothermal discharge at several sites in the western United States including sites in YNP. They collected discharge data for several years and used these data along with data collected by others (Allen and Day, 1935, Waring, 1965, Norton and Friedman, 1991) to find frequencies of hydrothermal discharge and heat flux at each site. Many sites showed strong seasonal frequencies, but few showed long-term trends, and none showed decadal-scale trends. They analyzed discharge fluctuations using daily average values reported at USGS gaging stations and they also analyzed heat discharge variations using Cl concentrations. Data for the Ingebretson et al. (2001) study were compiled from many sources (Allen and Day, 1935, Waring, 1965, Norton and Friedman, 1991). Sampling frequency for Cl concentrations was weekly, limiting the analysis to seasonal or longer

periods. Responses to major regional tectonic events, such as earthquakes or inflation/deflation cycles, were analyzed by visually analyzing Cl-flux data to check for anomalies before and after a major event. From this analysis, they determined that relative steadiness of the Cl flux in the major YNP streams since 1966 shows that the overall hydrothermal system shows little to no response from major regional tectonic events.

A study by Husen et al. (2004) suggested a 2002 Alaskan earthquake (magnitude 7.9 on the Richter scale) caused changes in YNP geyser eruption timing and frequency. They suggested that dynamic stress on the hydrothermal system may induce changes in permeability of aquifer material. The dynamic system-wide stress caused by the passage of surface waves from the Denali earthquake opened existing fractures that were previously obstructed with mineral precipitates thereby changing the geyser activity. They also suggested that redistribution of hydrothermal fluids and locally greater pore pressures trigged several smaller magnitude local earthquakes further propagating the effects on the local hydrothermal system. In their study, they monitored eruption times of 22 geysers by placing temperature sensors in runoff channels. Of the 22 monitored geysers, eight displayed statistically significant changes in their eruption timing

Variations in geyser eruptive cycles have been suggested to be influenced by seismic activity, earth tides, and/or barometric pressure changes (White, 1967; Rinehart, 1972; Marler and White, 1977; Hutchinson, 1985; Silver and Vallette-Silver, 1992; Streepey, 1996; Ingebritsen et al., 1996). However, a recent study by Ingebritsen et al. (2001

showed that changes in geyser eruption timing are much less sensitive to elastic deformation than previously hypothesized. In their study of geysers in the upper geyser basin of YNP, Ingebritsen et al. (2001) found no identifiable influences of earth tides or seismicity, and only minor influences from barometric-pressure changes of 5 mBars (500 Pa) or greater. Using a computer program called HYDROTHERM, they developed multiphase geothermal-simulation models to solve finite-difference approximations. By simulating different aspects of geyser systems, they were able to reproduce observed changes in eruption cycles. As an example, by altering conduit area and holding basal heat input constant, they were able to simulate a given change in eruption timing. They suggested that variations in geyser periodicity may be governed by the internal dynamics of geysers rather than external influences. In their study, they found that variations in eruption interval were significantly influenced by neighboring and distant geysers. Every geyser monitored was influenced by at least one other geyser. They suggested that these relationships indicate that the reservoir(s) supplying water to the geysers are generally connected by highly permeable pathways.

2.0 Description of Study Site

Streams dominantly fed by hot springs were selected for study. Streams influenced heavily by shallow non-thermal aquifers were not selected because they would not provide an accurate measure of hydrothermal discharge. Rabbit Creek and White Creek are two streams dominantly recharged by hot springs in Yellowstone National Park (Figure 10). Discharge data were also analyzed for Tantalus Creek, which drains the Norris Geyser Basin, Yellowstone National Park (Figure 10) even though the stream does have some geysers in its drainage. Tantalus Creek is composed entirely of thermal discharge from the Norris Geyser Basin.

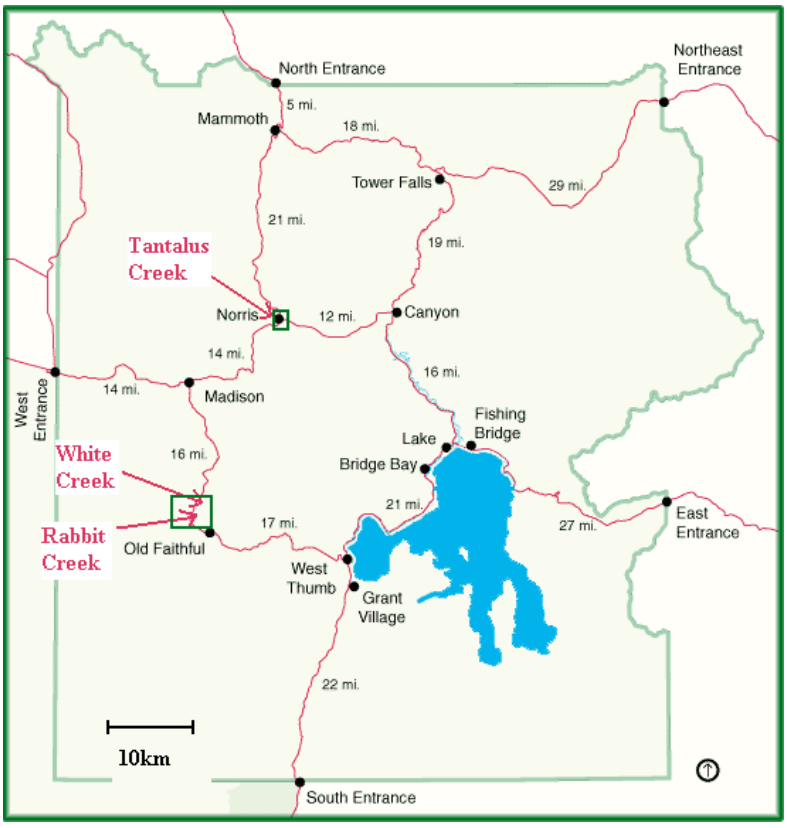

Figure 10. Yellowstone National Park Site Map (NPS, 2006)

2.1 Rabbit Creek

Rabbit Creek (UTM 44.516610° -110.819469°), approximately 6.3 km north of the Old Faithful Geyser Basin in the Upper Geyser Basin of YNP, drains a small basin of approximately 3.5 km^2 (Figure 11). The basin is roughly 2,225 m (7,300 ft) above sea level. Water input to Rabbit Creek comes primarily from discharging hot springs draining one or more hydrothermal aquifers. Four hot spring clusters occur in the basin. The western and central clusters are aligned east-west, while the other two clusters are aligned northwest-southeast (Figure 12). In total, Rabbit Creek flows for approximately 2 km from scattered hot springs sources to the confluence with the Firehole River in a general east west direction. The study site for Rabbit Creek was located approximately 1.5 km upstream from the confluence (Figures 12).

The Rabbit Creek basin lies within the most recent Yellowstone Caldera (caldera III) which in this area overlaps caldera I. A research drill hole, Y-5, (1967) was drilled in the southwest portion of the basin to a depth of 166 m (White et al., 1975; Keith et al., 1978) (Figures 11, 12). Glacial deposits of approximately five meters consisting of sand, gravel and silica precipitates, cover an extensive volcanic stratigraphy (Figure 13). Volcanic layers comprising the youngest breccia layer are encountered at depths between 5 and 10 m. Underlying the volcanic breccia, the Lava Creek Tuff extends from 10 m to below the deepest drilled depth of 166 m. The Lava Creek Tuff is densely-welded vitrified tuff. Hydrothermal fluid was encountered throughout drilling. However an abrupt rise in pressure was encountered at 74 m, which was interpreted by White et al.

(1975), as the presence of a major aquifer at this depth. Water pressure measured throughout drilling placed the static water level for the aquifer well above ground level, meaning water is confined and pressurized confirming that the aquifer is confined (White et al., 1975).

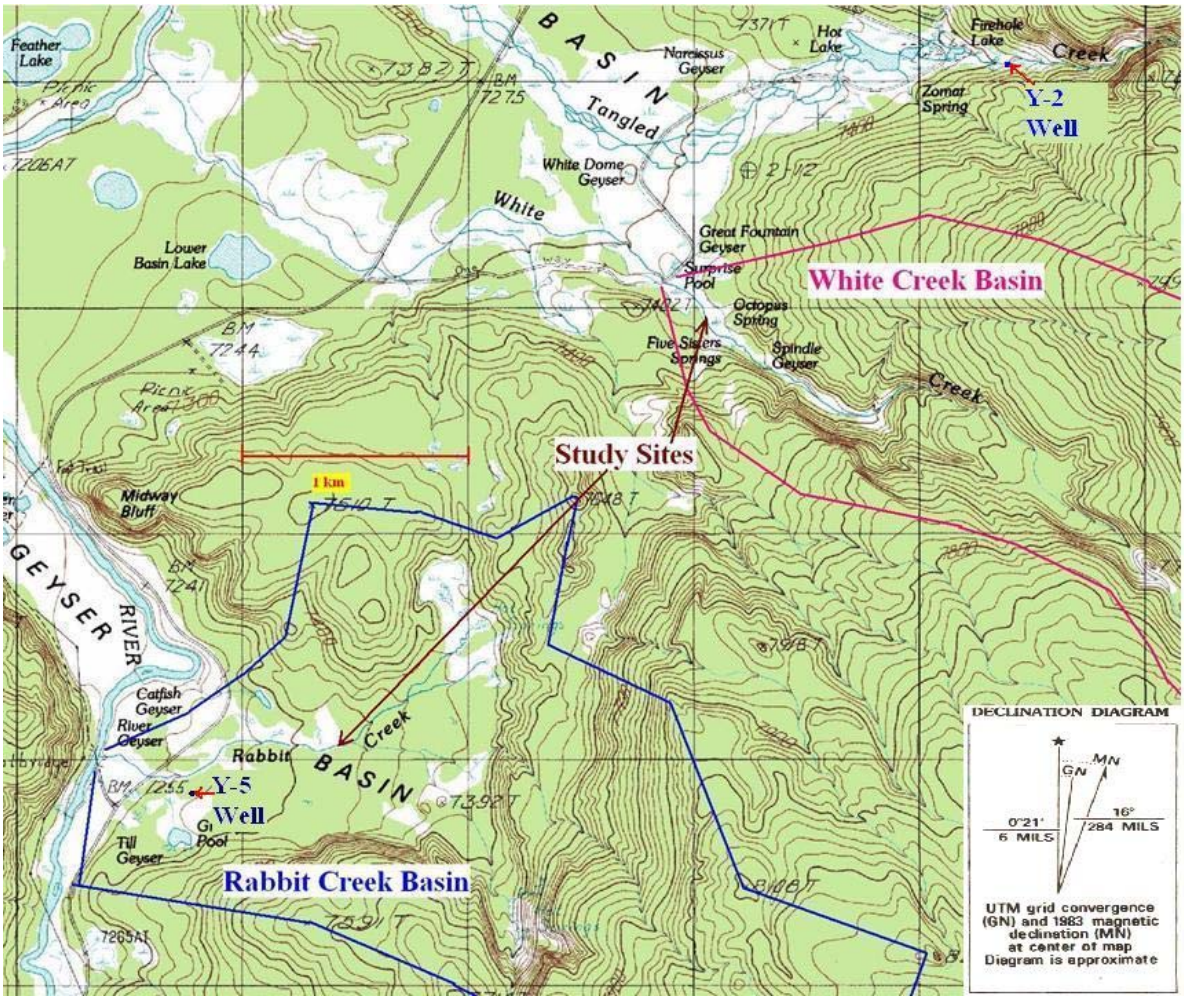

Figure 11. White Creek and Rabbit Creek with location of research well Y-2 and Y-5 (NPS, 1998).

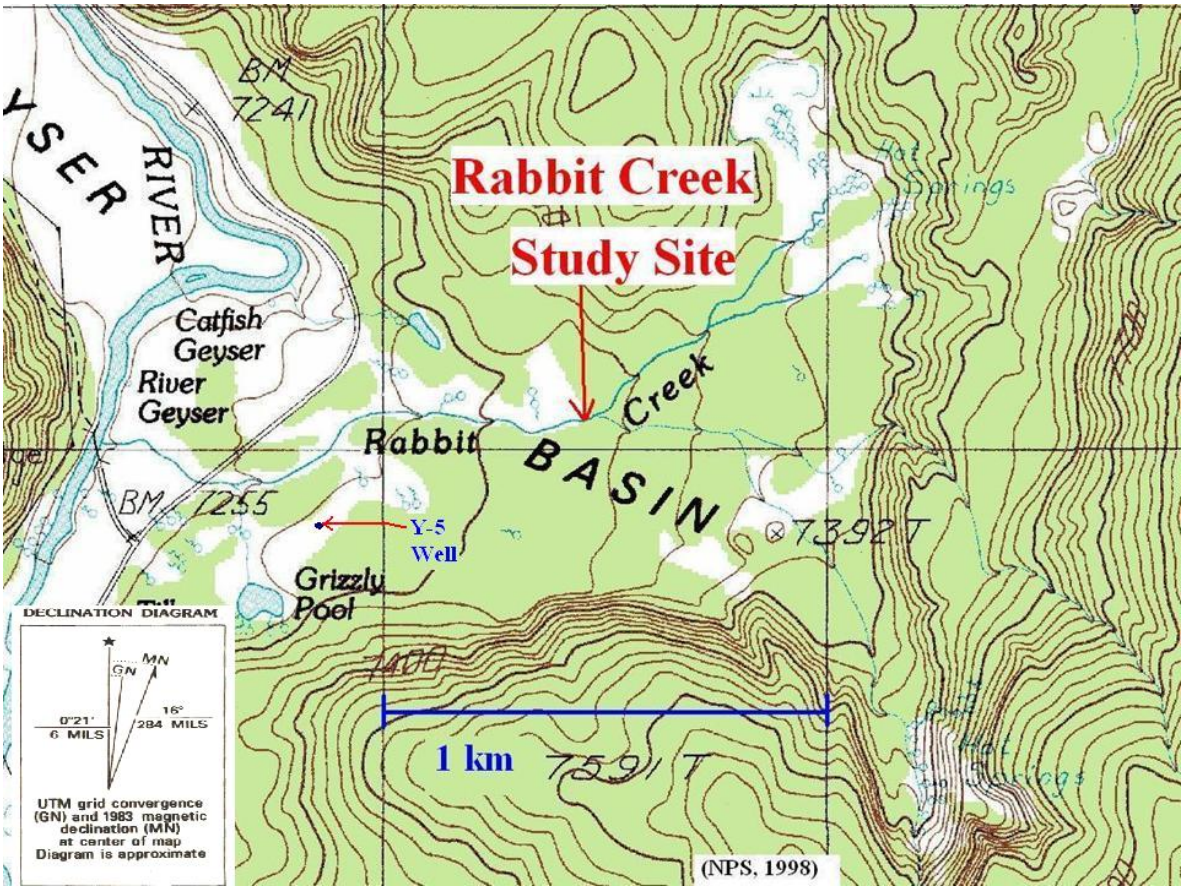

Figure 12. Rabbit Creek Basin withlocation of research well Y-5 (NPS, 1998).

Figure 13. Stratigraphy of Research hole Y-5 and Y-2. (White et al., 1975)

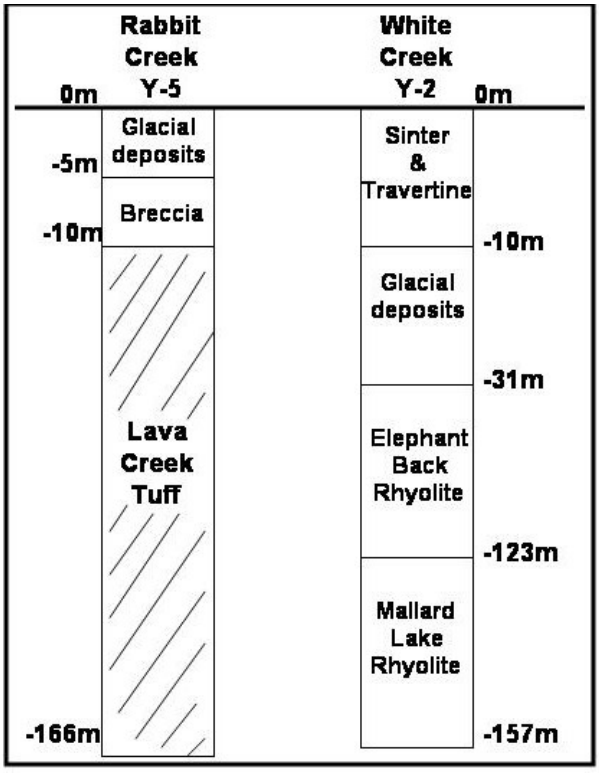

2.2 White Creek

White Creek (UTM 44.534139°, -110.799134°) is located in the Lower Geyser Basin of YNP and is approximately 2.5 km north-northeast of Rabbit Creek (Figure 11). White Creek drains a basin that is roughly 2,225 m (7,300 ft) asl (Figure 14). The basin is approximately 7 km^2 and is longer then it is wide (Figure 14). The primary source input is hot springs discharge, although there is a small but unquantified cold-water input above the highest hot spring that mixes with the thermal water (Gibson, 1999). In total, White Creek flows for approximately 4.8 km from the source to the confluence with the Firehole River. The study site for White Creek was located approximately 240 m upstream from Firehole Lake Drive (Figure 14).

Research drill hole, Y-2 (1967) is located near Hot Lake, a small hot lake approximately 1.25 km to the northeast of White Creek (Bargar and Beeson, 1980) and is the closest well to White Creek (Figure 11). Although it is 1.25 km to the northeast, it is the nearest location of known stratigraphy as to interpret what may exist beneath White Creek. The well was drilled to a depth of 157.4 m and plugged with cement and abandoned shortly thereafter (Figure 14). The upper 10.2 m comprises siliceous-sinter interbedded with thin layers of travertine. Deposits from the Pinedale Glaciation are observed from 10.2 to 31.7 m (Waldrop and Pierce, 1975). Rounded clasts of volcanic debris are included in the glacial deposits (Bargar and Beeson, 1981). Volcanic rhyolite from the Elephant Back flow dominated between 31.7 and 122.8 m (Christiansen and Blank, 1974; White et al., 1975). Mallard Lake (Third Caldera Cycle) rhyolite occurred between 122.8 and

157.4 m at the bottom of the borehole (White et al., 1975). The deepest rocks were dated at 150 ka using the K-Ar dating technique (Obradovich and Christiansen, USGS, unpub. data 1973).

While drilling, water was encountered at a depth of one meter, however hot water was not encountered until approximately 40.8 m in Y-2 (White et al., 1975), and a distinct rise in water pressure occurred at 107 m. White et al. (1975) speculated that this hot water is likely just up-flowing thermal water rising through fractures from a larger confined aquifer but did not assign this to a confined hydrothermal aquifer because water pressure of the aquifer was assumed to be much greater then what was encountered during drilling. However the occurrence of static water levels of 20 m above ground surface from this over-pressured hot water suggests a confined aquifer.

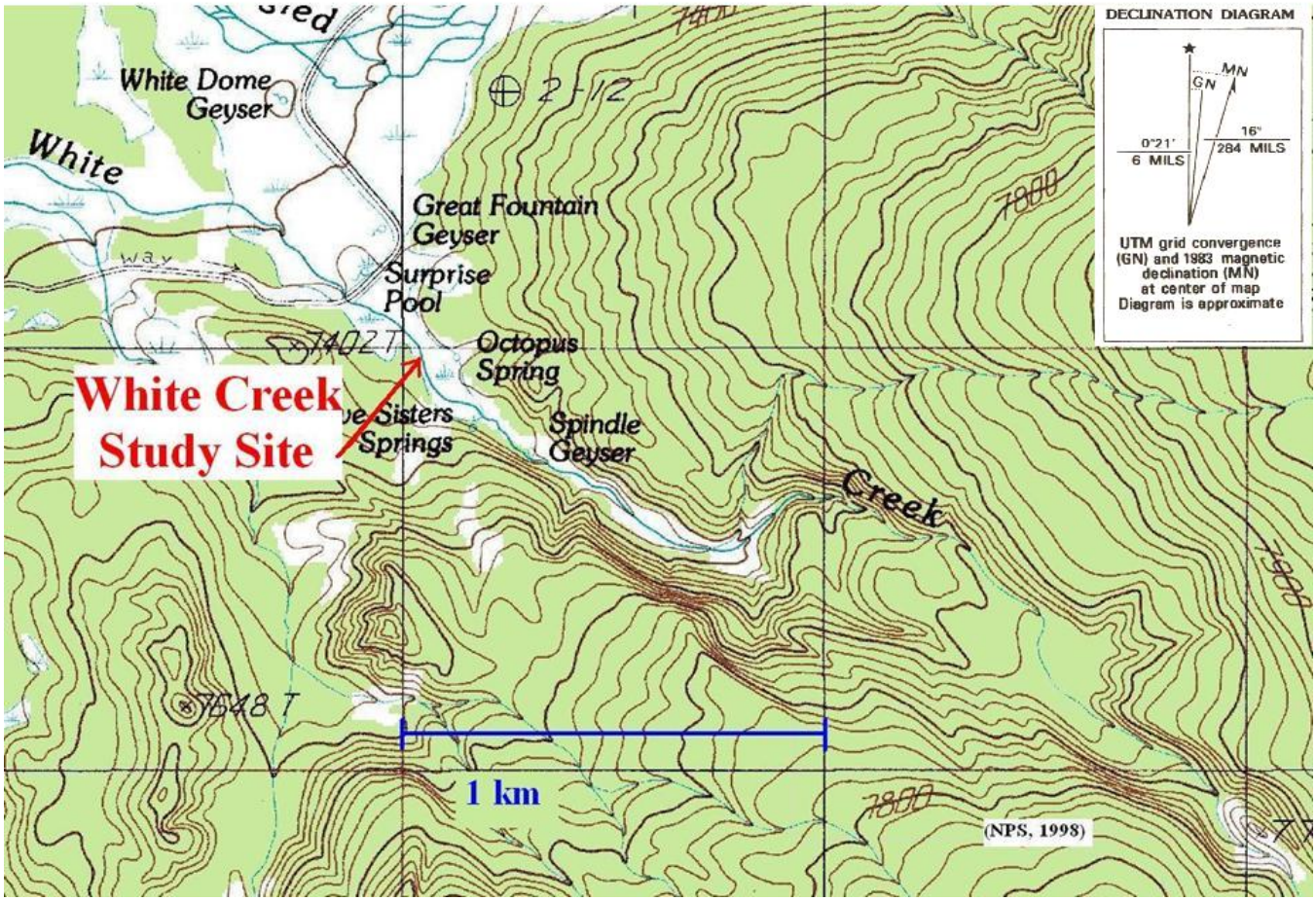

Figure 14. White Creek Basin (NPS, 1998)

2.3 Tantalus Creek

Tantalus Creek (UTM 44.733044°, -110.713617°) is hydrothermal in origin and drains Norris Geyser Basin, which is approximately 3.34 square kilometers (1.29 square miles) at an elevation of 2,273 m (7,460 feet) asl (White et al., 1988) (Figure 10,15). The stream is continuously monitored by a gaged weir box located about 100 m above the streams confluence with the Gibbon River. Data (gage height, discharge, precipitation, and water temperature) are available on the USGS website (http://waterdata.usgs.gov/nwis/uv?06036940).

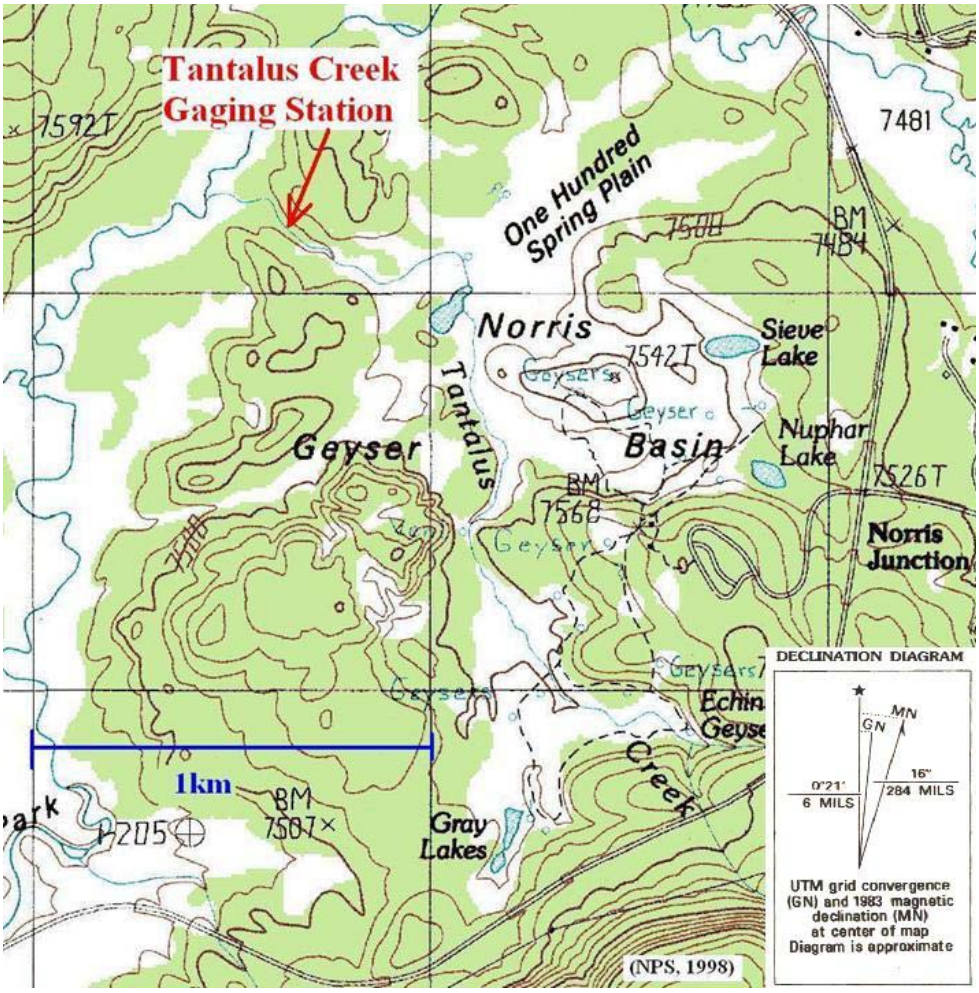

Figure 15. Norris Geyser Basin and Tantalus Creek USGS Gaging Station (NPS, 1998).

Norris Geyser Basin is located at the intersection of several large faults, which produce numerous thermal features (White et al., 1988) (Figure 2.). One major fault runs south from the Mammoth Hot Springs area and crosses another running from the Hebgen Lake area (White et al., 1988). This major fault intersection further adds to the area's hydrothermal potential by creating a complex fracture network (White et al., 1988). The waters of Norris Geyser Basin are alkaline chloride-type waters with high concentrations of Na and K (Table 3.) (White et al., 1975, White et al., 1988, Fournier, 1989), and analysis of data suggests the hydrothermal reservoir to be approximately 300°C (Kharaka et al., 1990, 1991).

White et al. (1988) suggest mineral precipitates in the geyser basin (montmorillonite and siliceous-sinter) are formed from near neutral pH waters with high concentrations of Cl and quartz (SiO_2).

Two research wells were drilled in Norris geyser basin; Y-9, and Y-12 drilled between 1967-68 (Figure 16). These wells followed the Carnegie wells drilled between 1929-1930 (drilled by Allen, Day and Fenner in 1929-1930 (1935)).

Norris Geyser Basin Geochemistry

Location	Porcelain Terrace	Cinder Pool	Echinus Geyser
Temp (°C)	93.5	92	93
pH	-	3.57	3.2
SiO2	654	329	278
Al	0.06	-	0.6
Ca	2.12	6.3	4.9
Mg	0.03	0.12	0.52
Na	404	346	166
K	81	81	50
Li	5.8	3.9	0.7
HCO3	47	0	0
SO4	31	147	337
Cl	669	569	108
F	5.8	6	5.6
B	9.9	8	3

Table 3. Norris Geyser Basin Geochemistry (Fourier, 1989).

Hole Y-9 was located in the basin in hopes of finding the hottest water in the Park by drilling through the thick Lava Creek Tuff. However, after drilling 250 m, there was no evidence that they were even half way through the unit so drilling ceased (White et al., 1975). Upwelling hydrothermal fluids prevented delineation of aquifer boundaries. Y-12 was completed at 330 m, and encountered similar units to those encountered in Y-9. At a depth of 330 m, 294 m of Lava Creek Tuff had been drilled with no sign of nearing the bottom contact of the unit. Highly permeable ground interpreted to be the hydrothermal aquifer was expected at the base of the Lava Creek contact. However the potential of uncontrollable fluid pressure forced cessation of drilling. Static water levels were 75 m above land surface (White et al., 1975) indicating the presence of an over-pressured and possibly confined aquifer.

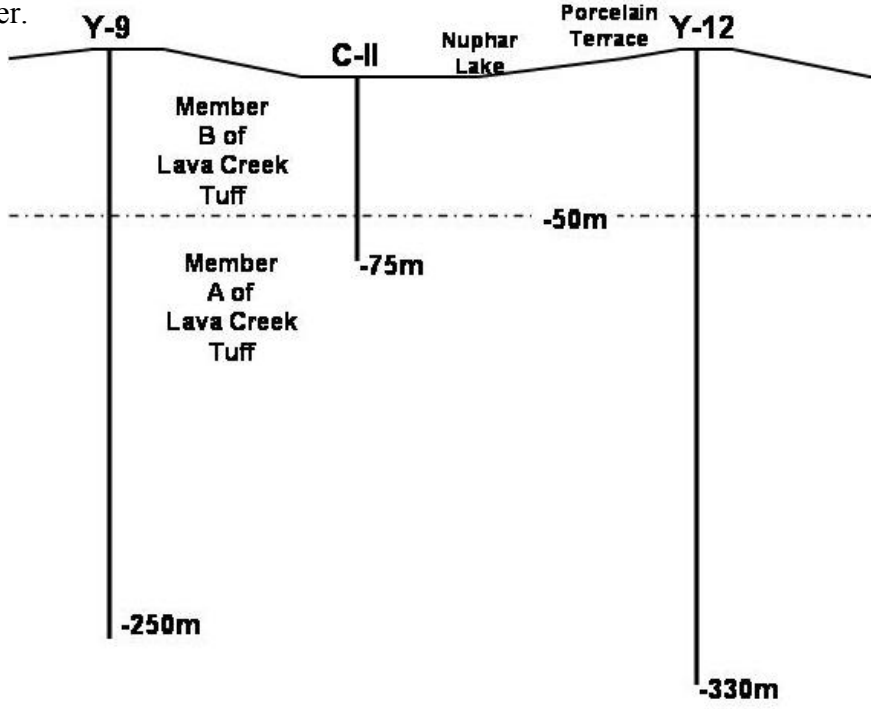

Figure 16. Research holes Y-9, C-11, Y-12 at Norris Geyser Basin (White et al., 1975).

3.0 Methods

Field work for this study was performed between August, 2006 and November, 2006. Stream water velocity and depth were measured using a discrete sampling recorder to estimate discharge and compared with discrete measurements at the time of deployment. Water temperature and GPS locations were taken during deployment. Additional information was provided by permanent U. S. Geological Survey (USGS) weir box gaging stations (http://waterdata.usgs.gov/nwis/uv?06036940), National Oceanic and Atmospheric Administration (NOAA) weather station (http://www4.ncdc.noaa.gov/cgi-win/wwcgi.dll?wwDI~StnSrch~StnID~20023004), Utah State University (USU) seismic monitoring stations (http://www.seis.utah.edu/), and verified tidal data from Depoe Bay, OR (http://tidesandcurrents.noaa.gov/station_info.shtml?stn=9435827+Depoe+Bay+%2C+OR). Tidal data from Depoe Bay, OR were selected because the station provides historic verified six-minute water level data which could easily be time corrected to Mountain Standard Time, and because it lies at similar latitude as our study sites. Tidal generating forces are experienced equally at similar latitudes around the globe, and by finding station data at similar latitude a time correction can be made to show at what approximate time high and low tidal effects should be observed.

3.1 Field Measurements

Field work started in the summer of 2006 and ended in November 2006. Discharge was measured using a Marsh McBierney (Loveland, CO) FloDar unit, which measures

velocity using radar, measures water depth using ultrasound, and calculates flow rate using a simply continuity equation of volume multiplied by velocity equals flow rate with an error of ±5% (FloDar, 2006). It also gives the user an option to multiply the flow by some factor determined from channel shape and roughness. Given an average flow rate at Rabbit Creek of 0.0857 m^3/s (3.03 cfs) during the study time, the FloDar could accurately measure changes in flow with a precision of ± 0.00428 m^3/s (0.151 cfs). At White Creek the average flow rate was 0.117 m^3/s (4.12 cfs) meaning the FloDar could accurately measure changes in flow with a precision of ± 0.00583 m^3/s (0.206 cfs). FloDar data were recorded using a data logger connected to the monitoring unit. Data were transferred from the data logger to a laptop computer. The FloDar can operate at a water depth precision of ± 0.635 cm under subaerial or submerged conditions, at air or water temperatures between -10˚C (14˚F) to 52˚C (125F) and in water depths between 0.634 cm to 569 cm. Further, it measures discharges between 0.0210 to 0.566 m^3/s, velocity changes of 0.5% with an error of ±0.03 m/s, and level changes of 1% with an error of ±0.64 cm (Flo-Dar, 2006). Factory calibration and a new internal lithium battery were installed in September of 2006. Initially the FloDar was deployed at Rabbit Creek, YNP, and was set to sample discharge (cfs later converted to m^3/s, 1.00 cubic foot/second = 0.0283 cubic meter/second) and water height (inches, later converted to centimeters, 1.00 in. = 2.54 cm.) every 15 minutes for 15 days. Discharge of Rabbit Creek was measured between October 13th, 2006 and October 29th, 2006. Discharge of White Creek was measured between October 29th and November 11th. Flow data for Tantalus Creek were downloaded for the time period of September 9th, 2006 to October 10th, 2006 (http://waterdata.usgs.gov/nwis/uv?06036940). The 15-minute sample interval was

originally selected for several reasons. A physical constraint to our data collection was the FloDar's level of precision which allowed us to accurately measure any changes in hot springs discharge greater then 5%. Hypothesized factors that could be analyzed using the spectral analyses (tides, barometric pressure, heating cycles) were expected to vary on at a time interval of hours to days. Although heating cycles in the confined aquifer may force discharge of thermal water at higher frequencies, these discharge changes must be greater then 5% of the average flow in order to be accurately measured by the FloDar. Conceptually, it was suspected that major discharge changes greater then 5% of the average stream flow rate were absent in short time periods. Therefore sampling at a finer scale then 15 minutes was thought to be unnecessary. Spectral analysis of discrete data at a 15-minute sample interval can illuminate time patterns of 30 minutes or more according to the Nyquist-Shannon sampling theorem and would, therefore, be adequate for determination of tidal and barometric effects. The Nyquist-Shannon sampling theorem (discussed further in methods 3.2b) states that in order to accurately determine time patterns, the sample interval must be two times greater then the shortest time pattern in the continuous period. Another reason for originally selecting a 15-minute sample interval was that reported values for the Tantalus Creek gaging station are given at a 15-minute interval, so our 15-minute sample interval would allow direct comparison. Finally, we selected a 15-minute sample interval to optimize battery power over the two-week period. Weak, or dead batteries found at the end of the study period could have compromised the entire data set. For this reason, the FloDar recorded battery power for each sample.

In the field, the FloDar hung over the center-most portion of the stream from a survey tripod using an adjustable rock climber's grade-spectra sling (Figure 17). The devise was leveled and locked in place as securely as possible. A long data cable connected the FloDar and the data logger. The data logger was labeled, sealed, and secured under a large log to camouflage it and secure it from any large curious mammals (LNT brochure, 2005). The cable was threaded through a 2 ½" flexible, black, PVC pipe to prevent damage from rodents and coyotes (Figure 17).

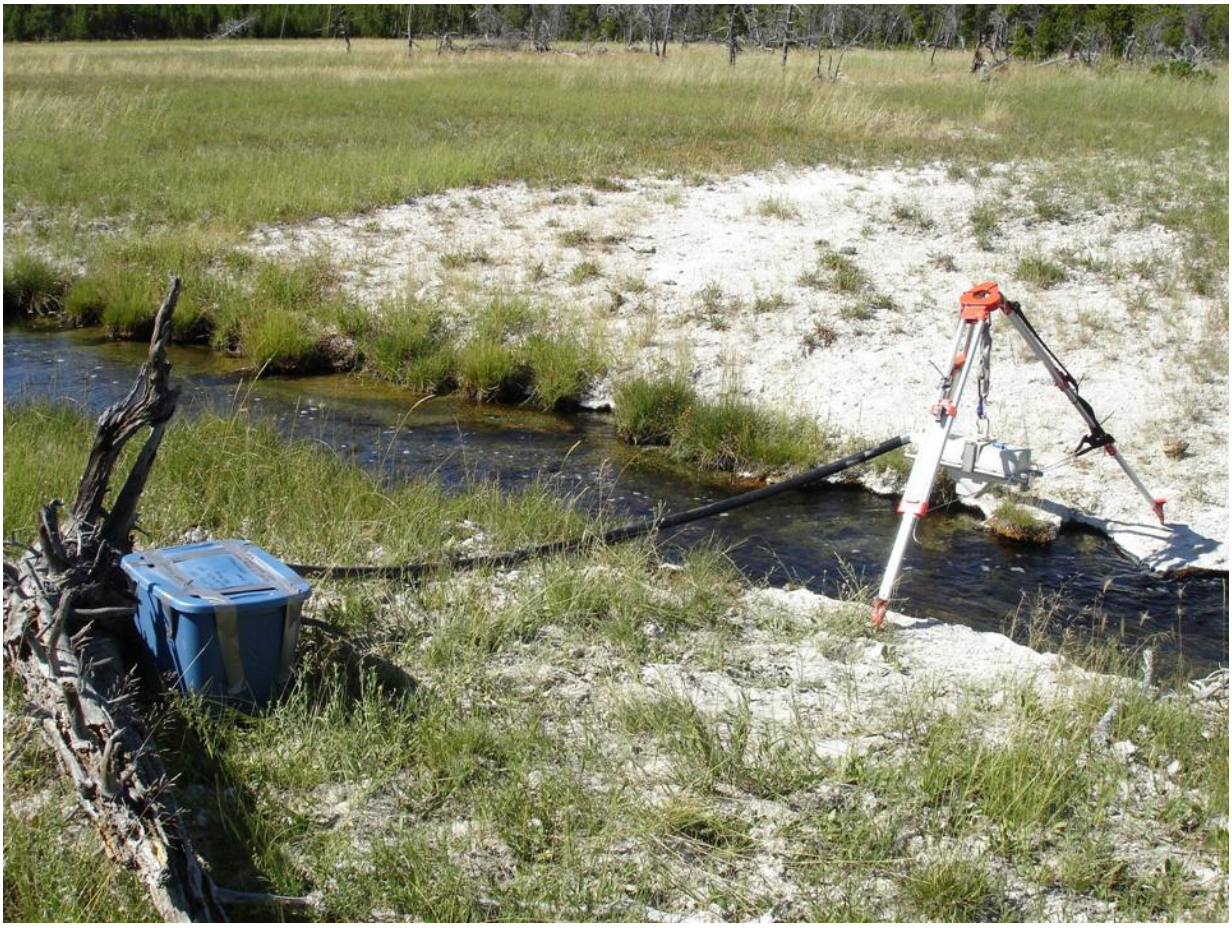

Figure 17. FloDar set up at Rabbit Creek 5 gallon storage tote for scale. Photo by Jacob Mohrmann, 2006

Field measurements including water temperature, air temperature, and barometric pressure were taken during deployment and retrieval for quality assurance including real-

time measurements from the FloDar to check for proper function. Water and air temperature measurements were taken using a Fluke 51 II thermometer.

3.2 Methods of Data Analysis

Data were analyzed using two methods: (1) visual or graphical representation of data and (2) analytical spectral analysis or a time-series frequency analysis to interpret data.

Two spectral analyses of each dataset were completed. Each used a fast Fourier transform (FFT) algorithm to complete a discrete Fourier transform (DFT) of each discrete data set (described further in 3.2 B.). Appendices A and B contain a detailed description of the steps used to analyze the data.

3.2 A. Graphical Analysis

Graphical analysis of data was done with one objective in mind, to visualize fluctuations in water discharge and compare those fluctuations with barometric pressure changes, earthquake occurrence, and rainfall events. Graphs were created that displayed stream discharge, observed tides from Depoe Bay corrected to Mountain Time zone, barometric pressure, precipitation, and earthquake occurrence. All data used are in electronic appendix (attached CD). Stream flow data were from FloDar measurements at Rabbit and White Creeks or from the USGS gaging station at Tantalus Creek (http://waterdata.usgs.gov/nwis/uv?06036940). Tidal data were from measured ocean

tides at the Depoe Bay, Oregon NOAA station due to its similar latitude to our test sites. (http://tidesandcurrents.noaa.gov/station_info.shtml?stn=9435827+Depoe+Bay+%2C+OR). Barometric pressure data from Norris Geyser Basin were provided by Dr. Henry Heasler (Yellowstone Center for Resources, NPS). Precipitation values came from Old Faithful, YNP, NOAA monitoring station (http://www4.ncdc.noaa.gov/cgi-win/wwcgi.dll?wwDI~StnSrch~StnID~20023004). Earthquake data were from the University of Utah's seismic monitoring program (http://www.seis.utah.edu/).

Static visualization is a commonly used tool when trying to understand overall trends and general relationships between data items (Card, 1999, Kaki, 2000, Ingebretsen, 2001). For this study, graphical representation of data was the only method used to determine a correspondence between precipitation and fluctuations in discharge and between earthquakes and fluctuations in discharge.

3.2 B. Spectral Analysis

Microsoft Office Excel 2003 was used for a variety of tasks as was Golden Software's Grapher 5.0. Bell Laboratories' R Project for Statistical Computing or simply "R" was used as well to perform spectral analysis using a Fast Fourier Transform (FFT). R was also used to graph results of its spectral analysis and to determine statistical significance of frequencies found.

Spectral analysis refers to an analysis that mathematically evaluates a series of discrete sequential numbers to find recurring frequencies (Brigham, 1988). Two different spectral analyses were completed, one using Excel and the other using R, and each method used the principle of Fourier transforms (FT's). The Fourier transform was named after Joseph Fourier, who first introduced the idea of decomposition of a function in terms of a sum of sinusoidal base functions, or the functions frequencies (Brigham, 1988). The decomposed function can be pieced back together to find the original function. This process of decomposition and re-composition was originally termed Fourier analysis and Fourier synthesis (Stein and Weiss, 1971). The term Fourier transform refers to the linear operator that transforms the original function into coefficients of the sinusoidal base function, or its frequencies (Brigham, 1988). The overall analysis has been called several things including: Fourier analysis, harmonic analysis, and spectral analysis (Brigham, 1988). The transform has applications in several scientific studies including: signal processing, probability theory, statistics, acoustics, oceanography, optics and diffraction (Rockmore, 1999). The Fourier transform can be evaluated for continuous or discrete data sets and is commonly evaluated using a computer to compute the continuous or discrete Fourier transform (DFT) (Dutt and Rokhlin, 1993, 1995). Computers are used to calculated the DFT using a fast Fourier transform algorithm. Several algorithms are used to the DFT, the most popular being the Cooley-Tukey FFT algorithm (Cooley and Tukey, 1965). Each algorithm uses slightly different mathematical formulas and most were created for specific applications. The Cooley-Tukey FFT algorithm is the most popular due to its stability and use in multiple applications (Rockmore, 1999).

The DFT is defined by the formula: $X_k = {}^{N-1}\Sigma_{N=0}\, X_n e^{-2\pi i/N(nk)}$ where X_k is the returned complex number, and k is an integer ranging from 0 to $N - 1$ (Oppenheim et al., 1999). The Cooley-Tukey FFT algorithm divides the equation in two at N/2 and first computes the DFT for the even discrete-data series numbers $e_m=x_{2m}$ ($x_0,x_2,\ldots,x_{n-2}$) and then the odd data series numbers $o_m=x_{2m+1}$ ($x_1,x_3,\ldots x_{n-1}$). When combined with the original DFT formula we can write M= N/2 and denote the DFT of even-series numbers e_m by E_j and the DFT of odd-series numbers o_m by O_j (M=0, … M – 1, j=0, …, M -1) (Oppenheim et al., 1999). It then follows:

$$\begin{aligned} X_k &= \sum_{m=0}^{\frac{N}{2}-1} x_{2m} e^{-\frac{2\pi i}{N}(2m)k} + \sum_{m=0}^{\frac{N}{2}-1} x_{2m+1} e^{-\frac{2\pi i}{N}(2m+1)k} \\ &= \sum_{m=0}^{M-1} e_m e^{-\frac{2\pi i}{M}mk} + e^{-\frac{2\pi i}{N}k} \sum_{m=0}^{M-1} o_m e^{-\frac{2\pi i}{M}mk} \end{aligned}$$

When computed the algorithm combines the two results to produce the Fourier transform of the whole data sequence. Because the data is divided and transformed in two pieces the algorithm is limited to evaluating N at a power of two. Results of the computed algorithm are complex numbers relating to magnitude of each frequency (1/total sampling time).

Because the data sets are not composed of continuous samples but rather discrete samples, the Nyquist-Shannon sampling theorem must be considered. The theorem states that uniformly spaced, discrete samples are a complete representation of the signal if its bandwidth is less than half the sampling rate (Shannon, 1949). The bandwidth (B) is a measure of the frequency range of a sample (f_s) (Shannon, 1949). The theorem states that in order to accurately represent the continuous time signal, the sampling frequency must

be greater than twice the signal bandwidth ($f_s > 2B$) (Shannon, 1949). The Whittaker-Shannon interpolation formula states that under certain limiting conditions, a function (x(t)) can be reconstructed exactly from its samples (x[n]= x(nT)), by the formula (Whittaker , 1915): $$x(t) = \sum_{n=-\infty}^{\infty} x[n] \cdot \mathrm{sinc}((t - nT)/T)$$

Where $T=1/f_s$ is the sampling interval, f_s is the sampling rate, and sinc(x) is the normalized sinc function $\left(\mathrm{sinc}(x) = \frac{\sin(\pi x)}{\pi x}\right)$. Some degree of error in the reconstruction process is inevitable as it, in theory, requires summing an infinite number of terms, however we are limited to a finite number of terms (Marks, 1991). Some approximation is necessary. Error introduced in the approximation is referred to as interpolation error (Marks, 1991). Also, a signal that is temporally limited can never be fully bandlimited or reconstructed to be exactly that of the original signal (Marks, 1991). Error introduced from bandlimiting is termed aliasing (Marks, 1991). If under sampling occurs ($f_s < 2B$) some frequencies may overlap. The overlapped frequencies will create an aliased signal of the same frequency but with different phase and amplitude (Marks, 1991). If aliased signals are present in our data analysis, statistically significant frequencies found may actually be a result of higher frequencies occurring at less then two times our sampling interval of 15 minutes.

Two methods can be used to avoid aliasing, first increasing the sampling rate to above twice the highest frequency, or second introduce anti-aliasing filters in the sampling process to restrict any undesirable frequencies (Venkataramani, 2000). Anti-aliasing is

the process of removing signals with higher frequencies than can be properly recorded by the recording device, in our case, the FloDar (Venkataramani, 2000). Generally anti-aliasing filters used to restrict undesirable frequencies are used in applications such as optics and harmonics, however for spectral analysis increasing the sampling rate is typically the only anti-aliasing method used (Venkataramani, 2000). The removal of unwanted frequencies is done before sampling at a lower resolution. If it is not done, under sampling may cause undesirable results.

A statistical signal processor was used to eliminate some noise in the results of our spectral analysis in order to magnify important frequencies. The statistical signal processor used in this study was a running average smoothing technique in the R program (Appendix B). The technique was used to smooth data using a running average of results of the Fourier transform. R was also used for calculation of statistical significance of frequencies (Appendix B). The smoothing filter minimizes noise that has corrupted signals, but does make an assumption that the signals are stochastic processes with known spectral characteristics. Figure 18 shows two graphed results of the spectral analysis using R. The first graph is the raw output data plotted, while the second is the data smoothed using the running average kernel command “daniell” (Shumway, 2006).

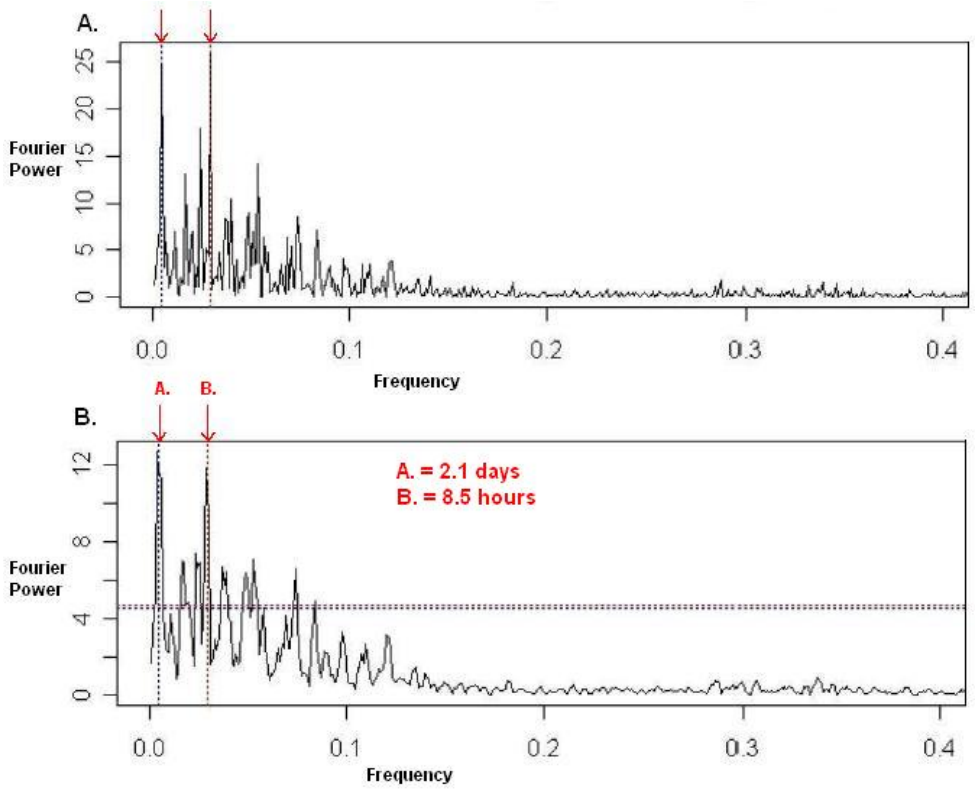

Figure 18. Example of smoothing technique to minimize noise in the frequency analysis. A is original output graph and B. is the graph with data that have been smoothed with the "daniel" kernel.

The "daniell" command uses the following formula beginning at time t = 0:

$s_o = x_o$ $s_t = \alpha x_t + (1 - \alpha)\, s_t - 1$ where s = output of the smoothing algorithm, x = the raw data sequence, and α is the smoothing factor and $0 < \alpha < 1$ (Shumway, 2006). The smoothing technique assumes the analyzed processes are random, and therefore, even though starting, ending, and midpoints are known, there are more possible outcomes that may occur, but that certain outcomes are more probable than others. Maintaining this assumption and using the program R, we were able to identify whether or not certain peaks were statistically significant results of the Fourier transform with 95% confidence.

Both R and Excel use the Cooley-Tukey FFT algorithm to compute the discrete Fourier transform (DFT). However, R completes the operation with fewer steps by the user. R is

a Linux based program and operates by commands entered by the user. With the proper command string, R is able to process a large amount of data, display the numeric transformed results, and graph these results all in a single step almost instantaneously. Statistical significance and data smoothing can also be calculated quickly. The biggest limitation to the program is the patience and accuracy of the user, as long strings of command are required to complete certain operations. (Please refer to Appendix B. for detailed description of how R was used).

The Fourier Transform used by Excel takes a sequence of linear discrete numbers and returns a complex number and its inverse for each number in the sequence. These complex numbers correspond to each frequency interval (f_s) in the period (T). $f_s = 1/T$ The complex number (n_i) returned from the Excel FT function must be normalized and assigned a power: the normalized number = $n_i * 1/N$, where N is the total number of samples (Shumway, 2006).

The power is assigned to better reflect the relative contribution of each frequency. Higher powers represent more significant frequencies. The power is determined by taking the absolute value of normalized numbers and multiplying this by the square root of 2. The power is then graphed against its corresponding frequency to visualize frequency distribution. (Appendix A).

The Cooley-Tukey FFT algorithm computes the DFT exactly (Welch, 1969), so no additional error is introduced into the analysis beyond that which is present from the

physical constraints of our measuring devise, the FloDar. Given that our sampling period of 15 minutes (900 seconds) in a total analyzed time of 15,360 minutes (921600 seconds), each frequency interval (f_s) in the total period (T) becomes 1.085069 $*10^{-6}$ Hz (Hz is 1 f_s per second) from the equation ($f_s = 1/T$).

4.0 Results and Interpretation

4.1 Graphical Analysis

Graphical analyses of datasets were done with the goal of visualizing changes in each dataset and visually inspecting plotted data to see if any correspondences exist. Graphs of data for Rabbit Creek revealed no correspondence between changes in flow and changes in precipitation or barometric pressure (Figure 19). Comparing plotted tidal records to changes in flow also showed no correspondence. Further, earthquakes did not appear to influence changes in flow (Figure 19).

Graphed data for White Creek did not show a correspondence between changes in flow and earthquakes, or precipitation over the entire sampling period (Figure 20, 21). However, a correspondence appears between flow changes and barometric pressure changes for certain narrow time periods (Figure 21). Nevertheless, the correspondence is absent for the majority of the test period (Figure 20). Tidal records showed no correspondence with flow changes at White Creek.

The Tantalus Creek hydrograph did not appear to respond to precipitation events or earthquakes (Figure 22). Changes in barometric pressure corresponded to fluctuations in discharge (Figure 23). Tidal records did not correspond to changes in flow at Tantalus Creek.

These graphs were created to visualize correspondence of indicators of hypothesized controls and observed fluctuations in discharge. However with the exception of Tantalus Creek discharge and barometric pressure changes, graphical analysis proved to be too simplistic to understand what controls hydrothermal discharge. A spectral analysis was the next step in understanding what controls discharge.

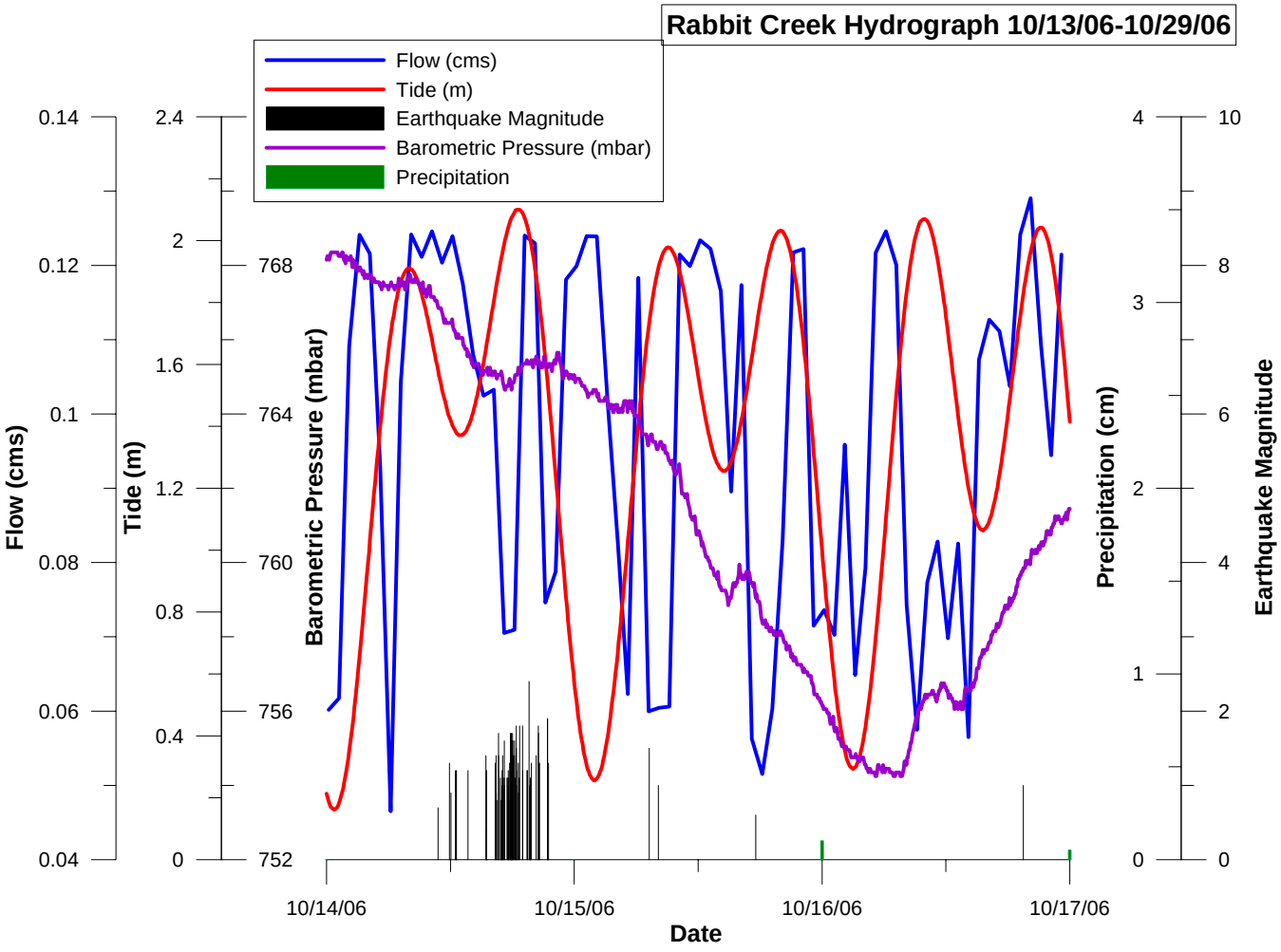

Figure 19. Visual representation Rabbit Creek hydrograph, flow rate, marine tide at Depot Bay, barometric pressure, precipitation and local earthquakes as a function of time over three days. Flow error at Rabbit creek is $\pm 4.28 \times 10^{-3}$ cms, which is below the resolution of the graph.

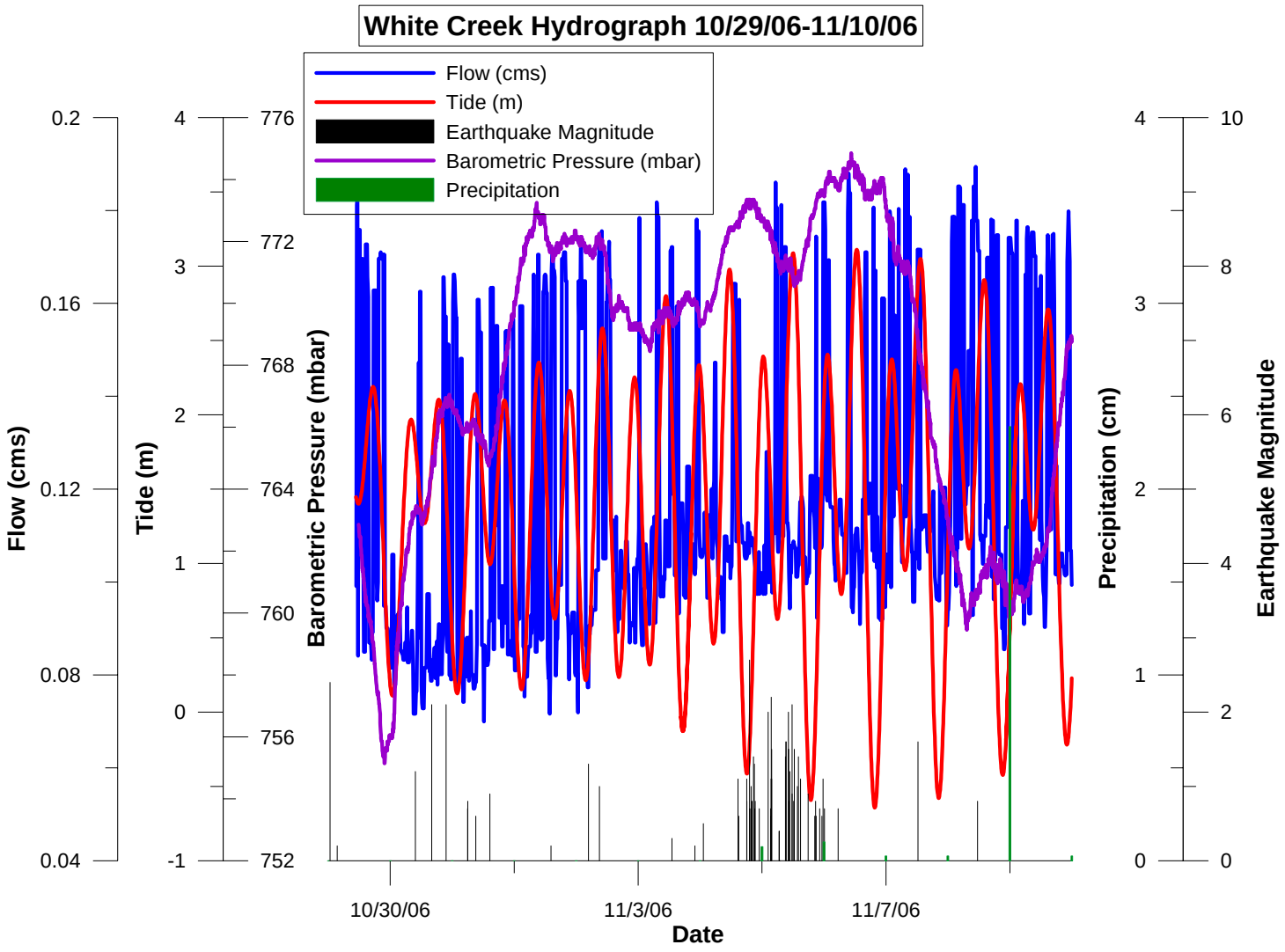

Figure 20. Full hydrograph record of White Creek. Datasets included on separate Y-axes: Flow rate, tides, barometric pressure, precipitation and earthquakes. Each set shares the same x-axis of time in date format. Flow margin of error at White creek is $\pm 5.83 \times 10^{-3}$ cms

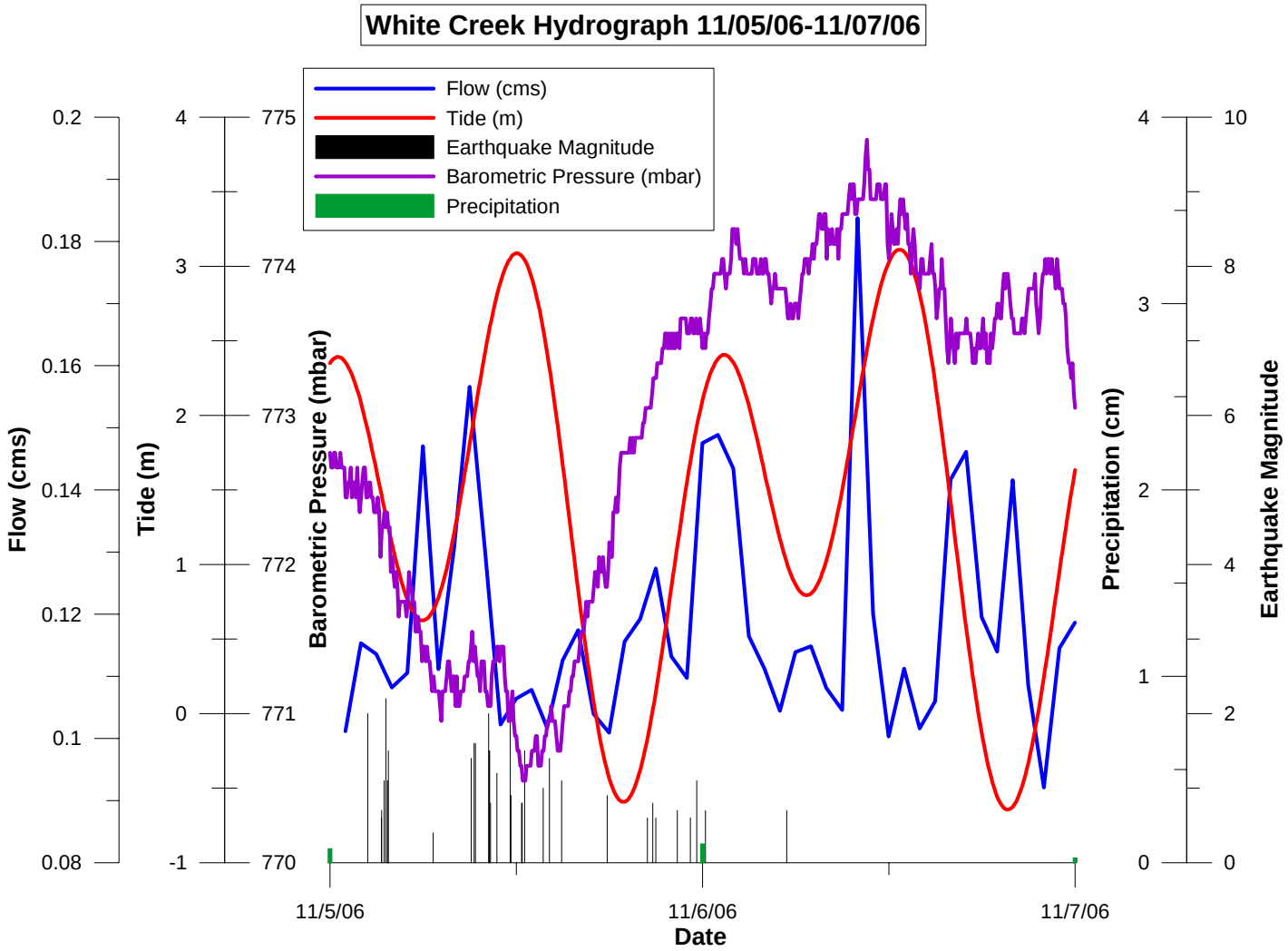

Figure 21. Short record hydrograph of White Creek. Datasets included on separate Y-axes: Flow rate, tides, barometric pressure, precipitation and earthquakes. Each set shares the same x-axis of time in date format. Flow margin of error at White Creek is $\pm 5.83 \times 10^{-3}$ cms

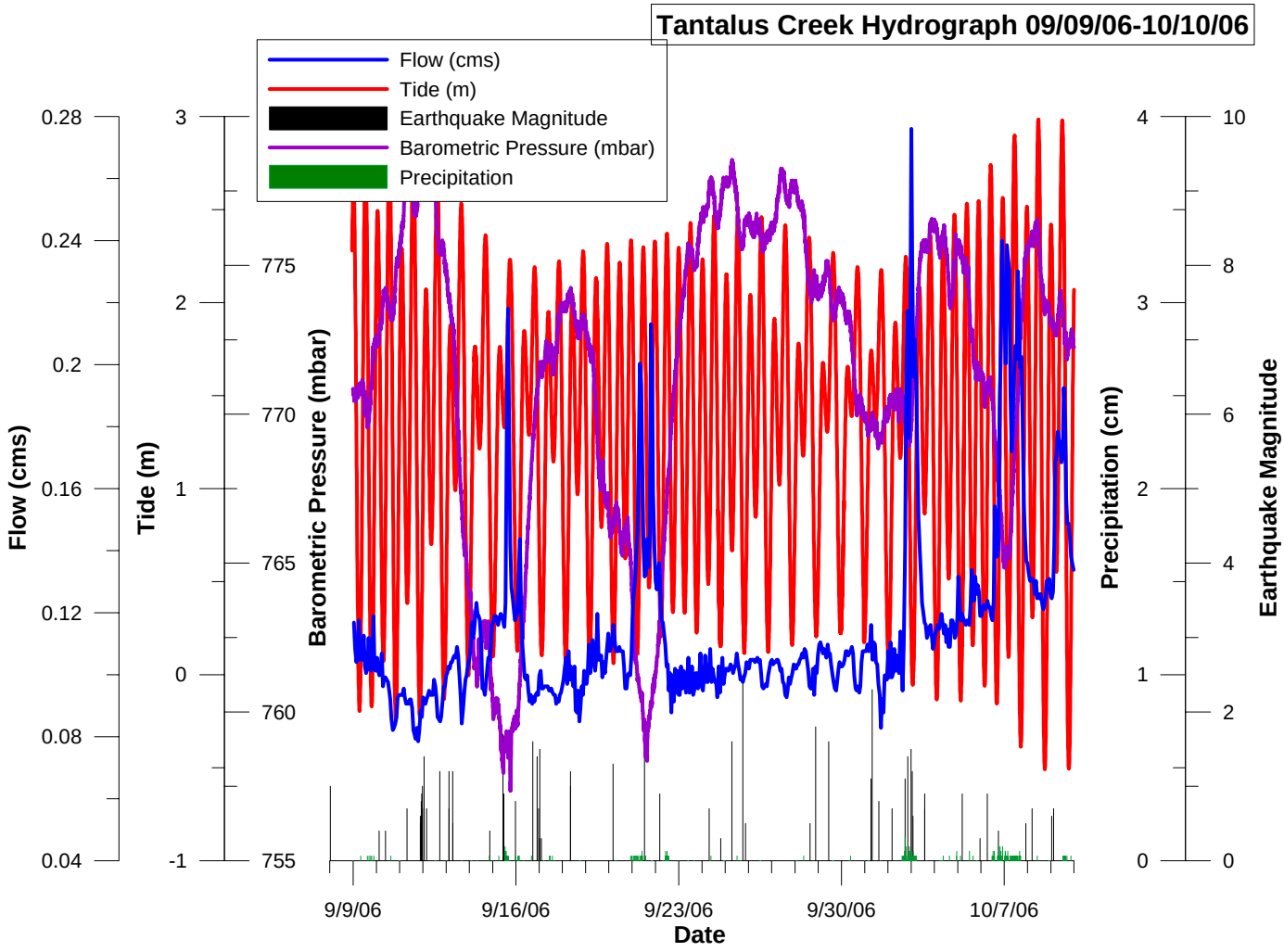

Figure 22. Tantalus Creek Full Record Hydrograph. Datasets included on separate Y-axes: Flow rate, tides, barometric pressure, precipitation and earthquakes. Each set shares the same x-axis of time in date format.

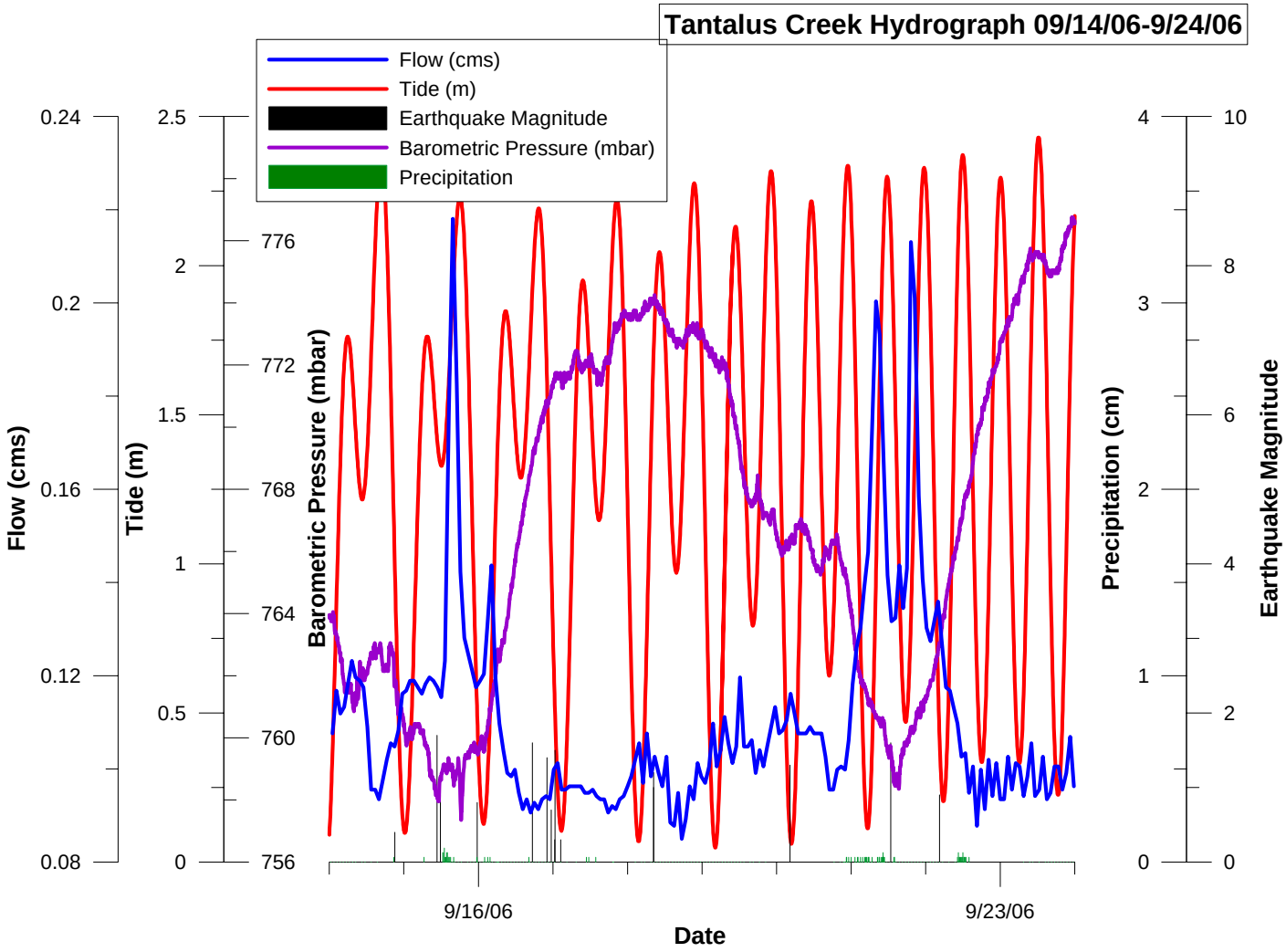

Figure 23. Tantalus Creek short record hydrograph. Datasets included on separate Y-axes: Flow rate, tides, barometric pressure, precipitation and earthquakes. Each set shares the same x-axis of time in date format

4.2 Spectral Analysis

Spectral analyses of datasets were done with the goal of determining frequencies in discrete data sets. Comparisons between similar frequencies found in datasets would help support or refute our hypothesized controls on hydrothermal discharge, but not provide absolute causal proof of controls based on this limited test of our hypotheses.

Total error at the end of the spectral analysis can be defined as the sum of data collection error, and interpolation error, or error introduced in the data analysis. Initially, an error of 5% was introduced by our data collection device, the FloDar. Error introduced by the FloDar resulted from calculation of flow, or the volume of water per time that passed a specific point in the stream. Some additional error is introduced in the spectral analysis process and is called interpolation error (Makrs, 1991). Each frequency interval (f_s) is calculated from the equation $f_s = 1/T$ where T is the total sampling time. Given that our total sampling time (T) was 15,360 minutes (921600 seconds), each frequency interval (f_s) was equal to 921600^{-1} or $1.085069 * 10^{-6}$ Hz (Hz is 1 f_s per second). Recall that the first step of the spectral analysis is to use the Cooley-Tukey FFT algorithm to computer the Discrete Fourier Transform (DFT). This step essentially takes the discrete dataset and outputs a non-real number that represents magnitude of each frequency interval. Frequency intervals start with the longest frequency of $1.085069 * 10^{-6}$ Hz and add to that another frequency interval of $1.085069 * 10^{-6}$ Hz, then another interval of $1.085069 * 10^{-6}$ Hz, and so on until the number of frequency intervals is equal to ½ of the total number of samples. Recall the frequency of $1.085069 * 10^{-6}$ Hz is equal to 921600 seconds ($1.085069 * 10^{-6}$ Hz^{-1}), by adding an additional frequency interval of $1.085069 * 10^{-6}$ Hz,

that frequency then becomes 2.17014 *10^{-6} Hz and is equal to 460800 seconds, a difference of 460800 minutes or 5.3 days. Meanings, when the DFT was computed, and frequencies were assigned magnitudes, any trends occurring ½ way between each frequency are grouped to the closest frequency. The error between those two smallest frequencies then becomes 2.67 days. As the frequency intervals near the largest point, error becomes smaller. For example the difference between the frequency intervals 1.1002*10^{-3} Hz (908.88 seconds) and 1.1013*10^{-3} Hz (907.98 seconds) is 0.9 seconds, or an error of 0.45 seconds between those intervals.

Spectral analysis in Rabbit Creek showed major changes in discharge with periods of 2.1 days and 8.5 hours (Table 4, Figure 24). Spectral analysis of tidal records from Depot Bay showed patterns with periods of 22.8 hours and 12.1 hours (Table 4, Figure 25). Spectral analysis of barometric pressure showed a pattern with a period of 7.1 days (Table 4, Figure 26). Error for major changes in discharge periods was ±5.3 hours at the 2.1 day period, and ±8.5 minutes at the 8.5 hour period. Error for observed tides was ±1.28 hour at the 22.8 hour period and ±21.3 minutes at the 12.1 hour period. Error for barometric pressure was ±2.97 days at the 7.1 days period.

Excel spectral analysis in White Creek revealed patterns of changes in discharge at 7.1 days, 23.3 hours, 8.5 hours, and 3.3 hours (Table 4, Figure 27). Analyzing tidal records revealed patterns at 23.3 hours and 12.8 hours (Table 4, Figure 28). Barometric pressure analysis revealed only one pattern, at 7.1 days (Table 4, Figure 29). Error for major changes in discharge periods was ±2.97 days at the 7.1 days period, ± 64 minutes at the

23.3 hour period, and ±8.5 minutes at the 8.5 hour period. Error for observed tides was ±1.28 hour at the 23.3 hour period and ±21.4 minutes at the 12.8 hour period. Error for barometric pressure was ±2.97 days at the 7.1 days period.

Excel spectral analysis in Tantalus Creek revealed only one pattern of change in discharge at 5.3 days (Table 4, Figure 30). Analyzing tidal records revealed patterns at 24.1 hours and 12.5 hours (Table 4, Figure 31). Barometric pressure analysis revealed only one pattern, at 5.3 days (Table 4, Figure 32). Error for major changes in discharge periods was ±1.78 days at the 5.3 day period. Error for observed tides was ±64 minutes at the 24.1 hour period and ±17.4 minutes at the 12.5 hour period. Error for barometric pressure was ±1.78 days at the 5.3 days period.

Many peaks appear that are not discussed. By visual determination, the strongest peaks in each analysis were chosen. Using the Excel method, there was not a convenient way to calculate statistical significance of each frequency observed, or to statistically smooth the data. A smoothing technique and statistical significance calculation was performed using the 'R' method.

Excel Spectral Analysis Results			
	Rabbit Creek	**White Creek**	**Tantalus Creek**
Dates Analyzed	10/13-10/29/06	10/29-11/10/06	9/9-10/10/06
Significant Discharge Patterns	2.13 days; **8.53 hours**	**3.6 days**; **23.3 hours** **8.53 hours**; 3.3 hours	**5.3 days**
Significant Earth Tide Patterns	**22.76 hours;** **12.05 hours**	**23.3 hours;** **12.8 hours**	**25.6 hours;** **12.8 hours**
Significant Barometric Pressure Patterns	**5.3 days**	**5.3 days**	**5.3 days**

Table 4. Results of Excel Spectral Analysis.

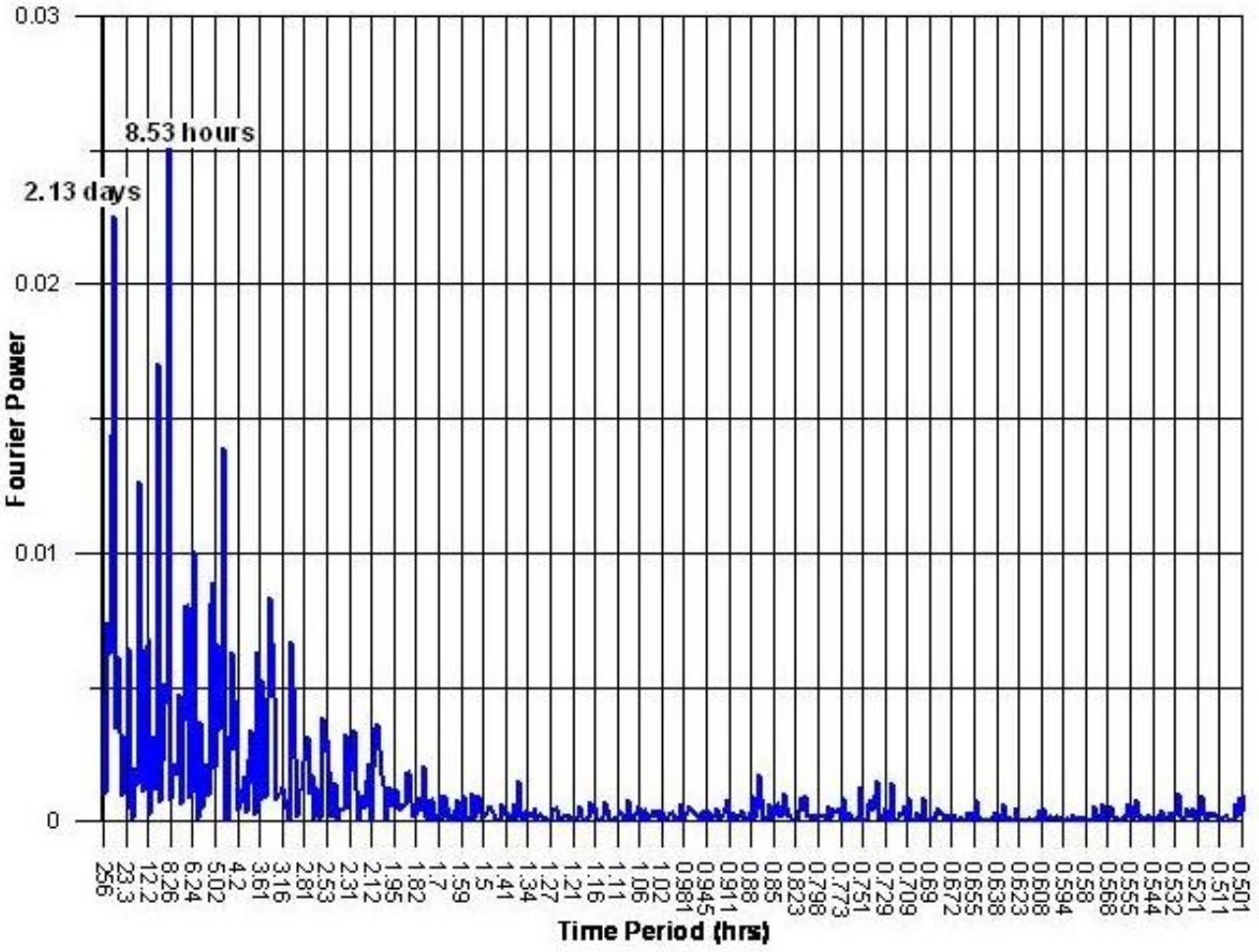

Figure 24. Rabbit Creek Excel spectral analysis of discharge.

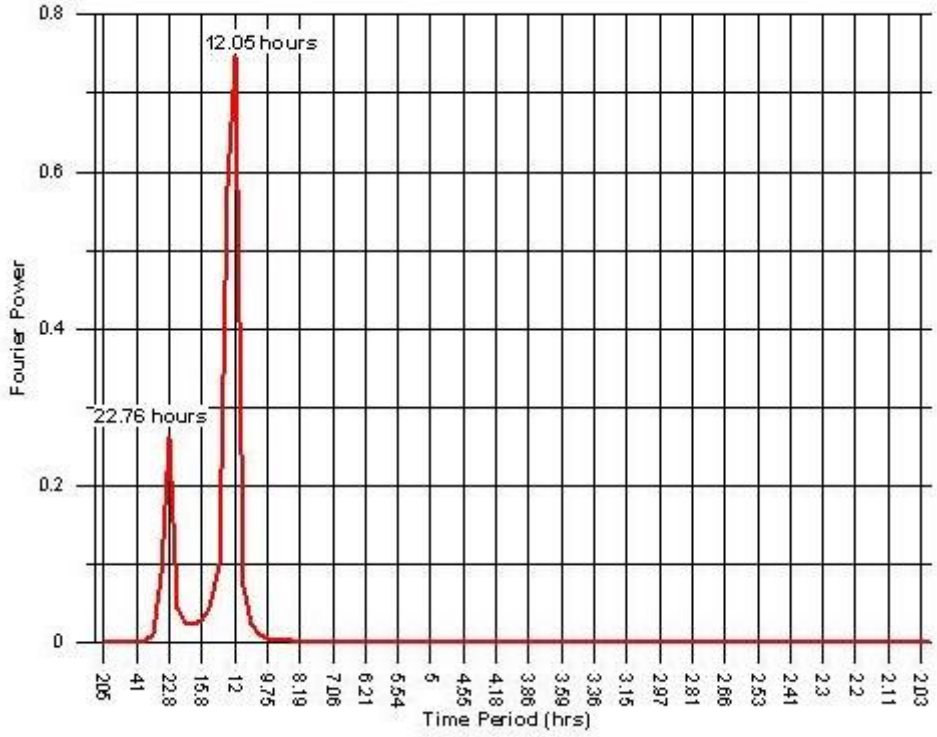

Figure 25. Excel spectral analysis of Depoe Bay observed tides during the Rabbit Creek test period.

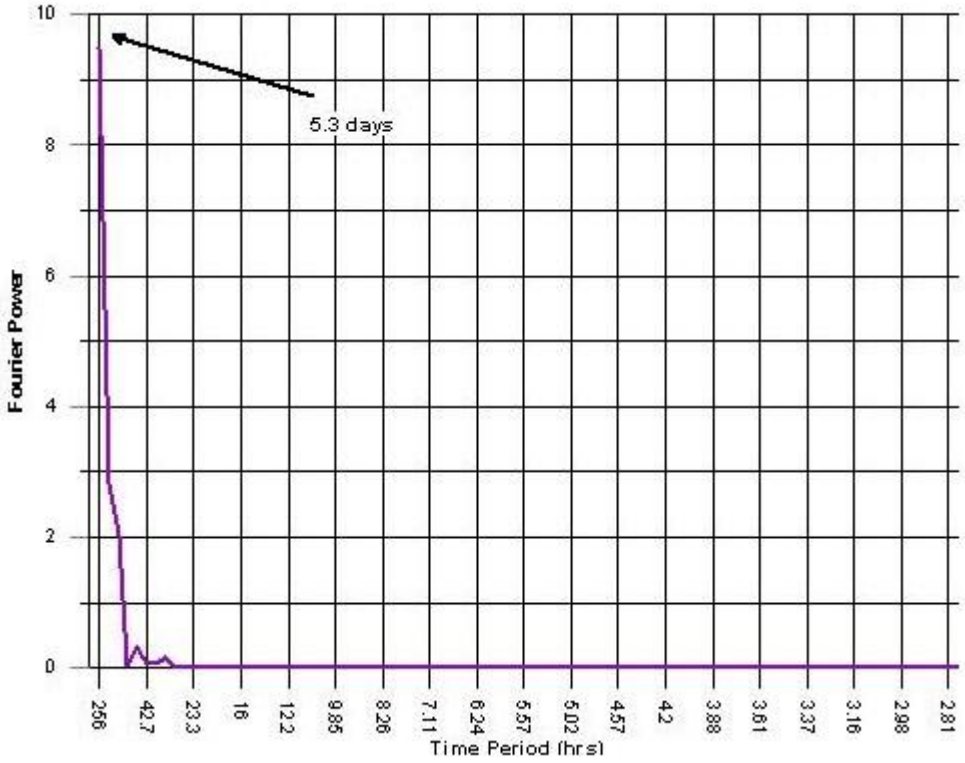

Figure 26. Excel spectral analysis of barometric pressure during the Rabbit Creek test period.

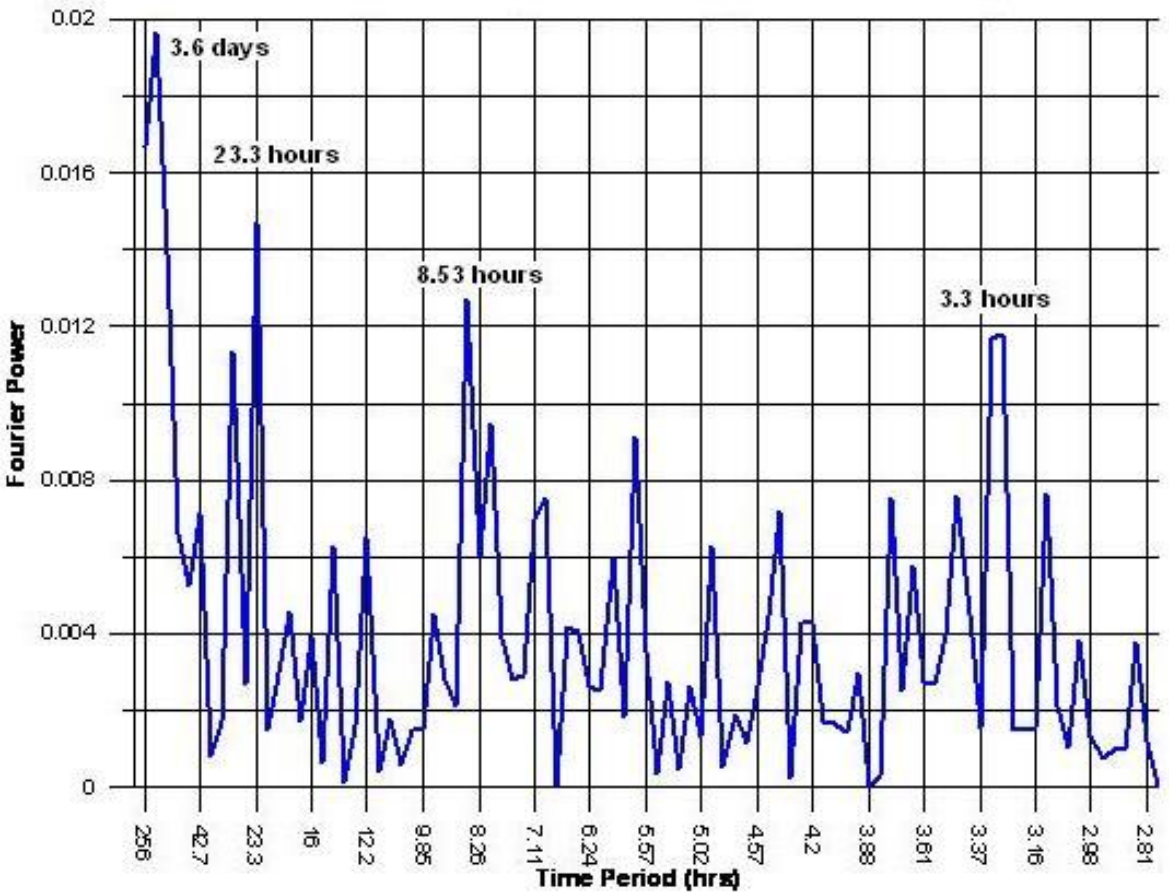

Figure 27. White Creek Excel spectral analysis of discharge.

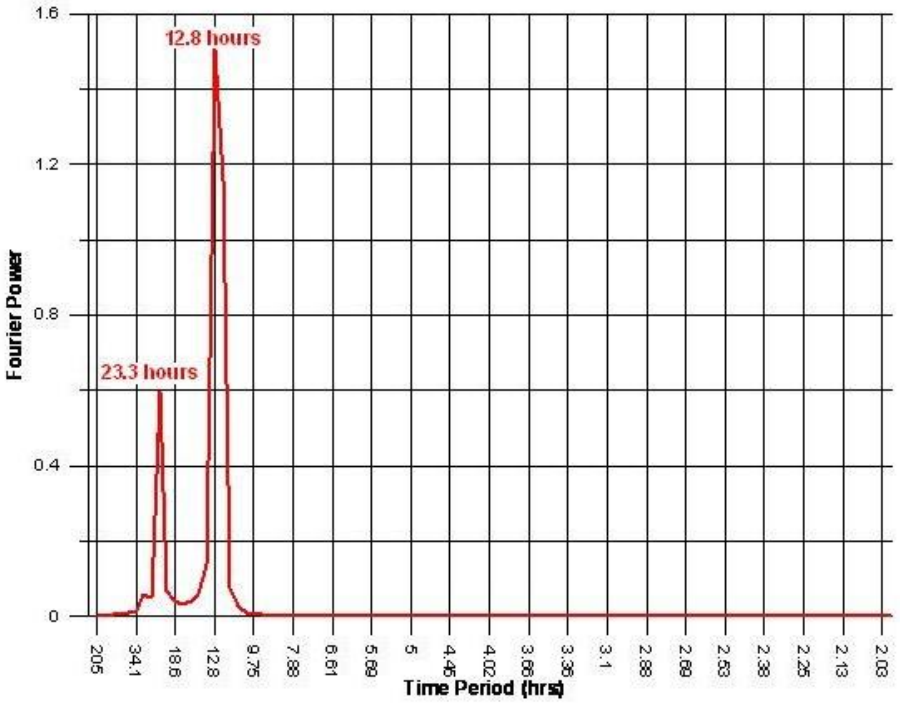

Figure 28. Excel spectral analysis of Depoe Bay observed tides during White Creek study period.

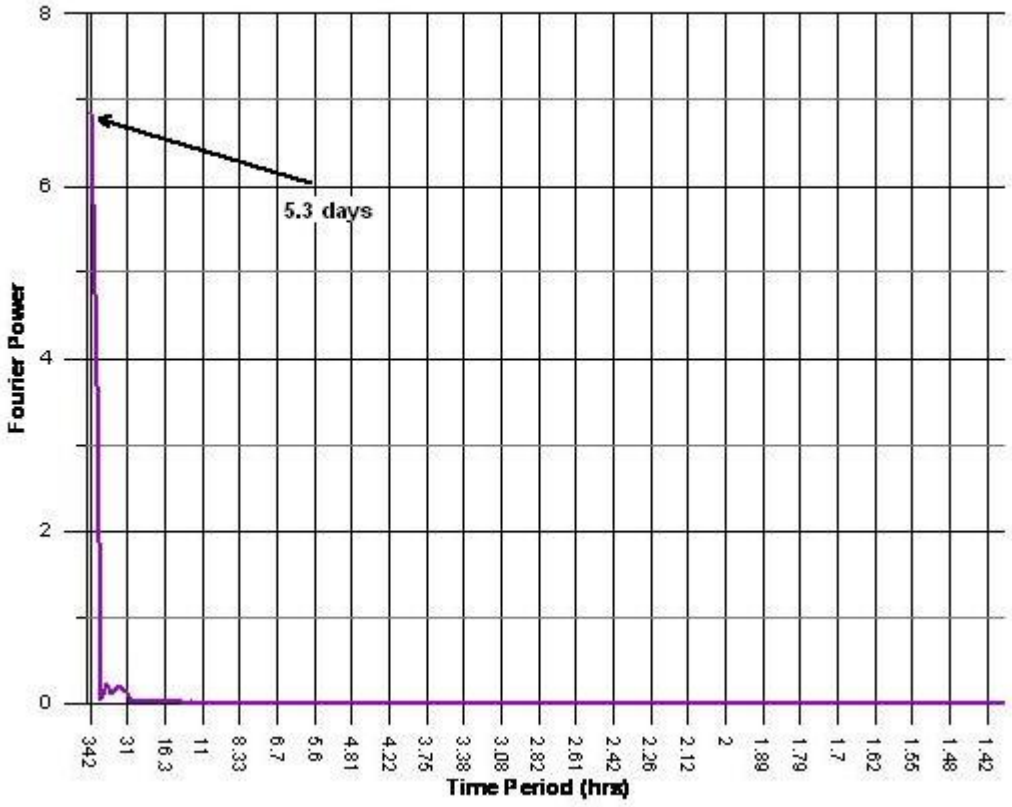

Figure 29. Excel spectral analysis of barometric pressure during White Creek study period.

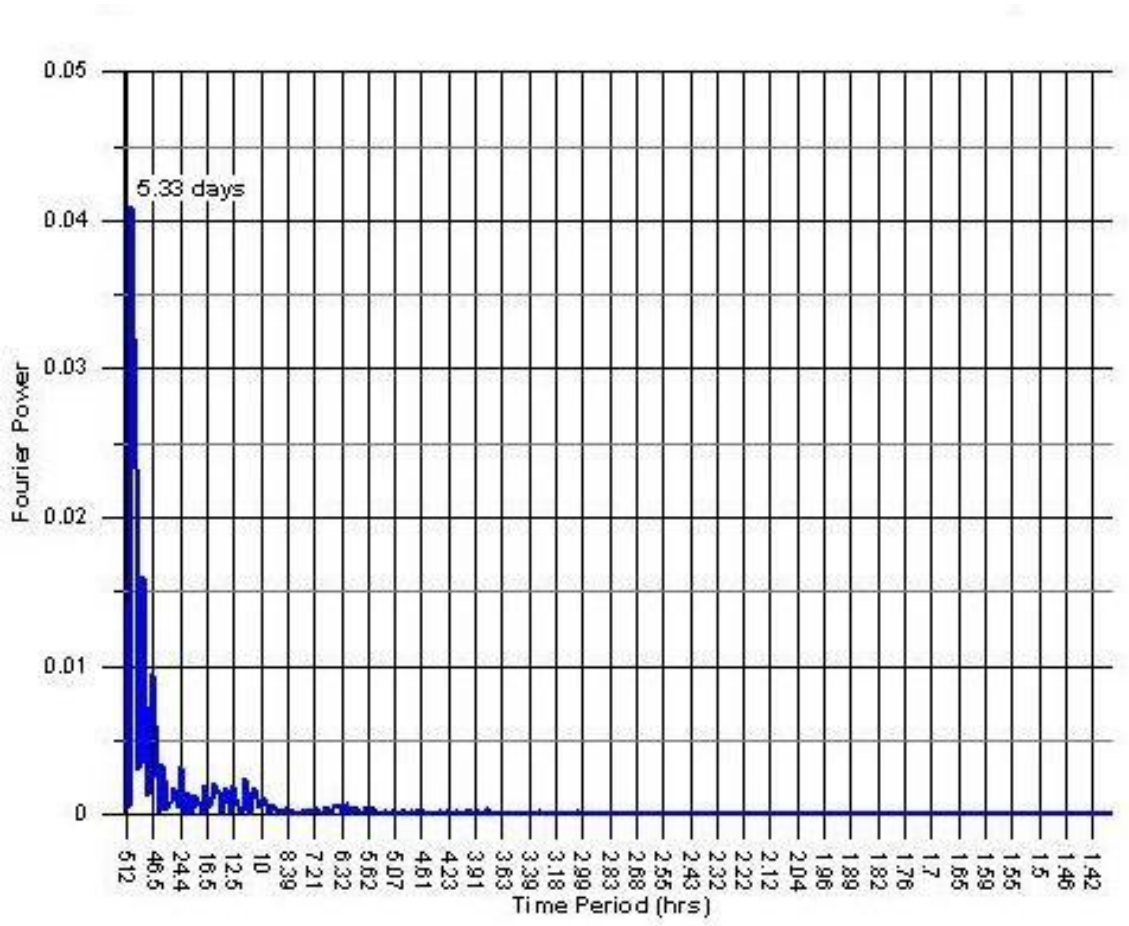

Figure 30. Tantalus Creek Excel spectral analysis of discharge.

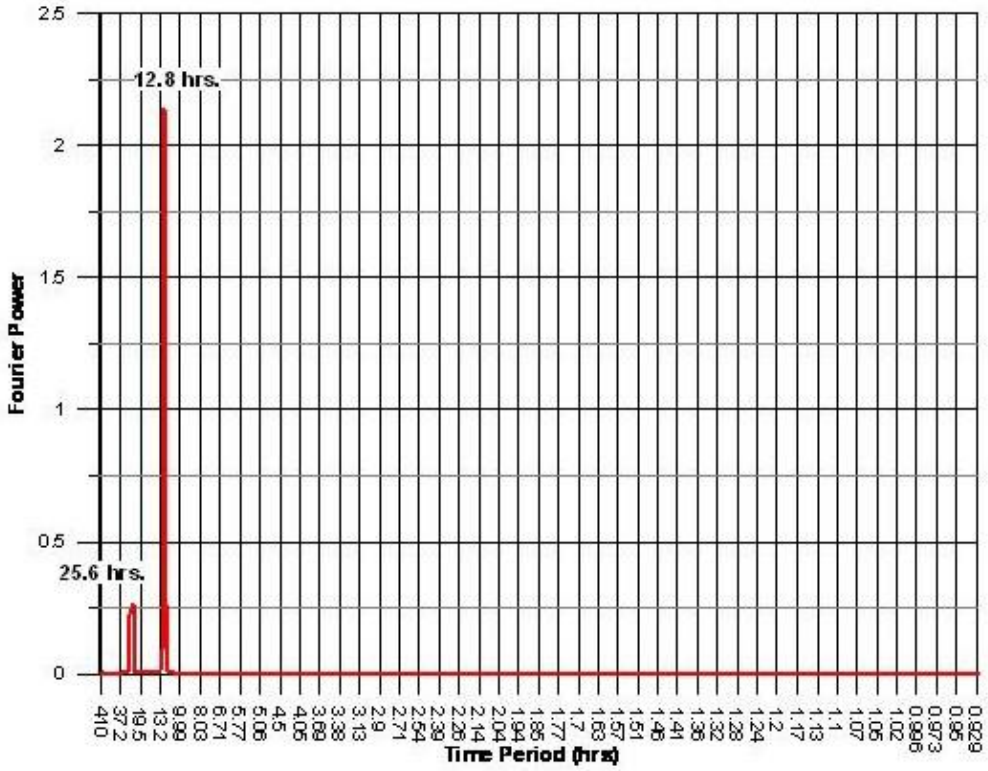

Figure 31. Excel spectral analysis of Depoe Bay observed tides during Tantalus Creek study period.

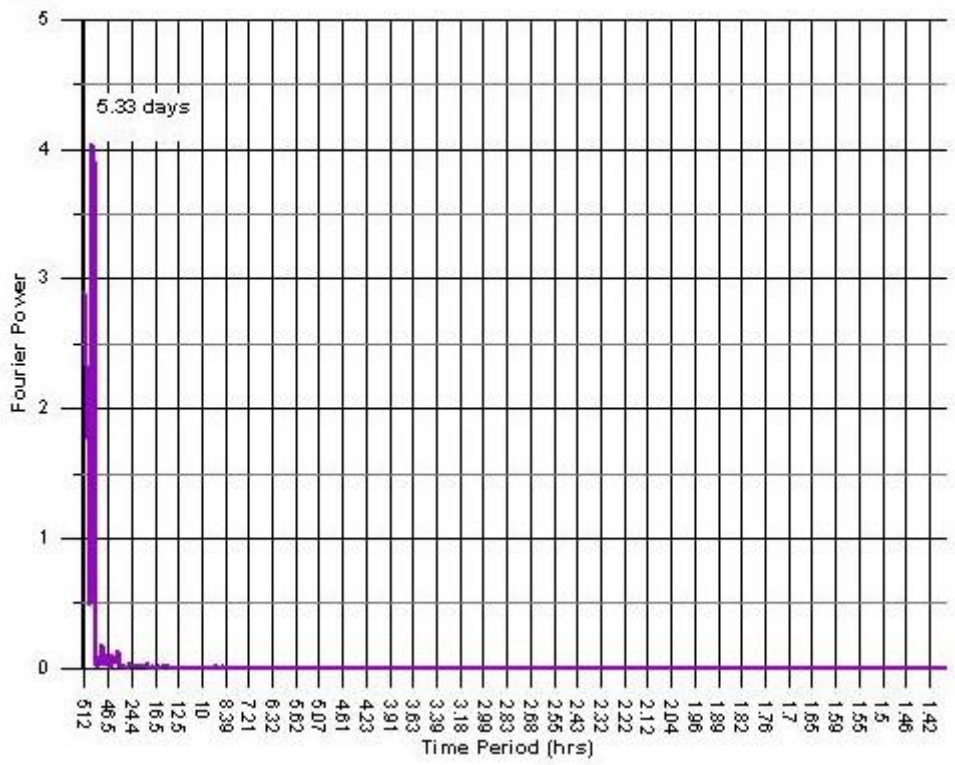

Figure 32. Tantalus Creek Excel spectral analysis of barometric pressure during Tantalus Creek study period.

A second spectral analysis was performed using R in order to boost confidence of results attained through the Excel. R proved to be much quicker, yet similar results were achieved negating a need for further methods.

R is a Linux based program and requires the user to input command codes in order to process data, create graphs, or to perform any of the other things it is capable of. Recall the sampling frequency (f_s) is equal to 1/total time, and the magnitude is calculated from the DFT (described in Methods 3.2a). Periods of significant frequencies has been calculated (f_s x total time = period) and is displayed on each graph. R was also used to find statistical significance of frequencies. Using the commands "U=qchisq(0.0125,df); L=qchisq(1-0.0125,df) (.0125 relates to our confidence interval of 95%)" we are able to calculate statistical significance with 95% confidence (Broman, 2006). Data smoothing was done once using the "daniel" command at a 95% confidence interval (described in Methods 3.2b). Observed tide data, and barometric pressure data were not smoothed due to the limited variability in the output data.

R's spectral analysis in Rabbit Creek revealed patterns of changes in discharge at 2.1 days and 8.5 hours (Table 5, Figure 33). Analyzing tidal records revealed patterns at 22.8 hours and 12.1 hours (Table 5, Figure 34). Barometric pressure analysis revealed only one pattern, at 4 days (Table 5, Figure 35). Error for major changes in discharge periods was ±5.3 hours at the 2.1 day period, and ±8.5 minutes at the 8.5 hour period. Error for observed tides was ±1.28 hour at the 22.8 hour period and ±21.3 minutes at the 12.1 hour period. Error for barometric pressure was ±1.4 days at the 4 day period.

R's spectral analysis in White Creek revealed significant patterns of changes in discharge at 3.6 days, 23.3 hours, 8.5 hours, and 3.3 hours (Table 5, Figure 36). Analyzing tidal records revealed patterns at 22.8 hours and 12.8 hours (Table 5, Figure 37). Barometric pressure analysis revealed only one pattern, at 5.3 days (Table 5, Figure 38). Error for major changes in discharge periods was ±16 hours at the 3.6 day period, ± 64 minutes at the 23.3 hour period, ±8.5 minutes at the 8.5 hour period, and ±1.3 minutes for the 3.3 hour period. Error for observed tides was ±1.28 hour at the 22.8 hour period and ±21.4 minutes at the 12.8 hour period. Error for barometric pressure was ±1.78 days at the 5.3 day period.

R's spectral analysis in Tantalus Creek revealed one significant patterns of changes in discharge at 5.3 days (Table 5, Figure 39). Analyzing tidal records revealed patterns at 25.6 hours and 12.8 hours (Table 5, Figure 40). Barometric pressure analysis revealed only one pattern, at 5.3 days (Table 5, Figure 41). Error for major changes in discharge periods was ±1.78 days at the 5.3 day period. Error for observed tides was ±1 hour 9 minutes at the 25.6 hour period and ±17.4 minutes at the 12.8 hour period. Error for barometric pressure was ±1.78 days at the 5.3 days period.

R Spectral Analysis Results			
	Rabbit Creek	**White Creek**	**Tantalus Creek**
Dates Analyzed	10/13-10/29/06	10/29-11/10/06	9/9-10/10/06
Significant Discharge Patterns (95% confidence)	2.1 days; **8.5 hours**	**3.6 days**; **23.3 hours** **8.5 hours**; 3.3 hours	**5.3 days**
Significant Tide Patterns (95% confidence)	**22.8 hours; 12.1 hours**	**22.8 hours; 12.8 hours**	**25.6 hours; 12.8 hours**
Significant Barometric Pressure Patterns (95% confidence)	**4 days**	**5.3 days**	**5.3 days**

Table 5. Results of R Spectral Analysis.

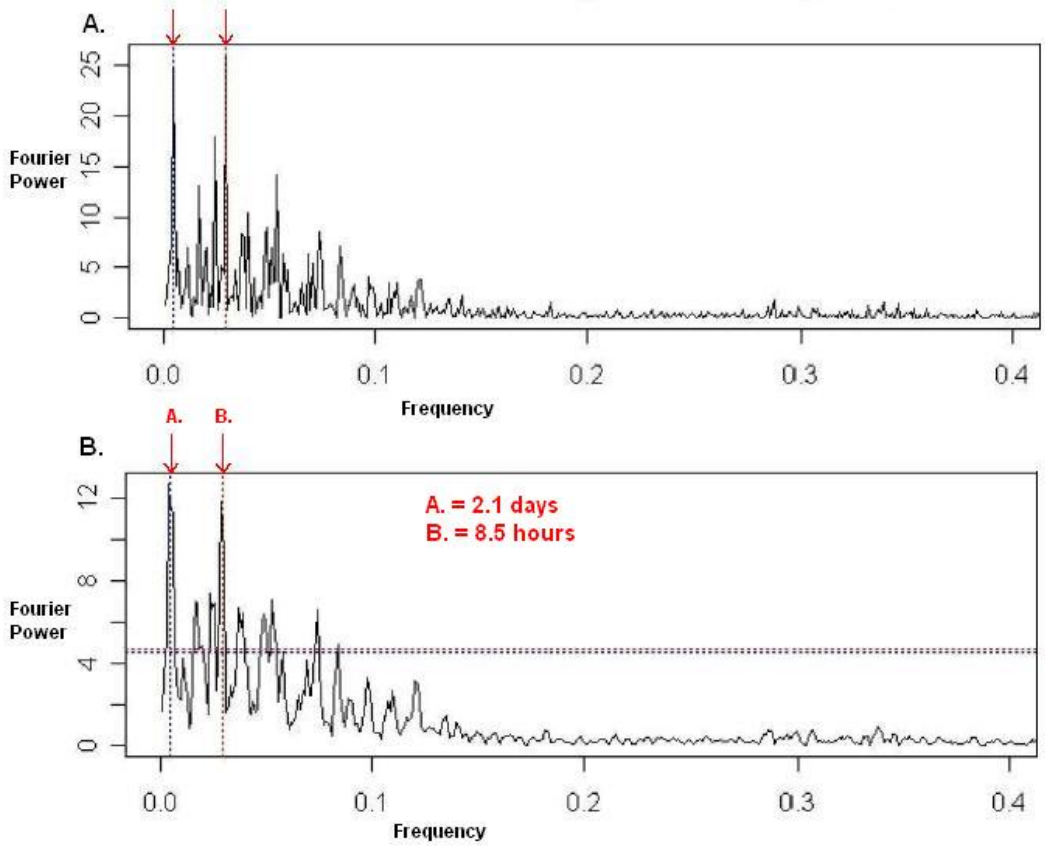

Figure 33. Rabbit Creek "R" Spectral Analysis of Discharge. Dashed vertical lines represent frequencies determined to be statistically significant. Horizontal dashed lines correspond with statistical significance calculation. Graph A. is initial graphed output of Fourier Transform, while B. is a once smoothed version of graph A. at 95% confidence.

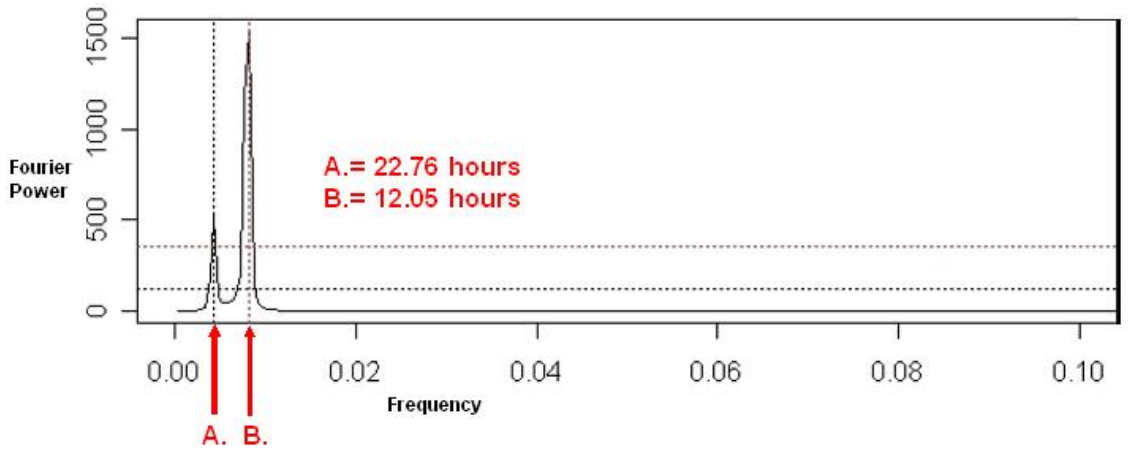

Figure 34. "R" Spectral Analysis of Depoe Bay observed tides during Rabbit Creek study period. Dashed vertical lines represent frequencies determined to be statistically significant. Horizontal dashed lines correspond with statistical significance calculation.

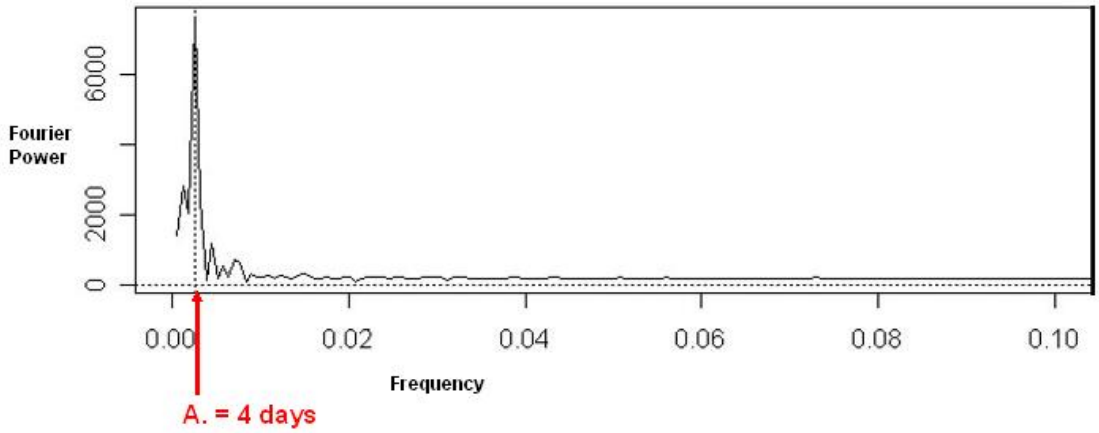

Figure 35. "R" Spectral Analysis of barometric pressure from Rabbit Creek study period. Dashed vertical lines represent frequencies determined to be statistically significant. Horizontal dashed lines correspond with statistical significance calculation.

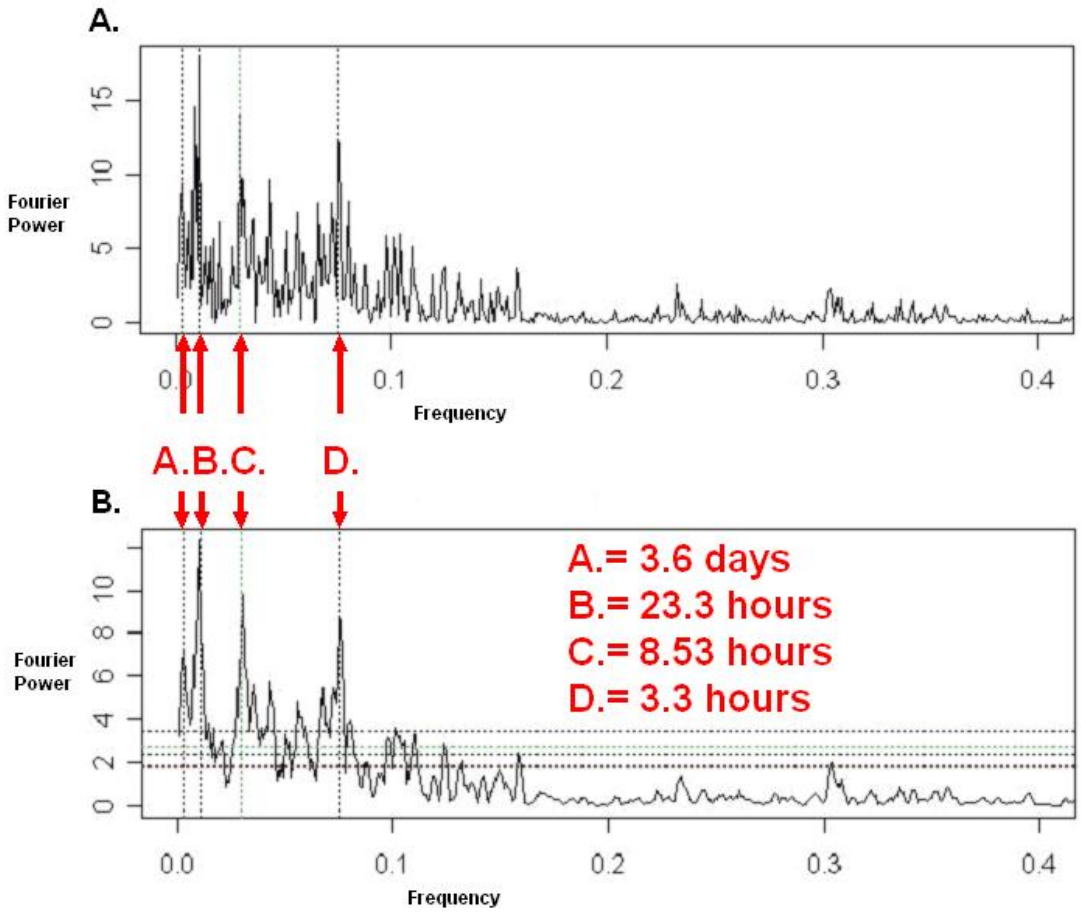

Figure 36. White Creek "R" Spectral Analysis of Discharge. Dashed vertical lines represent frequencies determined to be statistically significant. Horizontal dashed lines correspond with statistical significance calculation. Graph A. is initial graphed output of Fourier Transform, while B. is a once smoothed version of graph A. at 95% confidence.

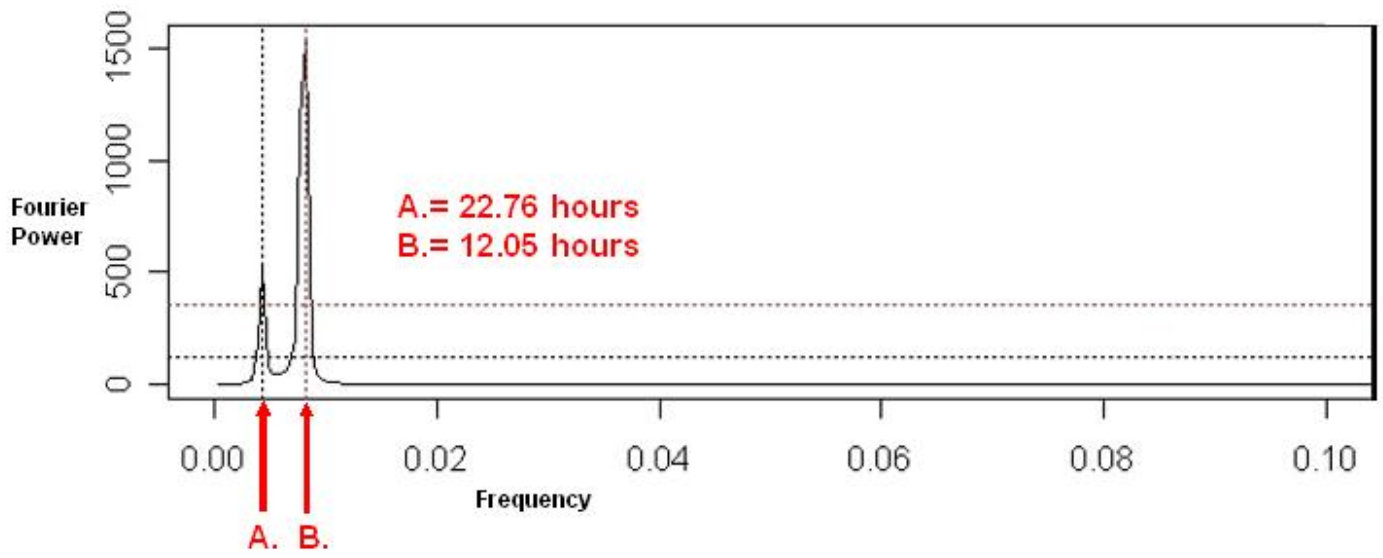

Figure 37. R" Spectral Analysis of Depoe Bay observed tides during White Creek study period. Dashed vertical lines represent frequencies determined to be statistically significant. Horizontal dashed lines correspond with statistical significance calculation.

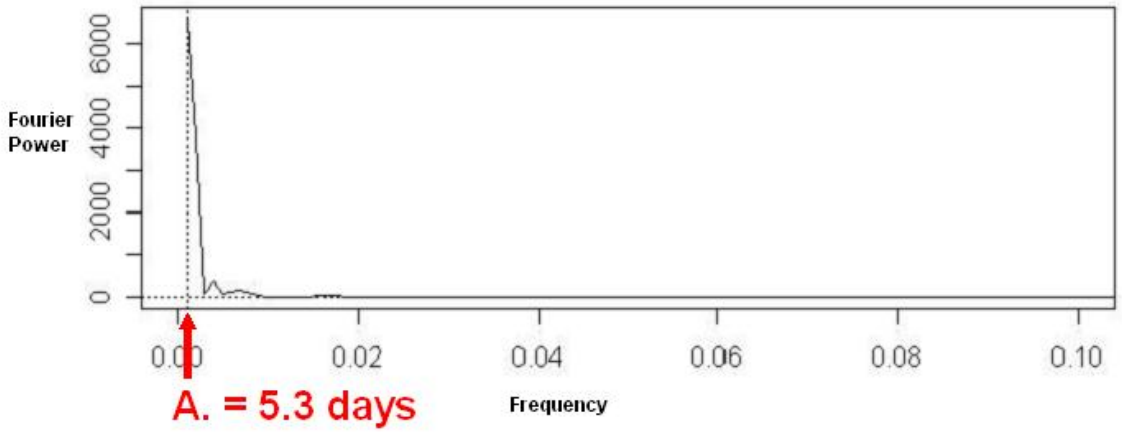

Figure 38. "R" Spectral Analysis of barometric pressure from Rabbit Creek study period. Dashed vertical lines represent frequencies determined to be statistically significant. Horizontal dashed lines correspond with statistical significance calculation.

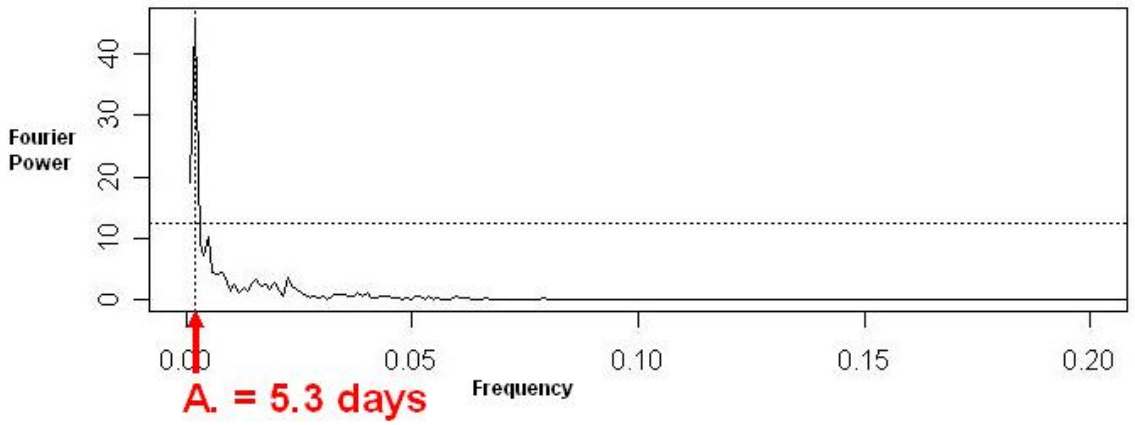

Figure 39. Tantalus Creek "R" Spectral Analysis of Discharge. Dashed vertical lines represent frequencies determined to be statistically significant. Horizontal dashed lines correspond with statistical significance calculation. Graph A. is initial graphed output of Fourier Transform, while B. is a once smoothed version of graph A. at 95% confidence.

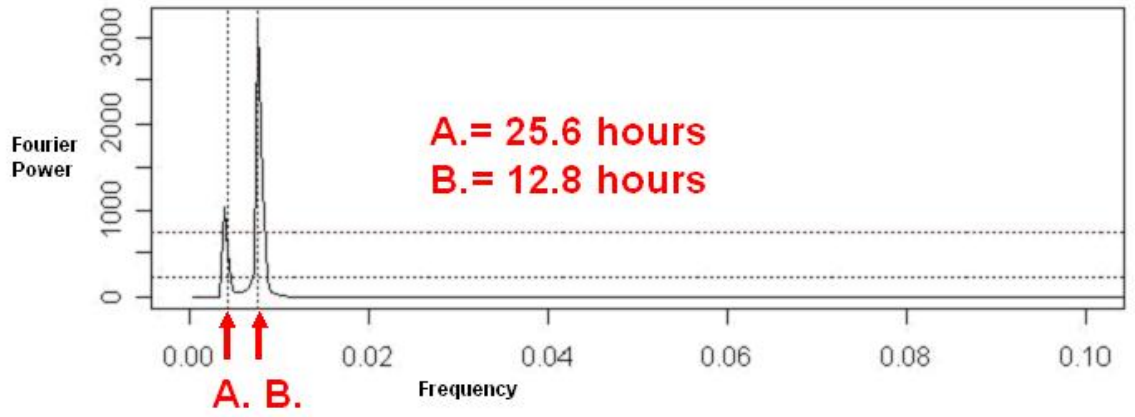

Figure 40. R" Spectral Analysis of Depoe Bay observed tides during Tantalus Creek study period. Dashed vertical lines represent frequencies determined to be statistically significant. Horizontal dashed lines correspond with statistical significance calculation.

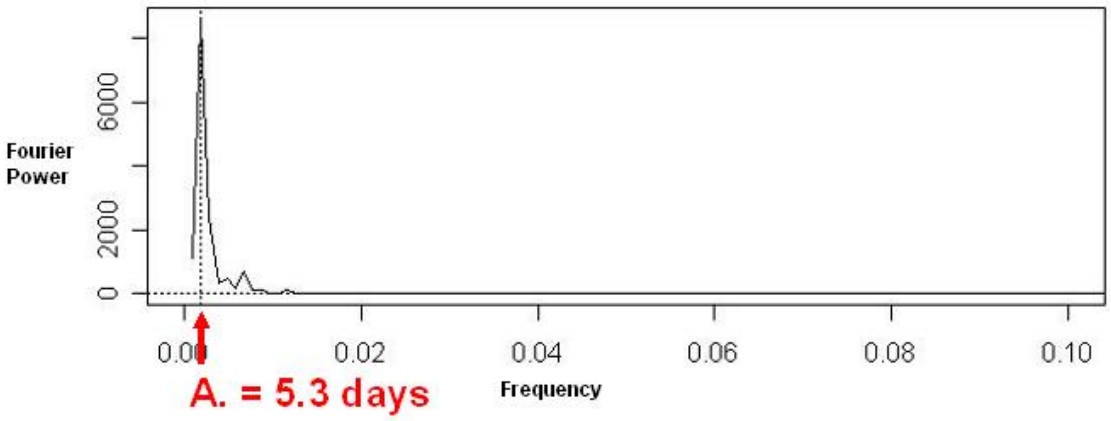

Figure 41. "R" Spectral Analysis of barometric pressure from Tantalus Creek study period. Dashed vertical lines represent frequencies determined to be statistically significant. Horizontal dashed lines correspond with statistical significance calculation.

5.0 Discussion

5.1 Graphical Analysis

Graphical analysis at Rabbit Creek did not show a visual correspondence between changes in flow and any of the hypothesized controls. Precipitation during the study period at Rabbit Creek was minimal (Figure 19). Discharge did not appear to change as a result of precipitation (Figure 19). However we cannot state that meteoric recharge does not affect discharge; only that in our study with minimal precipitation, we saw no noticeable changes in discharge caused by any precipitation event. No influence from earthquakes was observed (Figure 19). However with sample intervals of 15 minutes, if an earthquake did affect discharge we most likely missed recording the effect due to the short lived nature of earthquakes. In our study, if earthquakes did affect discharge, the effect was not lasting. Barometric pressure did not affect discharge. Aquifers have varying degrees of barometric efficiencies, or the degree of ability to be elastically compressed and contracted due to the effects of barometric pressure. The barometric efficiency of an aquifer is determined by its hydrologic properties (Fetter, 2000), ie. porosity, size, physical constraints. The aquifer feeding springs that discharge to Rabbit Creek could either have a very low barometric efficiency, or barometric pressure fluctuations during the study time were not powerful enough to cause noticeable fluctuations in discharge (Figure 19). Similarly with earth tides, no noticeable correspondence between discharge and tidal stage was observed (Figure 19). Reasons for an apparent lack of influence from earth tides are similar to those of barometric pressure, the aquifer is either simply not significantly affected by earth tide forces, or the forces

experienced during the test period did not fluctuate greatly enough to cause noticeable changes in discharge. The physical properties of the aquifer such as the aquifers porosity, depth, size, could be such that earth tides simply do not provide sufficient pressure differentials to cause noticeable changes in discharge.

Similar results were observed at White Creek to those at Rabbit Creek. Visual correspondences were not observed between flow and any of the hypothesized controls (Figure 20, 21). Precipitation, again, was minimal during the study interval, and influence from earthquakes, if any, were not lasting. Effects from both barometric pressure and earth tides both were absent visually.

Precipitation did not cause correspond with noticeable fluctuations in discharge in graphical analysis of Tantalus Creek data (Figure 22, 23). However we cannot state that meteoric recharge does not affect discharge, only that in our study with minimal precipitation, we saw no noticeable changes in discharge due to precipitation. Changes in barometric pressure and fluctuations in flow visually corresponded at Tantalus Creek (Figure 23). Barometric pressure changes inversely corresponded with flow changes. As barometric pressure increased, flow subsided. As barometric pressure fell, flow increased. The response shows convincing evidence that atmospheric loading on the aquifer is causing marked changes in discharge. This effect observed in hot springs discharge appears consistent with that of an open well tapping a confined aquifer. Barometric pressure acts directly on water in the well, or in this case, fractures that conduct water upwards. Earth tides, on the other hand, do not show a correspondence to

changes in flow. Thus, although an aquifer may show signs of a barometric pressure influence, it does not necessarily mean the aquifer will also show a response to earth tides. The magnitude of barometric pressure forces appears to be great enough to cause a noticeable impact on hydrothermal aquifer discharge. The magnitude of earth tide forces appears to be too weak to cause noticeable discharge fluctuations. Perhaps if the same type of study were done during a spring tide event (period when forces of high tide and low tide are at their greatest difference), a noticeable correspondence could be seen.

5.2 Spectral Analysis

By comparing results of spectral analysis of flow data, tide data, and barometric pressure data, correspondences can be drawn between fluctuation patterns seen in tide and barometric pressure and patterns found in flow data. Similarities found between patterns in flow and patterns found in barometric pressure or tides would not prove, but may help explain controls on hydrothermal aquifers. The link from correspondence to correlation between signals cannot be made absolutely. However by performing a visual and then, statistical analysis of patterns found, we can state with a certain degree of confidence that a correlation is likely or unlikely. Although there is error introduced in data collection and analysis (discussed in 4.2 Spectral Analysis Results), each frequency, assigned a power by the Fourier Transform, can be statistically determined significant or not.

Before discussing results of the spectral analysis, it is important to first discuss restrictions of the analysis. A major unavoidable restriction was that sample intervals in

analyzed data must follow rules of the Nyquist-Shannon sampling theorem. That is, the sample interval (f_s) used in each data set was greater then two times the highest frequency (B) (fs > 2B) (Shannon, 1949). Therefore with a sampling interval of 15 minutes, the smallest observable time pattern we could correctly identify would be a frequency with a period of 30 minutes. If higher discharge frequencies existed, they would be aliased. Aliased frequencies would be shown in the spectral analysis by repeated patterns at even frequency intervals. For example, if a high frequency with a time period of 2 minutes were present, we would see a spike in our graph at 30 minutes, 60 minutes, 90 minutes and so on, representing the 2 minute pattern. As our FloDar devise collected data, it would not see this 2 minute change in discharge at its first 15 minute sample, it would catch it at 30 minutes, miss it at 45 minutes, catch it at 60, and so on. Frequencies that could be aliased would have a time period at anything less then 30 minutes. Lower frequencies that would be aliased, would be represented by longer time periods. For example, a signal that repeated every 29 minutes would show up as a spike on our graph every 7 hours 15 minutes.

The 15-minute sample intervals would be sufficient to capture any affects earth tides may have on the hydrothermal aquifers. The highest tidal frequency (S_2) has a time period of around 12 hours. As oversampling does not create a problem in data analysis, the sample interval for tides has been well documented and generally accepted that using a two hour sample interval is sufficient for earth tide analysis (Ray and Cartwright, 2007). Nevertheless, many studies still use a one-hour sample interval, a 45-minute interval, and some even use less down to a six-minute time interval (Arabelos et al., 2003; Ray and

Cartwright, 2007). Analyzing six-minute time interval data collected at Depoe bay in this study was thought to be more then sufficient to reconstruct a continuous time sample from a discrete dataset as described by the Whittaker-Shannon interpolation formula (described in methods 3.2).

Barometric pressure analysis can be a bit more complicated as changes in barometric pressure are a result of atmospheric trends (Arabelos, 2001). A one-hour sample interval has been accepted as sufficient in order to properly reconstruct the continuous time sample from the discrete dataset. However many choose to err on the side of caution and sample at a smaller time interval such as 5 minutes (Arabelos, 2001). Analyzing barometric pressure data at a time interval of five minutes was also thought to be sufficient to prevent aliasing of a barometric signal.

Rabbit Creek

Spectral analysis of Rabbit Creek flow data revealed statistically significant (confidence interval of 95%) time patterns at 2.13 days and at 8.5 hours, neither of which corresponded to patterns in tides and barometric pressure. Assuming sampling intervals for tides (Arabelos, et al., 2003, Ray and Cartwright, 2007) and barometric pressure (Arabelos, 2001) were sufficient, we would expect to see similar time patterns of discharge in analysis of our recorded flow data. If such influences were present in Rabbit Creek, expected time patterns from earth tidal influence would be approximately 12.5 hours and 23 hours as determined by the spectral analysis of tidal data collected at Depoe

Bay during the same time period. Analysis of barometric pressure data during the Rabbit Creek study time revealed that if influence from barometric pressure were present, there should be a related time pattern in discharge data at around 4 days. As these time patterns are absent in the discharge data, it appears that neither of these hypothesized controls are present at Rabbit Creek. Statistically significant patterns found may be a result of aliased shorter time period patterns. However if earth tides and barometric pressure did have an influence on the aquifer, we would still expect to see statistically significant patterns at similar time intervals as were found in analysis of those datasets.

White Creek

Spectral analysis of White Creek flow data revealed statistically significant (95 % confidence) time patterns at 3.6 days, at 23.3 hours, at 8.5 hours, and at 3.3 hours. Statistically significant time patterns revealed in analysis of Depoe Bay observed tides were at 23 hours and 12.1 hours. Analysis of barometric pressure revealed a statistically significant time pattern at 5.3 days. Similar time patters exist at approximately 23 hours between stream-flow analysis and in observed tide analysis. This similarity suggests one of two things. Either there is some influence from earth tides on the aquifers feeding White Creek, or this similar time pattern is a coincidence.

White Creek and Rabbit Creek are relatively close geographically; however one major difference between the two streams is that White Creek has a small amount of cool, shallow ground water (not quantified) input at its source (Gibson, 1999). Why White

Creek may be showing some influence from earth tides while Rabbit Creek does not may be due to White's cool shallow ground water source. Earth tides may be acting on it, creating regular pulses in discharge, while the deeper thermal aquifer is not affected.

The difference between the observed tidal pattern at 23.3 hours and the normal tidal period (P_1) of 24.07 hours can be explained by the dynamic tidal theory (described in section 1.4 confined aquifer controls) where the complexities of the real world ocean tidal system often reveal observed timing to be slightly different then hypothesized.

Tantalus Creek

Spectral analysis of Tantalus Creek flow data revealed one statistically significant (95 % confidence) time pattern at 5.3 days. Observed tide analysis during the Tantalus Creek study time revealed time patterns at 12.8 hours and 25.6 hours. Barometric pressure analysis revealed a time patterns at 5.3 days. The similarity between patterns observed in barometric pressure fluctuations and fluctuations in discharge in Tantalus Creek suggest that the aquifer discharging to Tantalus Creek may be influenced by barometric pressure. This similarity helps to support the hypothesis of a barometric pressure control. However this similarity could simply be a coincidence. The 5.3 days pattern is not an aliased signal. If undersampling and aliasing had occurred, we would see in our spectral analysis more then one significant pattern. For example, if a major pattern occurred every 13 minutes and our sampling interval was 15 minutes, we may expect to see patterns in our analysis at 3 hours 15 minutes, another at 7 hours 30 minutes, another at 10 hours 45 minutes and so on, every 3 hours and 15 minutes we would catch the 13 minute pattern.

Aliased higher frequencies would show patterns at shorter periods. For example, if a pattern in discharge were present every two minutes, we would see major patterns more often, at 30 minutes, 60 minutes, 90 minutes, and so on. Aliased longer frequencies would show patterns at longer periods. For example, if a pattern in discharge were present at 29 minutes, we would see major patterns every 7 hours 15 minutes. Scatter in the spectral analysis graph may show some minor aliased signals, however the one major frequency observed at Tantalus Creek suggests that no major patterns in discharge were aliased.

8.5 hour time pattern at Rabbit and White Creek

Analysis of both Rabbit and White Creek revealed statistically significant (95 % confidence) time patterns at 8.5 hours. This pattern cannot be related to either earth-tide influences on the aquifer or to barometric-pressure influences as each influence would have shown time patterns of hours to days longer.

If this time period were related to an under sampled shorter time pattern we would expect to see similar strength patterns at 4 hours 15 minutes and other strong patterns at longer time periods associated with a 17-minute discharge pattern. As patterns are not seen at those times, we can state that the 8.5-hour pattern observed is not a result of an aliased signal.

The similarity in occurrence at each site suggests the possibility of a connection between the sites on some level. The common time pattern could also be the result of independent factors at work in each site, coincidentally causing a similar time pattern.

One explanation might be that this pattern is related to the hot springs discharging into each of these streams. The aquifer(s) feeding the hot springs may be controlled by a similar factor. A shared hydrothermal aquifer convectively heating and discharging fluid at surface springs may offer an explanation. As hydrothermal fluids are heated, they rise in plumes and discharge at the surface. Once the superheated fluids leave the aquifer, cooler recharge enters the aquifer, is slowly heated, and begins to become more pressurized by the expanding heat energy until at about 8.5 hours another plume is pushed up through fractures to again discharge at the surface.

	Geochemistry	
	White Creek	Rabbit Creek
pH	8.25	9.54
F	9.03	27.21
Cl	58.17	289.61
SO4	20.00	18.35
CACO3	127.53	297.88

Table 6. Geochemical data for waters of White Creek and Rabbit Creek. Values are averaged from seasonal sampling, and from 3 sites near the study area. Units are mg/l (Gibson, 1999; Vitale, 2002).

If the hot springs discharging into these streams do in fact share the same aquifer, similar geochemical compositions of fluid might be expected. However the only similarities observed are that both streams have fairly high pH and show similar values of SO_4 (table 3). All other measured constituents differ.

Variations in Cl and alkalinity ($CaCO_3$) can result from varying degrees of cooling, decompressional boiling and mixing with shallow groundwater (Fourier, 1989). The geochemical data do not support the hypothesis that a shared aquifer is feeding the two sites. However even if the streams share the same source aquifer, geochemistry of the waters can vary significantly over a distance of 2.5 km (Fourier, 1989). As the hydrothermal fluids circulate they react with local parent rock to dissolve minerals (Fourier, 1989). Upon reaching the surface, hydrothermal fluids cool and precipitate some minerals previously dissolved (Si, $CaCO_3$). Y-5 and Y-2 drill logs showed that stratigraphy in each area does differ, which may also explain some differences observed in the geochemical compositions. Y-5 drilled in the Rabbit Creek basin penetrated the Lava Creek Tuff while Y-2 drilled in the White Creek area penetrated the Elephant Back Rhyolite. Another factor potentially contributing differences in geochemistry could be the shallow cool groundwater source feeding White Creek, diluting the hydrothermal fluid. If shallow groundwater mixing was diluting the geochemistry of White Creek, we may still see proportionately similar ratios of certain chemicals, however no two of the values listed in table 6 have a similar ratio.

Although the geochemistry of the two steams does not outright support or refute a shared hydrothermal aquifer, the 8.5-hour discharge time pattern observed in each site may still be a sign of a similar aquifer control at Rabbit and White Creek. This pattern may be a result of convective heating in a shared aquifer, but could also be a similar heat source heating separate aquifers of similar sizes, volumes, and depths. If any one of those

factors were different, (ie. one aquifer is larger, or deeper, or holds a smaller volume of water) the heat source might still cause convective heating/discharge, but would do it at different rates in each aquifer. The 8.5-hour time pattern may be a result of a similar aquifer control, or may be a coincidence.

5.3 Further Study

Time constraints restricted data collection to periods of convenience rather than periods of maximum likelihood of observing physical impacts of tidal or barometric forces on hydrothermal discharge. When designing a similar future study, factors that should be addressed in the design process of the experiment include: study time selection, sample interval selection, and data acquisition. Selection of study time should include selecting sampling periods that occur during maximum likelihood of hypothesized forces on the aquifer. Sampling times should be selected that occur during springs tides (full moons) and neap tides (quarter moons). Although it is hard to predict, it would be useful to select another sample period that occurred during periods of dramatic changes in barometric pressure and sample periods where dramatic precipitation events were shortly followed by times of no precipitation. Selecting a sampling interval so that aliasing of signals is minimized is also important. In order to do this, knowledge of the shortest time pattern is important. A data recorder similar to a clock driven chart recorder used in several USGS gaging stations could be used to collect continuous flow data that could be analyzed to determine the shortest time patterns in flow changes. Once determined, subtracting a conservative amount of time would provide the necessary time sampling interval so

aliasing would be minimized. Over sampling does not pose a problem, however under sampling can lead to an unknown degree of uncertainty, as it did in this study. Data acquisition in a future study should include adding barometric pressure loggers to the field station equipment in order to collect accurate local barometric pressure measurements. Water temperature loggers should also be deployed with the FloDar to record fluctuations in heat discharge as well as flow discharge. Although some geochemical data exist for each site, future studies may also focus on analyzing the previously collected data and analyzing new data to determine source temperatures, decompressional boiling rates for certain springs, and if any mixing with shallow groundwater existed.

6.0 Conclusion

This study has shown that through both graphical analysis and spectral analysis, patterns found at Rabbit Creek did not appear to correspond to earth tides or barometric pressure. Graphical analysis of data for Rabbit Creek neither supports nor refutes the hypothesis of precipitation or earthquake influence on hydrothermal discharge. At White Creek, barometric pressure and earth tides appear to possibly have a control on thermal fluid discharge. Statistical correlation analysis was not performed for any of the data and therefore, the apparent control on discharge at White Creek from earth tides and barometric pressure can not be supported or refuted as the apparent similarities in time patterns may simply be coincidental. Graphical analysis for White Creek showed similar results to that of Rabbit Creek. The hypothesized controls from precipitation and earthquakes can also not be supported or refuted due to the lack of occurrence during the sampling periods. Spectral analysis of data for Tantalus Creek showed a correspondence between changes in flow and changes in barometric pressure. Only one significant time pattern of discharge was found at Tantalus Creek. This time pattern was similar to that found in analysis of barometric pressure, suggesting that barometric pressure does have an influence on discharge. This similarity in time patterns may actually be cause-and-effect, but also could simply be coincidental. Graphical analysis appeared to reveal a correspondence between changes in barometric pressure and changes in flow. Graphical analysis also appeared to show a response in flow changes due to precipitation, however as no further analysis was completed to determine whether or not the hydrothermal aquifer was responding due to the precipitation increasing the load on the land surface, or

if changes in flow observed were simply due to increased surface run off, the hypothesis of a precipitation control on hydrothermal discharge at Tantalus Creek cannot be supported or rejected. The hypothesized influence of barometric pressure controlling discharge at Tantalus Creek is likely, however cannot be supported as again, it may simply be coincidental.

A time pattern in discharge at 8.5 hours appears in both White Creek and Rabbit Creek. This pattern may be coincidental or it may represent an actual link between the sites. A possible connection between the sites could be a shared hydrothermal aquifer convectively releasing plumes of thermal fluids that discharge at surface springs at the same time interval, or it could also simply be coincidental.

In conclusion, the complexity of hydrothermal systems continues to provide potential for further research into this subject. Controls on thermal discharge are important to understand as they provide yet another building block in the knowledge base of thermal features. Understanding past and present variability in discharge can help predict future changes in the hydrothermal system.

References Cited

Allen, E. T., Day, A. L. (1935). Hot springs of the Yellowstone National Park. Carnegie Institute of Washington.525.

Arabelos, D. N., Asteriadis, G., Bloutsos, A., Contadakis, M.E., Spatalas, S.D. (2003). "Atmospheric tide disturbances as earthquake precursory phenomena." Natural Hazards and Earth Sciences **4**: 1-7.

Arabelos, D. N., Asteriadis, G., Contadakis, M.E., Spatalas, S.D. (2001). "An analysis of a twenty-seven years data for atmospheric tides disturbances in the area of Thessaloniki-North Greece and their correlation with the seismicity in this area." Geodesy and Surveying. 8.

Bargar, K. E., Beeson, M. H. (1980). Hydrothermal alteration in Yellowstone geyser basins, U.S. Geological Survey**: P-1175**: 59.

Barger, V. D., Olsson, M. G. (1973). Classical Mechanics, A Modern Perspective, McGraw-Hill, Columbus, OH**:** 265-274.

Benz, H. M., Smith, R. B. (1984). "Simultaneous inversion for lateral velocity variations and hypocenters in the Yellowstone region using earthquake and refraction data." Geophysical Research. **89**: 1208-1220.

Berrino, G., Coppa, U., Corrado, G. (1991). Tidal field and volcanic activity in Southern Italy. Proceedings 11th symp. Earth Tides, Helsinki, Schweizerbartsche Verlagsbuchhandlung Stuttgart. International Center for Earth Tides. 387-388.

Berrino, G., Coppa, U., Corrado, G., LoBascio, A., Luongo, G. (1988). Tidal field and dynamics at some active volcanoes in Southern Italy. Proceedings Kagoshima Int. Conference on Volcanoes. International Center for Earth Tides. 362-365.

Blackwell, D. D. (1969). "Heat-flow determinations in the northwestern United States." Geophysical Research**74**: 992-1007.

Boyd, F. R. (1961). "Welded tuffs and flows in the rhyolite plateau of Yellowstone Park, Wyoming." Geological Society of America Bulletin **72**(387-426).

Bredehoeft, J. (1967). "Well-aquifer systems and Earth tides." Geophysical Research **72**: 3075-3087.

Brigham, E. O. (1988). The fast Fourier transform and its applications. Englewood Cliffs, NJ, Prentice Hall.

Brown, E. W. (1925). "Tidal oscillations in Halemaumau." American Journal of Science. **5**: 9-95.

Christiansen, R. L. (1972). Volcanic stratigraphy of the Quaternary rhyolite plateau in Yellowstone National Park, U.S. Geological Survey. **729-B**: 18.

Christiansen, R. L. (1974). "Quaternary volcanism of the Yellowstone rhyolite plateau region, Wyoming-Idaho-Montana [abs.]." American Geophysical Union Transactions **56**: 1189.

Christiansen, R. L. (1979). "Cooling units and composite sheets in relation to caldera structure, in Chapin, C. E., eds., Ash-flow tuffs." Geological Society of America Special Paper **180**: 29-42.

Christiansen, R. L. (2001). The Quaternary and Pliocene Yellowstone Plateau volcanic field of Wyoming, Idaho, and Montana, U.S. Geological Survey. **729-G**: 145a.

Clark, W. E. (1967). Computing the barometric efficiency of a well. American Society of Civil Engineers, Journal of the Hydraulic Division Proceedings. **93(HY4)**: 93-98.

Cohee, G. V. (Chairman). (1962). Tectonic map of the United States. U.S. Geological Survey and American Association of Petroleum Geologists. Scale 1:2,500,000.

Cooley, J., Tukey (1965). "An algorithm for the machine calculation of complex Fourier series." Math Comput. **19**: 297-301.

Davis, P. M. (1981). "Gravity and tilt Earth tides measured on an active volcano, Mt. Etna, Sicily." Journal of Volcanology and Geothermal Research **11**: 213-233.

Dutt, R., V. (1993). "Fast Fourier transforms for nonsequispaced data." SIAM Journal of Science Comput. **14**(6): 1368-1393.

Dutt, R., V. (1995). "An improved fast multipole algorithm for potential fields." Technical report, Yale University **1089**.

Dzurisin, D. (1980). "Influence of fortnightly Earth tides at Kilauea volcano, Hawaii." Geophysical Research Letters **7**: 925-928.

Eaton, G. P., Christiansen, R. L., Iyer, H. M., Mabey, D. R., Blank, J. R., Zietz, I., Gettings, M. E. (1975). "Magma beneath Yellowstone National Park." Science **188**: 787-796.

Fadeli, A., Rydelek, P. A., Emter, D., Zurn, W. (1991). "On volcanic shocks at Merapi and tidal triggering." Volcanic tremor and magma flow, Forschungszentrum Julich, Germany. International Center for Earth Tides. 165-181.

Farnetani, C. G., Samuel, H. (2005). "Beyond the thermal plume paradigm." Geophysical Research Letters **32 LO7311**.

Farrar, C. D., Sorey, M. L., Rojstaczer, S. A., Junic, C. J., Winnett, T. L., Clark, M. D. (1985). Hydrologic and geochemical monitoring in Long Valley caldera, Mono County, California, U.S. Geological Survey Water Resources Investigations. **87-4090**: 71.

Fenneman, N. M. (1931). Physiography of the Western United States. New York, McGraw-Hill. 534.

Ferris, M. M., Nold, S. C., Santegoeds, C. M., Ward, D. M. (2001). Examining bacterial population diversity within the Octopus Spring microbial mat community. thermophiles: biodiversity, ecology and evolution. New York, Kluwer Academic/ Plenum Publishers, ed. Reysenbach et al.**:** 51-64.

Fetter, C. W. (2000). Applied Hydrogeology, Prentice Hall, Eglewood Cliffs, NJ. 691.

Finn, C. A., Morgan, L. A. (2002). "High-resolution aeromagnetic mapping of volcanic terrain, Yellowstone National Park." Journal of Volcanology and Geothermal Research **115**: 207-231.

Fitts, C. R. (2002). Groundwater Science, Academic Press, San Diego, CA. 450.

Fleming, S. W., Quilty, E.J. (2006). "Aquifer responses to El Nino-southern oscillation, Southwest British Columbia." Ground Water **44**(4): 595.

FloDar (2002). specification, Marsh-McBirney. http://www.marsh-mcbirney.com/Products/open_channel.htm (March, 2006).

Fournier, R. O. (1989). "Geochemistry and dynamics of the Yellowstone National Park hydrothermal system." Annual Reviews of Earth and Planetary Science **17**: 13-53.

Fournier, R. O., Pitt, A. M. (1985). The Yellowstone magmatic-hydrothermal system, U.S.A. Geothermal Resources Council International Symposium on Geothermal Energy. 319-327.

Fournier, R. O., Thompson, J. M., Hutchinson, R. A. (1994). "The geochemistry of hot spring waters at Norris Geyser Basin, Yellowstone National Park." Transactions-Geothermal Resource Council **18**: 177-179.

Fournier, R. O., White, D. E., Truesdell, A. H (1976). Convective heat flow in Yellowstone National Park. Second United Nations Symposium on Develpment and Use of Geothermal Resources Proceedings, San Francisco, CA. 731-739.

Freeze, R. A., Cherry, J. A. (1979). Groundwater. Englewood Cliffs, NJ, Prentice-Hall, Inc. 604.

Friedman, I., Norton, D.R., Hutchinson, R. A. (2000). Data used for calculating chloride flux out of Yellowstone National Park for the water years 1983-1999, U.S. Geological Survey**. OF-00-0194**: 48.

Fritz, W. J. (1985). Roadside Geology of the Yellowstone Country. Missoula, MT, Mountain Press.149.

Furbish, D. J. (1997). Fluid Physics in Geology: An introduction to fluid motions on Earth's surface and within its crust. New York, Oxford University Press.496.

Gibson, M. L. (1999). Hydrothermal water/groundwater interaction: a compatative study of electromagnetic terrain-conductivity mapping and standard hydrogeochemical techniques. Unpubl. Masters Thesis, University of Montana**:** 153.

Gieske, A., DeVries, J. (1987). "An Analysis of Earth-Tide-Induced Groundwater Flow in Eastern Botswana." Hydrology **82**(3-4): 211-232.

Gooch, F. A., Whitfield, J. E. (1888). Analysis of waters of the Yellowstone National Park, with an account of the methods of analysis employed, Chemical News and Journal of Industrial Science. 441.

Goodmajn, W. (1968). Introduction to Fourier Optics. San Francisco, CA, McGraw-Hill. 441.

Hamilton, W. L. (1973). "Tidal cycles of volcanic eruptions--fortnightly to 19 yearly periods." Geophysical Research. **78**(17): 3363-3375.

Henley, R. W., Truesdell, A. H., Barton, P. B., Whitney, J.A. (1984). "Fluid-Mineral Equilibria in Hydrothermal Systems." Soc of Economic Geologists. **001**: 235.

Hsieh, P. A., et al. (1987). "Determination of aquifer transmissivity from earth tide analysis." Water Resource **23**(10): 1824-1832.

Husen, S., Smith, R. B., Waite, G. P. (2004). "Evidence for gas and magmatic sources beneath the Yellowstone volcanic field from seismic tomographic imagin." Volcanology and Geothermal Res. **131**: 397-410.

Husen, S., Taylor, R., Smith, R. B., Healser, H. (2004). "Changes in geyser eruption behavior and remotely triggered seismicity in Yellowstone National Park produced by the 2002 M 7.9 Denali fault earthquake, Alaska." Geology **32**(6): 537-540.

Hutchinson, R. A. (1985). "Hydrothermal changes in the Upper Geyser Basin, Yellowstone National Park, after 1983 Borah Peak earthquake. In: Stein, R. S., Bucknam, R. C., Proceeding of workshop XXVIII on the Borah Peak earthquake." U.S. Geological Survey Open-File Report 85-290 **A**: 612-624.

Igarashi, G., Wakita, H. (1991). "Tidal responses and earthquake-related changes in the water level of deep wells." Geophysical Research. **96**(B3): 4269-4278.

Ingebritsen, S. E., Galloway, D. L., Colvard, E. M., Sorey, M. L., Mariner, R. H. (2001). "Time-variation of hydrothermal discharge at selected sites in the Western United

States: Implications for monitoring." Volcanology and Geothermal Research. **111**(I. 1-4): 1-23.

Ingebritsen, S. E., Rojstaczer, S. A. (1993). "Controls on Geyser Periodicity." Science **262**: 889.

Ingebritsen, S. E., Rojstaczer, S. A.Ge (1996). "Geyser periodicity and the response of geysers to deformation." Geophysical Research B: Solid Earth **101**(B10): 21891-21905.

Ingebritsen, S. E., Sorey, M. L. (1988). "Vapor-dominated zones within hydrothermal systems: evolution and natural state." Geophysical Research **93**(B11): 13635-13655.

Inkenbrandt, P. C., Doss, P. K., Pickett, T. J. (2005). Barometric and Earth-tide induced water level changes Inglefield sandstone in Southwestern Indiana. Proceedings of the Indiana Academy of Science, Denver, CO.

Iyer, H. M., Evans, J. R., Zandt, G., Stewart, R. M., Coakley, J. M., and Roloff, J. N. (1981). "A deep low-velocity body under the Yellowstone caldera, Wyoming: Delineation using teleseismic P-wave residuals and tectonic interpretation." Geological Society of America Bulletin, part II **92**: 1471-1646.

Jacob, C. E. (1940). On the flow of water in an elastic artesian aquifer. Transactions of the American Geophysical Union 21, Part II. 574-586.

Jaggar, T. A. (1924). "The lava tide, seasonal tilt, and the volcanic cycle." Monthly Weather Review **52**: 142-147.

Jentzsch, G. (1995). Mayon volcano: ocean tidal loading triggering activities. Proceedings 12th int. symp. on earth tides, Beijing, China, Science Press. 487-500.

Jern, M. (1999). "Visual intelligence-turning data into knowledge." Information Visualization. **1999**: 3-8.

Keefer, W. R. (1970). Structural geology of the Wind River Basin, Wyoming, U.S. Geological Survey**: 495-D**: 21.

Keith, T. E. C., Muffler, L. J. P. (1978). "Minerals produced during cooling and hydrothermal alteration of ash flow tuff from Yellowstone drill hole Y-5." Journal of Volcanology and Geothermal Research. **3:** (373-402).

Kharaka, Y. K., Mariner, R. H., Bullen, T. D., Kennedy, B. M., Sturchio, N. C. (1991). Geochemical investigations of hydraulic connections between the Corwin Springs known geothermal resources area and adjacent parts of Yellowstone National Park. Effects of potential geothermal development in the Corwin Springs known geothermal resources area, Montana, on the thermal features of Yellowstone National Park. M. L. Sorey**:** F1-F37.

Kharaka, Y. K., Thordsen, J. J., White, L. D. (2002). Isotopic and chemical compositions of meteoric and thermal waters and snow from the greater Yellowstone National Park Region, U.S. Geological Survey**:** 75.

Kvale, E. P. (2006). "The origin of neap--spring tidal cycles." Marine Geology **235**: 5-18.

Lanphere, M. A., Champion, D.E., Christiansen, R.L., Izett, G.A., Obradovich, J.D. (2002). "Revised ages for tuffs of the Yellowstone Plateau Volcanic field: Assignment of the Huckleberry Ridge Tuff to a new geomagnetic polarity event." Geological Society of America Bulletin. **114**(5): 559-568.

Lehman, J. A., Smith, R. B., Schilly, M. M., Braile, L. W. (1982). "Upper crustal structure of the Yellowstone caldera from seismic delay time analyses and gravity correlations." Geophysical Research. **87**: 2713-2730.

Licciardi, J. M., Clark, P. U., Brook, E. J., Pierce, K. L., Kurz, M. D., Elmore, D., Sharma, P. (2001). "Cosmogenic 3He and 10Be chronologies of the late Pinedale Northern Yellowstone ice cap, Montana, USA." Geology **29**(12): 1095-1098.

Lowenstern, J. B., Smith, R. B., Hill, D. P. (2006). Monitoring super-volcanoes: geophysical and geochemical signals at Yellowstone and other large caldera systems. Philosphical Transactions.

LTN-brochure (2005). "Performing environmentally sensitive field research in Yellowstone National Park." a guide for research scientists.

Marks, R. J. (1991). Introduction to Shannon Sampling and Interpolation Theory, Springer Text, New York. 332.

Marler, G. D., White, D. E. (1977). "Evolution of seismic Geyser, Yellowstone National Park." Earthquake Inf. Bulletin **9**: 21-25.

Melchior, P. (1974). "Earth Tides." Surveys in Geophysics **1**: 275-303.

Miller, D. S., Smith, R. B. (1999). "Pand S velocity structure of the Yellowstone volcanic field from local earthquake and controlled-source tomography." Geophysical Research. **104**(B7): 15105-15121.

Morrison, D., Owen, T. (1966). The Planetary System, Addison-Wesley.

Norton, D. R., Friedman, I., Mohrman, J., Hutchinson, R. A. (1989). Monitoring of thermal activity in the northern part of Yellowstone National Park and vicinity: Part I: Feb. 1985-June 1988, U.S. Geological Survey**:** 35.

NPS (1998). "Yellowstone National Park Digital Raster Graphics UTM Zone 12; NAD 83." Spatial Analysis Center Yellowstone Center for Resources.

NPS (2006). Yellowstone National Park basic road map, National Parks Service.

Obradovich, J. D. (1992). Geochronology of the late Cenozoic volcanism of Yellowstone National Park and adjoining areas, Wyoming and Idaho, U.S. Geological Survey**. 92-408**: 45.

Obradovich, J. D. C. (1973). "unpub. data." USGS.

Oppenheim, A. V., Schafer, R. W., Buck, J. R. (1999). Discrete-time signal processing. Upper Saddle River, NJ, Prentice Hall. 870.

Pascal, B. (1973). The physical treatises of Pascal. New York, Octagon Books.

Perkins, M. E., Nash, B. P. (2002). "Explosive silicic volcanism of the Yellowstone hotspot: the ashfall tuff record." Geological Society of America Bulletin **114**: 367-381.

Powers, H. A., Young, E. G., Barnett, P. R. (1958). "Possible extension into Idaho, Nevada, and Utah of the Pearlette ash of Meade County, Kansas [abs.]." Geological Society of America Bulletin. **69**: 1631.

Pugh, D. T. (1987). Tides, surges and mean sea level. New York, John Wiley and Sons.

Ray, R. D., and Cartwright, D.E. (2007). "Times of peak astronomical tides." Geophisical Research. **168**: 999-1004.

Richmond, G. M. (1986). "Stratigraphy and chronology of glaciations in Yellowstone National Park." Quaternary Science Reviews. **5**: 83-98.

Rinehart, J. (1972). "Fluctuations in geyser activity caused by variations in Earth tidal forces, barometric pressure, and tectonic stresses." Geophysical Research. **77**(2): 342-350.

Robinson, E. S., Bell, R. T. (1971). "Tides in confined well-aquifer systems." Geophysical Research. **76**: 1857-1869.

Robinson, T. W. (1939). "Earth-tides shown by fluctuations of water-levels in wells in New Mexico and Iowa." Transactions of the American Geophysical Union **20**: 656-666.

Rockmore, D. N. (1999). "The FFT- an algorithm the whole family can use." Departments of Mathematics and Computer Science, Dartmouth College, NH. 9.

Rojstaczer, S. A. (1988). "The response of the water level in a well to atmospheric loading." Water Resource Research. **24**(11): 1927-1938.

Rojstaczer, S. A., Galloway, D. L., Ingebritsen, S. E., Rubin, D. M. (2003). "Variability in geyser eruptive timing and its causes: Yellowstone National Park." Geophisical Research. **30**(18): 1953.

Ross, D. A. (1995). Introduction to Oceanography. New York, NY, Harper Collins**:** 236-242.

Rowe, J. J., Fournier, R. O., Morey, G. W. (1973). Chemical analysis of thermal waters in Yellowstone National Park, Wyoming, 1960-1965, U.S. Geological Survey**. 1303**: 31.

Shannon, C. E. (1949). "A mathematical theory of communication." Bell System Technical Journal **27**: 379-423, 623-656.

Shumway, R. H., Stoffer, D. S. (2006). Time series analysis and its applications with R examples, Springer. 572.

Silver, P. G., Valette-Silver, N. J. (1992). "Detection of hydrothermal precursors to large Northern California earthquakes." Science **257**(5075): 1363-1368.

Smith, R. B., Braile, L. W. (1984). "Crustal structure and evolution of an explosive silicic volcanic system at Yellowstone National Park, in explosive volcanism: Washington." National Academy of Sciences: 96-109.

Sophocleous, M., Bardley, E., Healey, J., Engard, B. (2004). "Can precipitation loading be detected at 300-meter depth or greater?" Kansas Geological Survey Open-file Report 2004-46.

Sorey, M. L., ed. (1991). Effects of potential geothermal development in the Corwin Springs known geothermal resources area, Montana, on the thermal features of Yellowstone National Park, U.S. Geological Survey Water Resources Investigations. **91-4052**: 207.

Sorey, M. L., Evans, W. C., Kennedy, B. M., Farrar, C. D., Hainsworth, L. J., Hausback, B. (1998). "Carbon dioxide and helium emissions from a reservoir of magmatic gas beneath Mammoth Mountain." Geophysical Research. **103**: 15303-15323.

Spane, F. A. (1999). Effects of barometric fluctuations on well water-level measurements and aquifer test data. Richland, WA, Pacific Northwest National Laboratory. **PNNL-13078**: 59.

Stein, E. M., Weiss, G. (1871). Introduction to Fourier analysis on Euclidean spaces, Princeton University Press. 312.

Streepey, M. (1996). Geysers and the Earth's plumbing systems, University of Michigan publications. **GS662**: 8.

Thompson, J. M., DeMonge, J. M. (1996). Chemical analysis of hot springs, pools, and geysers from Yellowstone National Park, Wyoming, and vicinity, 1980-1993, U.S. Geological Survey**. OF-96-0068**: 66.

Thompson, J. M., Presser, T. S., Barnes, R. B., Bird, D. B. (1975). Chemical analyses of the waters of Yellowstone National Park, Wyoming, from 1965-1973, U.S. Geological Survey**. 75-25**: 59.

Thompson, J. M., Yadav, S. (1979). Chemical analyses of waters from geysers, hot springs, and pools in Yellowstone National Park, Wyoming, from 1974-1978, U.S. Geological Survey**. 79-704**: 49.

Thordsen, J. J., Kharaka, Y. K., Mariner, R. H., White, L. D. (1992). Controls on the distribution of stable isotopes of meteoric water and snow in the greater Yellowstone National Park region. USA Proceedings of the 7th International Symposium on Water-Rock Interaction. Ed. A. A. Balkema. **1**: 591-595.

Thornbury, W. D. (1965). Regional geomorphology of the United States. New York, NY, Wiley. 418.

Thurman, H. V. (1994). Introductory Oceanography. New York, NY, Macmillan**:** 252-276.

Toll, N. J., Rasmussen, T. C. (2007). "Removal of barometric pressure effects and Earth tides from observed water levels." Ground Water. **45**(1): 101-105.

Venkataramani, R. B., Y. (2000). "Perfect reconstruction formulas and bounds on aliasing error insub-Nyquist nonuniform sampling of multiband signals." Information Theory, IEEE Transactions. **46**(6): 2173-2183.

Vitale, M. V. (2002). Factors controlling the formation of mineral precipitates lining the channel in Rabbit Creek, Yellowstone National Park, Wyoming, Unpubl. Master's Thesis, University of Montana**:** 176.

Vorhis, R. C. (1964). "Earthquake-induced water-leve fluctuations from a well in Dawson County, Georgia." Seismological Society of America Bulletin. **54**: 1023-1133.

Vorhis, R. C. (1995). "Interpretation of hydrologic data resulting from earthquakes." Geologische Rundschau. **43**: 47-52.

Wahr, J. (1995). Earth Tides. Global Earth Physics, A Handbook of Physical Constants, AGU Reference Shelf**:** 40-46.

Waite, G. P., Schutt, D. L., Smith, R. B. (2005). "Models of lithosphere and asthenosphere anisotropic structure of the Yellowstone hot spot from shear wave splitting." Geophysical Research. **110**: B11304.

Waite, G. P., Smith, R. B. (2002). "Seismic evidence for fluid migration accompanying subsidence of the Yellowstone caldera." Geophisical Research B: Solid Earth **107:** 9.

Waite, G. P., Smith, R. B., Allen, R. M. (2005). "Vp and Vs structure of the Yellowstone hot spot from teleseismic tomography: evidence for an upper mantle plume." Geophysical Research. **111**: B04303.

Waldrop, H. A., Pierce, K.L. (1975). "Surficial geologic map of the Madison Junction quadrangle, Yellowstone National Park, Wyoming." U.S. Geological Survey Miscellaneous Investigations **Map**(I-615).

White, D. E. (1967). "Some principles of geyser activity, mainly from Steamboat Springs, Nevada." American Journal of Science. **256**: 641-684.

White, D. E., Fournier, R. O., Muffler, L. J. P., Truesdell, A. H. (1975). Physical results of research drilling in the thermal areas of Yellowstone National Park, Wyoming, U.S. Geological Survey**. 892**: 77.

White, D. E., Hutchinson, R.A., Keith, T.C. (1988). "The geology and remarkable thermal activity of Norris Geyser Basin, Yellowstone National Park, Wyoming." U.S. Geological Survey. **P 1456**: 84.

Yahoo (2006). Yahoo Maps. www.maps.yahoo.com. March, 2006.

Yaun, H., Dueker, K. (2005). "Teleseismic P-wave tomogram of the Yellowstone plume." Geophisical Research. **32**: L07304.

Zarriello, P. J., Barlow, P.M., Duda, P.B. (2001). "Simulating the effects of ground-water withdrawals on streamflow in a precipitation runoff model." Civil Engineering. **103**: 407.

Appendix A

Using Excel for Spectral Analysis

By using Excel we are able to calculate the complex coefficients from the time series data. Excel's Fourier transform routine requires that the number of samples in the time series be a power of 2, i.e. $n=2^n$. Output data are 15 digit real and imaginary numbers. The first and last output numbers are real and represent the zero frequency. Output data is duplicated around n/2 (the second ½ of data are a mirror of the first half).

Step 1.) Determine sampling parameters.

Parameters of Sampling			Explanation/Formulas
N_points	1024		Total Number of sample points
total_time	921600	seconds	Total time represented by number of samples (=time_bin*N_points)
time_bin	900	seconds	Seconds Per Cycle (=15 minutes*(60 seconds/minute))
f_folding	0.000556	Hz	Mid data Frequency, where data is mirrored (=N_points/2*total time)
freq_bin	1.09E-06	Hz	frequency value per output number (=2*f_folding/N_points)

Step 2.) Process Data with Excel FT.

a.) Click "data analysis" under "tools" header, select "Fourier Analysis"

b.) Select Input and output range (remember number of input data must be a power of 2.)

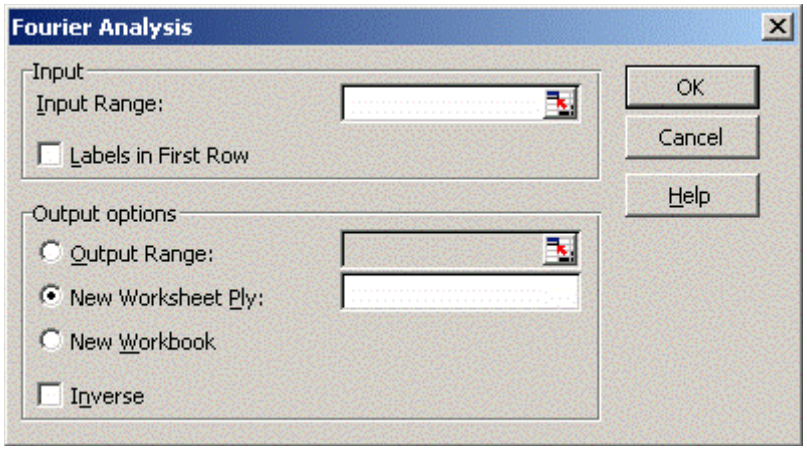

Step 3.) Normalize the Excel FFT output. This step multiplies the Excel output number by 1 over the number of samples. This is done to see better the relative contribution of each component. The command "improduct" is used here to multiply a non-real number. The command is (=improduct(excel_output, 1/n_points))

Step 4.) Determine magnitude of frequency. Using the function IMABS we can find the absolute value of the non-real number. By multiplying this by the square root of 2, we can find the magnitude of the Fourier coefficient.
This command is (=sqrt(2)*IMABS(normalized_output))

Step 5.) Determine Fourier Power of the frequency. The power of each frequency is used to determine significant frequencies.

If only the relative power of each frequency is required, normalization is not necessary, however allows us to compare magnitude of each frequency easier, and determine significance.

Step 6.) Determine Frequencies. In a separate column, begin with the zero frequency (the Excel FT assigned this frequency a real number output), in the next row, add 1 value of the frequency bin, in the next, add another value of the frequency bin, ect...

0	This is the first frequency value
1.09E-06	This is 1 frequency bin added to 0
2.17E-06	this is 2 frequency bins added to 0, or 1 to the previous frequency
3.26E-06	ect..
4.34E-06	ect..
5.43E-06	ect...

Spreadsheet Example of Excel FT

			White Creek Flow Spectral Analysis				
Parameters of Sampling						**Magnitude**	
N_points	1024		**Freequency**	**Excel**	**Normalized**	**Of Fourier**	**Fourier**
total_time	921600	seconds	**Hz**	**FFT Output**	**Excel FFT Output**	**Analysis**	**Power**
time_bin	900	seconds	0	30852.23	8.33663802421098E-003	0.01179	6.95E-05
f_folding	0.00056	Hz	1.0851E-06	-20.6362786291485-1.52019184	-2.23917953875309E-005-1.6495	3.2E-05	5.04E-10
freq_bin	1.1E-06	Hz	2.1701E-06	72.2044588186247+24.6003514	7.83468520167369E-005+2.66930	0.00012	6.85E-09
			3.2552E-06	65.9782794653164-1.642177498	7.15910150448312E-005-1.78187	0.0001	5.13E-09
			4.3403E-06	2.94400115881649-12.9333293	3.19444570184081E-006-1.40335	2E-05	2.07E-10
			5.4253E-06	9.61904696270592-18.62414182	1.04373339439083E-005-2.02084	3.2E-05	5.17E-10
			6.5104E-06	-5.3592843498746+51.89363159	-5.81519569213824E-006+5.6308	8E-05	3.2E-09
			7.5955E-06	8.20954873979327-2.932674802	8.90793049022707E-006-3.18215	1.3E-05	8.95E-11
			8.6806E-06	-28.1640396382601+21.9784518	-3.05599388435982E-005+2.3848	5.5E-05	1.5E-09
			9.7656E-06	80.2431641621112-47.16205910	8.70694055578464E-005-5.11741	0.00014	1.02E-08
			1.0851E-05	-27.1908427279083+15.3260424	-2.95039526127477E-005+1.6629	4.8E-05	1.15E-09
			1.1936E-05	-3.08229283927885+33.2661432	-3.34450177873139E-006+3.6096	5.1E-05	1.31E-09
			1.3021E-05	5.37506842904877+21.9428059	5.83232251415882E-006+2.38094	3.5E-05	6.01E-10
			1.4106E-05	13.373033550946+9.796548956	1.45106700856619E-005+1.06299	2.5E-05	3.24E-10
			1.5191E-05	-16.2200110497878+13.3953917	-1.7599838378676E-005+1.45349	3.2E-05	5.21E-10
			1.6276E-05	-33.8944956491676-1.83454633	-3.67778815637669E-005-1.9906	5.2E-05	1.36E-09
			1.7361E-05	-5.0936671954029-12.35965215	-5.52698263390072E-006-1.3411	2.1E-05	2.1E-10
			1.8446E-05	24.7666419393961-20.78302037	2.6873526409935E-005-2.255102	5E-05	1.23E-09
			1.9531E-05	12.6569349668206+16.7792641	1.37336533928175E-005+1.82066	3.2E-05	5.2E-10
			2.0616E-05	25.2997808636567+12.7038393	2.74520191662942E-005+1.37845	4.3E-05	9.44E-10
			2.1701E-05	-13.3509732731169+20.1153184	-1.44867331522536E-005+2.1826	3.7E-05	6.86E-10
			2.2786E-05	-13.407931021653-0.228248177	-1.45485362648145E-005-2.4766	2.1E-05	2.12E-10
			2.3872E-05	-7.62186722867587+2.42056240	-8.27025523944864E-006+2.6264	1.2E-05	7.53E-11
			2.4957E-05	5.02176810104858-4.894364650	5.44896712353362E-006-5.31072	1.1E-05	5.79E-11
			2.6042E-05	1.7917074330437+1.999311350	1.94412698897971E-006+2.16939	4.1E-06	8.49E-12
			2.7127E-05	-10.6556882156578-7.43559016	-1.1562161692337E-005-8.06813	2E-05	1.99E-10
			2.8212E-05	0.295584760126742+2.2595508	3.20729991456968E-007+2.45176	3.5E-06	6.11E-12
			2.9297E-05	-0.693631655700271-11.636630	-7.52638515299773E-007-1.2626	1.8E-05	1.6E-10
			3.0382E-05	-0.383826370633025+8.0317614	-4.16478266745904E-007+8.7150	1.2E-05	7.61E-11
			3.1467E-05	-1.92198410332009+2.69240580	-2.08548622322058E-006+2.9214	5.1E-06	1.29E-11
			3.2552E-05	1.40062008563338-1.533622920	1.51977005819594E-006-1.66408	3.2E-06	5.08E-12
			3.3637E-05	-3.26385730554289-6.46493085	-3.54151183327136E-006-7.0148	1.1E-05	6.18E-11
			3.4722E-05	-2.8631569856349+0.436275866	-3.10672415976009E-006+4.7338	4.4E-06	9.88E-12
			3.5807E-05	-2.09089459287149-0.26104313	-2.26876583427896E-006-2.8324	3.2E-06	5.23E-12

Appendix B

Using R for Spectral Analysis

R is a language and environment of statistical computing and graphing. R can provide a variety of statistical modeling, and spectral analyses. R can produce user defined graphs of publication quality. It is available as free software under the terms of the Free Software Foundation's GNU General Public license. The windows version is available for download at: http://cran.r-project.org/bin/windows/base/

To process data, the user must create a separate comma separated value spreadsheet with a single column of data points to be analyzed. The number of data points analyzed does not have to be a power of two, as the program will automatically add zeros up to the next power of two.

For each stream, a comma separated file (CSV) was created for tide data, another for barometric pressure data, and another for flow data. Using Microsoft Excel a single column of each data type was entered and then saved as a CSV file. This file must be located in a known folder and R must be told where to look for that file. This is done by clicking "File", then "Change Directory".

For additional information on coding, and time series analysis please refer to:
Time Series Analysis and Its Applications: with R examples, 2nd ed. Shumway and Stoffer, 2006.

An example of the command string used is as follows, with minor revisions of file names for each site.

```
tctide<-
read.csv("tctide.csv",header=T)
par(mfrow=c(2,1))
tctide.per=spec.pgram(tctide,tap
er=0,log="no",xlim=c(0,0.2),ylab
="Power",main="Tantalus Creek
Spectral Analysis of Earth
Tides",xlab="Frequency")
abline(v=0.0078125,lty="dotted")
abline(v=0.00390625,lty="dotted"
)
#cbind(tctide.per$freq,tctide.pe
r$spec)
```

Command Summary

reads the file named "tctide.csv" and performs the FFT spectral analysis, and graphs results on a graph occupying 1/2 of page, dotted vertical lines are drawn at frequencies 0.0078125 and 0.00390625

The Pound character tells the program not to run a certain line, it can be removed to run the line. The Cbind command reveals data output from the previous step.

```
df=tctide.per$df
U=qchisq(0.0125,df)
L=qchisq(1-0.0125,df)
tctide.per$spec[8]
df*tctide.per$spec[8]/L
df*tctide.per$spec[8]/U
abline(h=df*tctide.per$spec[8]/L
,lty="dotted")
tctide.per$spec[16]
df*tctide.per$spec[16]/L
df*tctide.per$spec[16]/U
abline(h=df*tctide.per$spec[16]/
L,lty="dotted")
```

Lines beginning at df=tctide.per and ending at L, lty="dotted"), are the commands used to compute and draw statistical significance of certain frequency spikes.
Spike frequencies were found using the "cbind" command earlier.

```
tcflow<-
read.csv("tcflow.csv",header=T)
par(mfrow=c(2,1))
tcflow.per=spec.pgram(tcflow,tap
er=0,log="no",xlim=c(0,0.2),ylab
="Power",main="Tantalus Creek
Spectral Analysis of
Discharge",xlab="Frequency")
abline(v=0.001953125,lty="dotted
")
#cbind(tcflow.per$freq,tcflow.pe
r$spec)
df=tcflow.per$df
U=qchisq(0.025,df)
L=qchisq(1-0.025,df)
tcflow.per$spec[2]
df*tcflow.per$spec[2]/L
df*tcflow.per$spec[2]/U
abline(h=df*tcflow.per$spec[2]/L
,lty="dotted")

k=kernel("daniell",1)
tcflow.ave=spec.pgram(tcflow,k,t
aper=0,log="no")
abline(v=0.00216,lty="dotted")
abline(v=0.0108,lty="dotted")
abline(v=0.0306,lty="dotted")

k=kernel("modified.daniell",c(3,
3))
flow.smo=spec.pgram(flow,k,taper
=0,log="no")
abline(v=0.00216,lty="dotted")
abline(v=0.0108,lty="dotted")
abline(v=0.0306,lty="dotted")
```

The K=kernel "daniell" command string smoothes the data from earlier graphs. Daniell command smoothes the data by doing a running average computation, and the daniell modified smoothes the data previously smoothed by the first daniell command.

```
tcbaro<-
read.csv("tcbaro.csv",header=T)
par(mfrow=c(2,1))
tcbaro.per=spec.pgram(tcbaro,tap
er=0,log="no",xlim=c(0,0.1),ylab
="Power",main="Tantalus Creek
Spectral Analysis of Barometric
Pressure",xlab="Frequency")
abline(v=0.0019531250,lty="dotte
d")
#cbind(tcbaro.per$freq,tcbaro.pe
r$spec)
df=tcbaro.per$df
U=qchisq(0.025,df)
L=qchisq(1-0.025,df)
tcbaro.per$spec[2]
df*tcbaro.per$spec[2]/L
df*tcbaro.per$spec[2]/U
abline(h=df*tcbaro.per$spec[2]/L
,lty="dotted")
```